BIOBASED AND BIODEGRADABLE POLYMER NANOCOMPOSITES

A Dissertation

Presented to the Faculty of the Graduate School

of Cornell University

In Partial Fulfillment of the Requirements for the Degree of

Doctor of Philosophy

By

Kaiyan Qiu

August 2012

BIOBASED AND BIODEGRADABLE POLYMER NANOCOMPOSITES

Kaiyan Qiu, Ph.D.

Cornell University 2012

In this dissertation, various noncrosslinked and crosslinked biobased and biodegradable polymer nanocomposites were fabricated and characterized. The properties of these polymer nanocomposites, and their relating mechanisms and corresponding applications were studied and discussed in depth.

Chapter 1 introduces the research background and objectives of the current research.

Chapter 2 presents the development of a novel low cost carbon source for bacterial cellulose (BC) production and fabrication and characterization of biobased polymer nanocomposites using produced BC and soy protein based resins. The carbon source, soy flour extract (SFE), was obtained from defatted soy flour (SF) and BC yield achieved using SFE medium was high. The results of this study showed that SFE consists of five sugars and *Acetobacter xylinum* metabolized sugars in a specific order.

Chapter 3 discusses the fabrication and characterization of biodegradable polymer nanocomposites using BC and polyvinyl alcohol (PVA). These polymer nanocomposites had excellent tensile and thermal properties. Crosslinking of PVA using glutaraldehyde (GA) not only increased the mechanical and thermal properties but the water-resistance.

Chapter 4 describes the development and characterization of microfibrillated cellulose (MFC) based biodegradable polymer nanocomposites by blending MFC suspension with PVA.

Chemical crosslinking of the polymer nanocomposites was carried out using glyoxal to increase the mechanical and thermal properties as well as to make the PVA partially water-insoluble.

Chapter 5 reports the development and characterization of halloysite nanotube (HNT) reinforced biodegradable polymer nanocomposites utilizing HNT dispersion and PVA. Several separation techniques were used to obtain individualized HNT dispersion. The results indicated uniform dispersion of HNTs in both PVA and malonic acid (MA) crosslinked PVA resulted in excellent mechanical and thermal properties of the materials, especially for the crosslinked PVA.

Chapter 6 presents the biodegradation of PVA based resins and nancomposites in a composting medium. The results suggest that biodegradation of PVA based materials is mainly by enzymes secreted by fungi. The three factors, namely, crystallinity, additives and crosslinking, may be utilized effectively to enhance the life of these materials in real life applications.

Chapter 7 presents broad conclusions of the the entire study and possible suggestions for future research.

BIOGRAPHICAL SKETCH

Kaiyan Qiu was born in Haining, China on October 8, 1981. He was then raised by his grandparents in his family's hometown, Shanghai, China before his mother returned to Shanghai. After graduating from Donghua University in June 2004 with a Bachelor of Science degree in Chemical Engineering, he received a Master of Science degree in Chemical Engineering at the same university in 2007. He enrolled in the Fiber Science Program in 2007, at Cornell University. He received a Doctor of Philosophy degree from Cornell in the August of 2012.

ACKNOWLEDGEMENTS

I first thank my advisor, Prof. Anil N. Netravali, for his guidance. I also thank my committee members, Prof. Yong L. Joo, Prof. Dan Luo and Prof. C.C. Chu for their valuable suggestions and discussions.

I wish to thank Prof. Antje Baeumner, Prof. John March and Prof. Prof. Jocelyn Rose of Cornell University for allowing the use of their facilities. I also thank Cornell Center for Materials Research (CCMR) for allowing me to use various equipments.

I would also thank my department colleagues for their help and my parents for their support during my PhD study.

TABLE OF CONTENTS

LIST OF FIGURES

LIST OF TABLES

Charpter 1 Introduction

Kaiyan Qiu, Anil N. Netravali*
Fiber Science Program, Cornell University, Ithaca, NY 14853-4401

1.1 Biobased and Biodegradable Polymers

Most commercial polymers used today are prepared using non-biodegradable constituents. Most of these polymers are also derived from petroleum, a non-sustainable resource. These materials at the end of their useful life cannot be easily consumed and simply pile up as waste and cause significant damage to the environment [1]. Over 30 million and 15 million tons of non-biodegradable polymeric waste, in the US and western Europe, respectively, are generated each year [2-4]. At the end of their life majority of the conventional plastics are traditionally disposed of in landfills where they may stay as is for several decades without degrading making that land unusable for any other applications. About 6-7% of the petroleum produced today is used for making polymers, fibers and other chemicals [2-3]. It is estimated that we are currently consuming petroleum at an 'unsustainable' rate, 100,000 times faster than the nature can create it [3]. At the current rate of consumption, it is estimated that the current petroleum reserves will last for only 50-60 years [2]. These concerns have forced the development of environmentally friendly biobased and biodegradable polymers and their composites in recent years [2-4].

Biobased and biodegradable polymers are generally defined as those polymers that can decompose in natural aerobic (composting) and anaerobic (landfill) environments [2]. Biobased polymers are those that are derived from renewable plant based raw materials and tend to be inherently biodegradable [2-4]. They almost always have oxygen or nitrogen atoms in their polymer backbones which is the feature that is mainly responsible for their biodegradability [2]. Biobased polymers can be further subdivided into two categories, natural biopolymers and

synthetic biopolymers [2]. Natural biopolymers often refer to those biobased polymers found directly in nature, including carbohydrates (starch, cellulose, chitin, agar, carrageenan, etc.), lignin, proteins and bacterial produced polyesters [2-4]. Synthetic biopolymers are polymers that are not found in nature but are made commercially from monomers that are found abundantly in nature [2]. Polylactic acid (PLA) and polyamino acids (PAA) are examples of important synthetic biopolymes [2]. Biodegradable polymers normally refer to petroleum-based biodegradable synthetic polymers, such as polyvinyl alcohol (PVA), polyglycolic acid (PGA), polycaprolactone (PCL), polyethylene oxide (PEO) etc. [2-4]. Biodegradation of biobased and biodegradable polymers can be achieved by enabling microorganisms in the environment to metabolize the polymer to produce an inert humus-like material that are less harmful to the environment and can get easily blended with the natural soil [2-4].

1.2 Polymer Composites

Although polymers are being employed more and more as structural materials, their use often is limited by their relatively low levels of stiffness and strength compared, for example, with metals [2, 5-7]. Because of the needs to be light weight and high stiffness as well as to possess other functionalities (wear resistance, thermal stability, electrical property, low-cost and high-volume etc.) for materials to be used in diverse applications, advanced polymer composites have been developed over recent years with extremely high properties [5-7].

Polymer composites consist of two or more distinct phases, normally including a polymer matrix (continuous) phase and fibrous or particulate material dispersed phase [2]. Based on their geometries, polymer composites can be categorized into three main classifications: particulate composites, continuous fiber composites and discontinuous fiber composites [5-7].

The polymers most commonly used as matrix materials at present are thermosetting network polymers such as unsaturated polyesters and epoxy resins [5, 8]. There have been developments in the field of thermoplastic polymer matrix composites using nylon or polypropylene as matrix. For dispersed phase, silicate-based minerals, glass, carbon and other high-modulus polymeric fibers are universally used as reinforcements in polymer composites, based on the properties desired [5, 8]. The dispersed phase size has become smaller to a few nanometers where significant benefits may be derived due to their small size. These nanocomposites are described later. Recently, polymer composites using biobased and biodegradable polymers and natural fibers have been widely studied and developed due to the increasing environmental and energy concerns [9-12].

1.3 Nanomaterials and Its Applications

1.3.1 Nanotechnology

The field of nanotechnology is currently one of the most popular areas that deal with small structures or small-sized materials [13-16]. By definition, at least one dimension of the structures and materials must be between a nanometer to several hundred nanometers for it to be called a nanomaterial. Extremely high specific area, as a result of the small size of the nanomaterials, allows packing of more functionalities in a given space. Some specific properties of nanomaterials are remarkable and distinctively different from those of bulk materials [13-15]. For example, crystals at nanometer scale have low melting points and reduced lattice constant, since the number of surface atoms or ions becomes a significant fraction of the total number of atoms or ions and the surface energy plays a significant role in the thermal stability. Bulk semiconductor becomes insulator when the characteristic dimension is sufficiently small, a couple of nanometers. Another good example is of gold. Although bulk gold does not exhibit

catalysis properties, gold nanocrystal demonstrates to be an excellent low temperature catalyst [16].

In general, nanotechnology can be understood as a technology of design, fabrication, and applications of nanostructures and nanomaterials. Nanotechnology also includes fundamental understanding of physical properties and phenomena of nanomaterials and nanostructures. In the United States, nanotechnology has been defined as being 'concerned with materials and systems whose structures and components exhibits novel and significantly improved physical, chemical and biological properties, phenomena and processes due to their nanoscale size' [16, 17].

1.3.2 Nanostructures and Nanomaterials

Nanostructures of the nanomaterials possess a large fraction of surface atoms per unit volume. The ratio of surface atoms to interior atoms changes dramatically if one successively divides a macroscopic object into smaller and smaller parts [18]. Such a dramatic increase in the ratio of surface atoms to interior atoms in nanostructures and nanomaterials might illustrate why changes in the size range of nanometers are expected to lead to great changes in the physical and chemical properties of materials [16].

Top-down and bottom-up are two common approaches to the synthesis of nanomaterials and the fabrication of nanostructures [15, 16]. Attrition or milling is a typical top-down method in making nanoparticles, whereas the colloidal dispersion is a good example of bottom-up approach in the synthesis nanoparticles. Lithography may be considered as a hybrid approach, since the growth of thin films is bottom-up whereas etching is top-down, while nanolithography and nanomanipulation are common bottom-up approaches [15, 16]. Both top-down and bottom-up approaches to nanomaterials play very important roles in modern industry, and most likely, in nanotechnology as well.

Structures of nanomaterials can be roughly categorized into zero-dimensional, one-dimensional and two-dimensional nanostructures [16]. In zero-dimensional nanostructures category, nanoparticles and heteroepitaxial core-shell nanomaterials are two main examples. Nanomaterials with one-dimensional nanostructures have been called by a variety of names including: whiskers, fibers or fibrils, nanowires, and nanorods. In many cases, nanotubes and nanocables are also included in one-dimensional nanostructures. Thin films or sheets such as exfoliated nanoclay possess typical two-dimension nanostructures [16].

Many applications for nanostructures and nanomaterials have been vastly investigated and developed. Examples include nanoscale and molecular electronics, catalysis of gold nanocrystals, nanobots, nanoparticles as biomolecular probes, bandgap-engineered quantum devices, nanomechanics, carbon nanotube emitters, photoelectrochemical cells, lithium-ion rechargeable batteries, hydrogen storage, thermoelectrics, environmental applications, photonic crystals, plasmon devices, etc. [16]. However, using nanoparticles as fillers to fabricate polymer nanocomposites has been one of the most common applications as of yet [16].

1.4 Polymer Nanocomposites and Biobased and Biodegradable Polymer Nanocomposites

Polymer nanocomposites are polymers or copolymers having dispersed in its nanomaterials. These nanomaterials may be of different shape (e.g., platelets, fibers, spheroids), but at least one dimension must be in the range of nanoscale (normally less than 100 nm) [13, 19-24]. The addition (loading) of nanomaterials to polymers leads to significant changes in their physical, mechanical as well as thermal properties [19, 20]. For example, nanocellulose can improve the mechanical properties of polymer while nanoclays often increase thermal stability of polymers [21-24]. Many diverse topics, including composite reinforcement, barrier properties, flame resistance, electro-optical properties, cosmetic applications and bactericidal properties, exist in

the field of polymer nanocomposites [1]. At present, polymer nanocomposites have revolutionized the research in the field of material composites, providing significant enhancements in the composite properties at low nanomaterial (fillers) loading [21, 22]. This is a result of the uniform dispersion of the nanomaterials in the polymer matrices. The fabricated polymer nanocomposites have been shown to possess excellent mechanical properties [1, 5, 13,]. However, most of them are non-biodegradable. Recently, many polymer nanocomposites using biobased and biodegradable polymers and nanomaterials with excellent mechanical and thermal properties as well as other functionalities have been reported [21-24]. These biobased and biodegradable polymer nanocomposites have the potential to replace traditional non-biodegradable plastic materials in many applications, including tennis/badminton/squash racket frames, ski pole, circuit board, automobile inside panels, etc. [1, 20-24].

1.5 Nanomaterials and Biobased and Biodegradable Polymers Used in Present Research

1.5.1 Nanomaterials Used in Present Research

All nanomaterials used in present research possess one-dimensional nanostructures. They include bacterial cellulose (BC), microfibrillated cellulose (MFC) and halloysite nanotubes (HNTs). While BC nanofibers were harvested from cellulose synthesis achieved through *Acetobacter xylinum* through media culture, MFC and HNTs were obtained from plant cellulose and halloysite mineral using top-down milling approach, respectively. They are either biobased or produced by nature and are benign to the environment.

1.5.1.1 BC

Bacterial cellulose (BC) is a promising nanomaterial derived from biobased raw materials with excellent potential as reinforcement for composites. BC is pure cellulose primarily produced by *Acetobacter xylinum*, a Gram-negative, obligately aerobic bacterium, in a nutritional

fermentation medium maintained at 30 ℃. Traditionally, the medium requires carbon sources (e.g., mannitol, sucrose, fructose or others) and nitrogen sources (e.g., peptone, typtone, yeast extract, etc.), with optimum pH of 5.0 [25-29]. BC has the same chemical structure as other plant-based cellulose and is produced as fibers with diameters in the range of 70 to 90 nanometers. It displays many unique properties including higher purity (up to 99% or higher), higher degree of polymerization (up to 20,000), higher crystallinity (up to 68%), higher tensile strength and modulus (up to 114 GPa for modulus) and stronger biological adaptability [25-29]. The BC material is already being used in many niche applications including artificial skin and blood vessels, binding agent for fibers and other materials, loud speaker diaphragms, high quality paper, foods, textiles, composite membranes, etc. [29-34]. BC can also be ground in to shorter fibers or hydrolyzed into BC nanowhiskers for further applications [35-38]. Though BC has excellent mechanical properties, the production cost is relatively high because of the high cost of the carbon source. Therefore, a low-cost carbon source from defatted soy flour (SF) for BC production was investigated and developed in the present research [21].

1.5.1.2 MFC

Microfibrillated cellulose (MFC) can be obtained by mechanical treatment, primarily shearing, of pulp cellulose fibers to small diameter fibrils through refining and high-pressure homogenization processes [39-42]. Since the widths or diameters of many of the fibrils in MFC are in submicron range, they may also be considered as nanofibers [39, 40, 43-45]. Being pure cellulose, MFC is biodegradable. The MFC has high aspect ratio and high tensile properties as a result of high orientation and crystallinity. Their modulus is estimated at 140 GPa and tensile strength between 2 and 6 GPa [39]. Much of the efforts until now have been focused on fabrication of MFC based composites using nonbiodegradable phenolic and other resins [39, 43-

47]. Such composites, although greener, cannot be not fully biodegradable and hence still need to be disposed of in landfills at the end of their life. This situation presents a significant opportunity to use MFC with biodegradable resins to fabricate fully biodegradable composites that can be composted at the end of their life. MFC can also be combined with green resins to fabricate fully green composites [10, 22]. MFC blended resin may also be used with natural or biodegradable fibers to form hybrid composites.

1.5.1.3 HNTs

Halloysite is based on aluminosilicate clay nanoparticles that have hollow nanotubular structure and are mined from natural deposits [47, 48]. While the ideal unit formula for halloysite is $Al_2Si_2O_5(OH)_4$. n H_2O (where n = 0 for halloysite-(7Å) and n = 2 for hydrated halloysite-(10Å)), the chemical composition is subject to variation due to the presence of impurities such as Fe oxides [48]. Halloysite occurs widely throughout the world in weathered rocks as well as in soils and has been identified as having formed by the alternation of a wide variety of igneous and non-igneous rocks [47-49]. It is often intermixed with dickite, kaolin, montmorillonite and other clay minerals [49]. The dominant morphology of halloysite is tubular when it is derived from crystalline minerals and hence it is commonly termed as halloysite nanotubes (HNTs) [48]. Unlike other nanostructured clays that must be exfoliated, HNTs naturally occur as cylinders with average diameters typically smaller than 100 nm and typical lengths ranging from 500 nm to over 1.2 μm [49]. HNTs have been used as bioreactor, time-release capsules, catalysts of polymer degradation, templates for deposition of other nanoparticles, ceramic applications and polymer filler or property modifier [47].

1.5.2 Biobased and Biodegradable Polymers Used in Present Research

Biobased and biodegradable polymers used in our research include biobased soy protein based resin and biodegradable PVA. These are described below.

1.5.2.1 Soy Protein based Resin

Defatted soy flour (SF) was used as a soy protein based resin. Defatted soy flour (SF) is obtained as a by-product after extracting oil from the soybeans. It is commercially available and consists mainly of protein (52-54%), carbohydrates (sugars) (30-32%), dietary fiber (2-3%), minerals and ash (3-6%) and moisture (6-8%). SF is also very inexpensive, about $0.25/lb. The soybean is a legume species native to East Asia and is classified as an oilseed. It is an annual and economic crop and has been abundantly produced and used in many countries for over 5,000 years [50]. Currently, it is an important global crop and provides major amount of edible oil and protein worldwide [51]. As mentioned earlier, SF contains carbohydrates in the form of various sugars and protein. It is possible to dissolve and extract water soluble sugars from SF, termed as soy flour extract (SFE). After removing SFE, the residual protein product, termed as modified soy flour (MSF) has higher protein content of between 60 and 70%. MSF based resin has been shown to have better tensile properties than those of SF resin [52]. MSF resin also has higher interfacial bonding with ramie fiber compared to SF resin [52]. As a result, composites using MSF resin could be expected to have much better mechanical properties than those using SF resin [52].

1.5.2.2 PVA

Polyvinyl alcohol (PVA) is a thermoplastic and biocompatible polymer prepared from the polymerization of vinyl acetate followed by alcoholysis. It has been widely used making films, fibers, paper coating and adhesives due to the attractive properties of PVA [53, 54]. However,

unlike most of petroleum based polymers, it is one of the rare polymers with a carbon-carbon single bond backbone that is fully biodegradable in the presence of suitably acclimated microorganisms and their enzymes [2, 53, 54]. In addition, because of the hydroxyl (-OH) groups on alternating carbon atoms PVA is strongly hydrophilic and soluble in water (depending on molecular weight), which also helps to promote its degradation through hydrolysis [2, 53, 54].

1.6 Development of Low-Cost Carbon Source for Production of BC Nanomaterials

Many pure sugars such as glucose, sucrose, fructose, etc. and sugar alcohols such as mannitol, xylitol, sorbitol, etc. have been used as carbon source for BC culture [55-59]. Among them glucose, fructose and mannitol are the most common and have shown excellent results in terms of BC production [55-61]. However, these sugars and sugar alcohols are expensive and hence they are not considered to be ideal for large commercial scale BC production which needs to be inexpensive. As a result, many attempts have been made to obtain higher BC yields as well as to reduce the cost of the carbon sources. Some of these efforts have been successful. For example, konjac powder hydrolyzate [55], sugarcane molasses [62], beet molasses [63] and processed rice bark [64] have been found to be useful in BC production. While some of these sources may be used for industrial BC production in the near future, there is significant scope to further reduce the cost of BC production by using inexpensive waste products and expand its use in many mass volume applications.

As mentioned earlier, soybeans contain decent amount of sugars, including fructose, glucose, sucrose, raffinose and stachyose [21, 65]. Out of these, fructose, glucose and sucrose have been used routinely as carbon sources for BC production [66]. It has also been reported that raffinose and stachyose can be metabolized by lactic acid bacteria [67]. To obtain higher protein content from SF, the sugars are extracted in the form of soy flour extract (SFE), a by-product. Therefore,

the SFE, a mixture of five sugars with ideal sugar concentrations (using high performance liquid chromatography (HPLC) for the analysis), can be expected as an inexpensive carbon source to produce BC for reducing the cost of BC production. The present research has successfully shown that SFE can be used for BC production and that the BC yields are comparable to commonly used sugars.

1.7 Methods for Polymer Nanocomposite Fabrication, Crosslinking and Characterization

1.7.1 Methods for Polymer Nanocomposite Fabrication

Polymer nanocomposites have commonly been prepared using several different synthetic routes [68]. The first method is *in situ* polymerization synthesis. It is based on the intercalation of the clay in the monomer followed by polymerizing the monomer in the presence of nanomaterial, thus trapping the nanomaterial within the polymer structure. The second method is melt intercalations. In this case, the polymer is melted at high temperature, and the nanomaterial filler is slowly added to the melt being sheared in the compounder. The nanomaterial filler is sheared during compounding and kneading in the compounder and thus are well mixed with the polymer phase. The third method for synthesizing polymer nanocomposites is solvent intercalation. The polymer is dissolved in the same solvent in which the nanomaterial is also dispersed. Evaporation of the solvent leads to entrapment of the polymer chains in between the nanomaterial layers [1, 68-70].

1.7.2 Crosslinking of Polymers and Polymer Nanocomposites

Crosslinking is the process of chemically joining (linking) two or more molecules at different locations along the polymer chains by covalent bonds or ionic bonds [71]. Crosslinking has been commonly used to improve the mechanical and thermal properties as well as to eliminate or reduce dissolution of polymers in solvents [71-75]. When used as resin, crosslinked polymers

can also improve composite properties. As in the case of resins, the resulting modifications of mechanical and physical properties of the composites depend strongly on the crosslink density [76]. Very low crosslink densities can decrease the viscosities of polymer melts. Intermediate crosslink densities transform gummy polymers into materials that have elastomeric properties and potentially high strengths. Very high crosslink density can cause materials to become stronger and rigid or glassy by increasing their glass transition temperature [76].

Crosslinking can be induced in polymers that are normally thermoplastic through exposure to radiation source, such as electron beam exposure, gamma radiation or ultraviolet light (UV) [77, 78]. More commonly, for polymers that have reactive (functional) groups crosslinks are formed by chemical reactions with crosslinkers that are initiated by heat, pressure, change in pH or radiation [22-24]. Crosslinkers are often selected on the basis of their chemical reactivity with the functionalities present on the polymers [71]. Glutaraldehyde (GA) and glyoxal are two universally used crosslinkers for polymers and their nanocomposites that contain amine and hydroxyl groups, such as proteins, PVA and cellulose [21-24, 72-76, 79]. Although both of them are effective in crosslinking polymers, they are relatively toxic [80]. Therefore, less toxic crosslinkers are of interest in the crosslinking reaction, particularly to maintain the biodegradability of the polymers. Malonic acid (MA) is a dicarboxylic acid produced from chloroacetic acid and can be used as a crosslinker [81]. In terms of toxicity, it is a significantly better choice as a crosslinker compared to GA or glyoxal [80]. Some researchers have shown crosslinking of PVA using dicarboxylic acids, including MA, where sulphuric acid was used as a catalyst to obtain esterification [82, 83]. In the present research, crosslinking was carried out for soy protein based resin as well as PVA using GA, glyoxal and MA and polymer nanocomposites were prepared using crosslinked resins.

1.7.3 Characterization of Polymers and Polymer Nanocomposites

Morphology of nanomaterials in polymer matrix is one of the key factors that influence the properties of nanocomposites. Transmission electron microscopy (TEM) and scanning electron microscopy (SEM) allow a direct morphological observation of polymers and polymer nanocomposites [84-86]. Currently, Föster resonance energy transfer (FRET) technique and laser scanning confocal microscopy (LSCM) were also jointly applied to reveal the interface between nanomaterial and polymer in polymeric nanocomposites [87].

Chemical structure, as well as elemental composition, crystalline, thermal, tensile, water-absorbent, soluble properties of nanocomposites are also of great interest since they determine their applications. Therefore, several techniques have been used to characterize their properties. These include attenuated total reflectance-Fourier transform infrared spectroscopy (ATR-FTIR), energy dispersive X-ray (EDX) analysis, wide-angle X-ray scattering (WAXS), thermogravimetric analysis (TGA), differential scanning calorimetry (DSC), tensile test, moisture content, swelling and sol-gel test are often applied to characterize the polymer nanocomposites [21-24]. Most of these techniques were used in the course of the present research and are described in the chapters.

1.8 Biodegradation for Biobased and Biodegradable Polymers and Polymer Nanocomposites

Biodegradation can be regarded as a process in which the degradation results from the action of microorganisms such as bacteria, fungi or algae [1, 88]. Biodegradation can be generally divided into two steps. The first step is depolymerization or chain cleavage where the longer polymer chain undergoes backbone scission into smaller oligomeric fragments with the help of enzymes secreted by microorganisms. The second step is mineralization, which occurs inside

the cell in which small oligomeric fragments are converted to biomass, minerals and salts, water and gaseous substances such as carbon dioxide under aerobic environments and methane under anaerobic environments [88-96]. Biobased and biodegradable polymers and their composites may be broken down by the enzymes secreted by microorganisms. Once broken down to monomeric level, the polymer is used as the carbon source for the microorganism metabolism. The biodegradation process is chemical in nature but the source of the attacking chemicals (enzymes) is from microorganisms [89-93]. Biodegradation of the materials produces carbon dioxide under aerobic environments or methane under anaerobic environments, in addition to humus [1, 88]. The susceptibility of polymers and their composites to microbial attack generally depends on enzyme availability, availability of a site in the polymers for enzyme attack, enzyme specificity for that polymer and the presence of coenzyme [94]. Biodegradation results in the changes in surface properties since it begins at the surface where the microorganisms are present. Once progressed, it results in loss of strength, assimilation by microorganisms, degradation by enzymes or breakage of backbone chains and subsequent reduction in the average molecular weight of polymers [1, 88-94].

The biodegradation and its mechanism under the effect of microorganisms for different polymers and their composites, including poly (butylene succinate) (PBS) and its silicate reinforced nanocomposites, poly (lactic acid) (PLA) and its silica and calcium carbonate reinforced nancomposites, whey protein, soy protein isolate (SPI), poly (ε-caprolactone) (PCL), poly (hydroxybutyrate-co-hydroxyvalerate) (PHBV), noncrosslinked PVA etc., have been extensively studied [1, 2, 97-110]. Many factors can influence the biodegradation process, including surface area, hydrophilic/hydrophobic properties, chemical structure, molecular weight, crystallinity and melting temperature. Polyesters with side chains and higher melting

temperature are less assimilated than those without side chains [97-110]. PCL with higher molecular weight degraded more slowly than that with low molecular weight [97-110]. The rate of biodegradation of PLA was shown to decrease with an increase in crystallinity since the enzymes mainly attack the amorphous domains of polymers [1, 97-100]. Addition of a dispersed phase also has an effect on the rate of biodegradation [107-110]. The relative rate of biodegradation for PBS-silica nanocomposites was faster than that of neat PBS which was attributed to the relatively low crystallinity of PBS in the PBS-silica nancomposites [107, 108]. It was also observed that addition of layered silicate and calcium carbonate increased the rate of biodegradation of PLA [109, 110]. Besides, the degradation rate of PLA in compost was delayed with the introduction of crosslinks [111].

PVA is a widely used thermoplastic and biocompatible polymer. However, unlike most of petroleum based polymers, it is one of the rare polymers with a carbon-carbon single bond backbone that is fully biodegradable in the presence of suitably acclimated microorganisms and their enzymes [2, 101, 102]. In addition, because of the hydroxyl (-OH) groups on alternating carbon atoms PVA is strongly hydrophilic and soluble in water, which also helps to promote its degradation through hydrolysis [2, 53, 54, 101, 102, 112]. Therefore, both enzymatic and hydrolytic degradations can occur in all regions for hydrophilic PVA with moisture absorption [103]. Nevertheless, degradation of hydrophobic polymers, e.g., poly(hydroxybutyrate-co-hydroxyvalerate) (PHBV) in compost medium is enzymatic rather than hydrolytic and occurs from the surface [102].

The first microorganisms capable of assimilating PVA as their sole carbon source were isolated from soil samples and identified as *Pseudomonas* species [54, 102, 105, 106, 113]. Further studies have confirmed that other aerobic bacteria, such as *Alcaligenes* and *Bacillus*,

were also active in the degradation of PVA [54, 104, 113-115]. Fungal strains, such as *Aspergillus niger, Pycnoporus cinnabarinus, Fusarium and Phanerochaete chrysoporium*, have been reported to change not only the polymer (like PVA) surface from smooth to rough, but even to disrupt the polymer through enzymatic degradation [9, 116, 117]. It was observed that specific microbial strains were able to induce a rapid decrease of the viscosity of aqueous culture media containing PVA. It was therefore assumed that at least the initial microbial attack should be consistent with a random cleavage of the polymer chains. At the same time, the occurrence of oxidative reactions of the tertiary carbon atoms of PVA chains, leading to the formation of hydrolysable β-hydroxylketone and 1, 3-diketone groups along the polymer backbone, was established. These reactions were catalyzed by specific oxidases and dehydrogenases that were isolated mainly as extracellular proteins from different bacterial species [54, 104, 101, 102].

It has been reported that PVA can be degraded under different environmental conditions, including aerobic composting, soil burial, aqueous media and even anaerobic conditions [104, 118-121]. Among these paths for biodegradation, composting is an effective technique to characterize the biodegradation of PVA and other biodegradable polymers and their composites [102]. Composting is defined as an exothermic bio-oxidative decomposition of organic materials by indigenous microorganisms in a controlled moist and warm aerobic environment leading to the production of 'compost', a mixture of carbon dioxide, water, minerals and a stabilized organic matter [105, 122]. As the compost pile becomes active, a succession of mesophilic and thermophilic microorganisms secret depolymerase enzymes. These enzymes attack the substrate as nutrient in the presence of optimal moisture, temperature and nutrients [105, 120]. This being an exothermic process causes the temperature to rise above the ambient temperature of 23^{o}C. If the temperature increases to 40-45^{o}C, the mesophilic bacteria, actinomycetes and fungi give way

to thermophilic organisms and if it reaches 70-75^{o}C, the microbial activity is drastically reduced resulting in cooling down of the material and eventual maturity [105, 120]. It has been reported that hydrolytic degradation can occur in some polymers with high moisture sensitivity under the slightly acidic pH conditions [102, 103, 105, 106]. Composting of crosslinked PVA and PVA based nanocompostes can be expected to unveil the effects of crosslinking and nanomaterials on the biodegradation rate of PVA.

1.9 Objective and Potential Applications

The objective of this research was to fabricate and characterize biobased and biodegradable nanocomposites using different polymers and nanomaterials, and deeply understand their properties, relating mechanisms and corresponding applications. A low cost 'green' carbon source obtained as a by-product from soy protein production process, soy flour extract (SFE), has been first utilized in BC production to reduce the cost of BC production. The individual sugar components present in the carbon source and their consumption pattern during fermentation have been studied with the help of HPLC in this dissertation. Nanomaterials, including fully degradable BC and MFC, and natural occurred clay HNTs have been used in biobased soy protein based resin and biodegradable PVA to fabricate biobased and biodegradable polymer nanocomposites using solvent intercalation approach. BC-soy protein resin and BC-PVA nanocomposites are continuous fiber composites, MFC-PVA nanocomposites are discontinuous fiber composites, while HNT-PVA nanocomposites possess particulate composites structure. Chemical crosslinking using different crosslinkers (GA, glyoxal and MA) has been applied to further increase these properties. Tensile, thermal, structural properties as well as water-absorbency, solubility, crystallinity, of these polymer nanocomposites have been characterized using different testing approaches to understand the role each component plays. In addition,

nanomaterial dispersion and interfacial properties were also characterized. Composting was used to test the biodegradability and characterize changes in the properties for some of these biobased and biodegradable polymers and their nancomposites in this dissertation.

It can be observed that tensile properties of these biobased and biodegradable polymer nanocomposites were comparable or higher than many traditional plastic materials based on theoretical calculation (rule of mixture), including polyethylene (Young's modulus: 800 MPa; fracture stress: 15 MPa), polypropylene (Young's modulus: 1900 MPa; fracture stress: 40 MPa), and nylon 6 (Young's modulus: 1800 MPa; fracture stress: 70 MPa) [123]. In addition, the synthesized polymer nanocomposites can also obtain other useful properties based on the nanomaterials' properties and resin crosslinking, including higher thermal stability and enhanced water-resistance [9-12, 115]. As a result, these nanocomposites have the potential to replace these traditional non-biodegradable plastic materials in many applications, including racket frame, ski pole, circuit board, automobile inside, etc. [21-24, 124]. These biobased and biodegradable polymer nanocomposites can be easily protected from water by applying varnish or other water-resistant coatings to increase their durability [21-24, 124].

References

[1] Mittal V. Nanocomposites with biodegradable polymers: synthesis, properties and future perspectives. Oxford, UK: Oxford University Press, 2011. p. 1-27.

[2] Stevens ES. Green plastics: an introduction to the new science of biodegradable plastics, Princeton University Press, Princeton, NJ, 2002, pp.10-30.

[3] Netravali AN, Chabba S. 'Composites get greener'. Materials Today, 2003, 6 (4): 22-29.

[4] Georgia Tech Research Institute . 'Breaking down plastics: new standard specification may facilitate use of additives that trigger biodegradation of oil-based plastics in landfills'. http://gtresearchnews.gatech.edu/biodegradation-of-plastics/, Accessed November 2011.

[5] Young RJ, Lovell PA. Introduction to polymers, 3rd edition. Boca Raton, FL: CRC Press, 2011. p. 591-622.

[6] McGarry FJ. Polymer composites. Annu Rev Mater Sci 1994; 24: 63-82.

[7] Sheikh-Ahmad JY. Machining of polymer composites. New York; London: Springer 2009. p.1-36.

[8] Netravali AN. Carbon fiber/epoxy interfacial shear strength: effects of plasma surface treatment and nano-particle addition Vol. 5. In: Mittal KL. Polymer surface modification: relevance to adhesion. Leiden, the Netherlands: VSP 2009. p. 237-253.

[9] Huang X, Netravali AN. Characterization of flax yarn and flax fabric reinforced nano-clay modified soy protein resin composites. Compos Sci Technol 2007; 67: 2005-2014.

[10] Huang X Netravali AN. Environmentally friendly green materials from plant-based resources: modification of soy protein using gellan and micro/nano-fibrillated cellulose**.** J Macromol Sci Pure 2008; 45: 899-906.

[11] Kim JT, Netravali AN. Mercerization of sisal fibers: effect of tension on mechanical properties of sisal fiber and sisal fiber composites. Compos Part A-Appl S 2010; 41: 1245-1252.

[12] Kim JT, Netravali AN. Mechanical and thermal properties of sisal fiber-reinforced green composites with soy protein-gelatin blend resins. J Biobased Mater Bio 2010; 4 (4): 338-345.

[13] Paul DR, Robeson LM. Polymer nanotechnology: Nanocomposites. Polymer 2008; 49: 3187-3204.

[14] Microscopy and histology catalog. Warrington, PA: Polysciences, 1993-1994.

[15] Shi DL. Functional thin films and functional materials: new concepts and technologies. Berlin: Tsinghua University Press and Springer-Verlag, 2003. p. 1.

[16] Cao G, Wang Y. Nanostructures and nanomaterials: synthesis, properties, and applications, 2nd edition. Singapore: World Scientific, 2011. p. 61-142.

[17] National nanotechnology initiative 2000 leading to the next industrial revolution, a report by the interagency working group on nanoscience, engineering and technology (Washington DC: committee on technology, national science and technology council), http://www/nano.gov.

[18] Nützenadel C, Züttel A, Chartouni D, Schmid G, Schlapbach L. Critical size and surface effect of the hydrogen interaction of palladium clusters. Eur Phys J D 2000; 8 (2): 245-250.

[19] Greiner A, Wendorff AL, Yarin AL, Zussman E. Biohybrid nanosystems with polymer nanofibers and nanotubes. Applied Microbiol Biotechnol 2006; 71:387-393.

[20] Godovsky DY. Application of polymer-nanocomposties. Adv Polym Sci 2000; 153: 165-205.

[21] Qiu K, Netravali AN. 'Green' composites based on bacterial cellulose produced using novel low cost carbon source and soy protein resin. Recent advances in adhesion science & technology: Mittal festschrift. Boston: Brill; 2012 Accepted.

[22] Qiu K, Netravali AN. Biodegradable composites of polyvinyl alcohol reinforced with microfibrillated cellulose. J Mater Sci 2012; 47 (16): 6066-6075.

[23] Qiu, K, Netravali, AN. Fabrication and characterization of biodegradable composites based on microfibrillated cellulose and polyvinyl alcohol. Compos Sci Technol 2012; 72 (13): 1588-1594.

[24] Qiu, K, Netravali, AN. Halloysite nanotube reinforced biodegradable nanocomposites using noncrosslinked and malonic acid crosslinked polyvinyl alcohol. Compos Part A-Appl S 2012; Sumbmitted.

[25] Iguchi M, Yamanaka S, Budhiono A. Bacterial cellulose - a masterpiece of Nature's arts. J Mater Sci 2000; 35(2): 261-270.

[26] Baeckdahl H, Helenius G, Bodin A, Nannmark U, Johansson BR, Risberg B, Gatenholm P. Mechanical properties of bacterial cellulose and interactions with smooth muscle cells. Biomaterials 2006; 27(9): 2141-2149.

[27] Klemm D, Schumann D, Udhardt U, Marsch S. Bacterial synthesized cellulose - artificial blood vessels for microsurgery. Prog Polym Sci 2001; 26(9): 1561-1603.

[28] Klemm D, Heublein B, Fink HP, Bohn A. Cellulose: Fascinating biopolymer and sustainable raw material. Angew Chem Int Ed 2005; 44(22): 3358-3393.

[29] Fink HP, Weigel P, Purz HJ, Ganster J. Structure formation of regenerated cellulose materials from NMMO-solutions. Prog Polym Sci 2001; 26(9): 1473-1524.

[30] Wan Y, Hong L, Jia S, Huang Y, Zhu Y, Wang Y, Jiang H. Synthesis and characterization of hydroxyapatite - bacterial cellulose nanocomposites. Compos Sci Technol 2006; 66(11-12): 1825-1832.

[31] Fontana JD, De Souza, AM, Fontana CK, Torriani IL, Moreschi JC, Gallotti BJ, De Souza, SJ, Narcisco GP, Bichara JA, Farah LFX. Acetobacter cellulose pellicle as a temporary skin substitute. Appl Biochem Biotechnol 1990; 24-25: 253-264.

[32] Shibazaki H, Kuga S, Onabe F, Usuda M. Bacterial cellulose membrane as separation medium. J Appl Polym Sci 1993; 50(6): 965-969.

[33] Svensson A, Nicklasson E, Harrah T, Panilaitis B, Kaplan DL, Brittberg M, Gatenholm P. Bacterial cellulose as a potential scaffold for tissue engineering of cartilage. Biomaterials 2005; 26(4): 419-431.

[34] Westland JA (Bothell, WA), Stephens SR (Auburn, WA), Johnston Jr., WC (Puyallup, WA), Rosenkrans HJ (Seattle, WA). Bacterial cellulose binding agent. United States, Weyerhaeuser Company (Tacoma, WA) 1993; 5207826. http://www.freepatentsonline.com/5207826.html. Accessed June 2011

[35] Dobre LM, Stoica-Guzun A, Stroescu M, Jipa IM, Dobre T, Ferdeş M, Ciumpiliac Ş. Modeling of sorbic acid diffusion through bacterial cellulose-based antimicrobial films. Chem Pap 2012; 66 (2): 144-151.

[36] Mart ńez-Sanz M, Lopez-Rubio A, Lagaron JM.. Optimization of the nanofabrication by acid hydrolysis of bacterial cellulose nanowhiskers. Carbohyd Polym 2011; 85: 228-236.

[37] Mart ńez-Sanz M, Okson RT, Lopez-Rubio A, Lagaron JM. Development of electrospun EVOH fibers reinforced with bacterial cellulose nanowhiskers. Part I: characterization and method optimization. Cellulose 2011; 18: 335-347.

[38] Park WI, Kang M, Kim HS, Jin HJ. Electrospinning of poly(ethylene oxide) with bacterial cellulose whiskers. Macromol Symp 2007; 249-250 (1): 289-294.

[39] Nakagaito AN, Yano H. The effect of fiber content on the mechanical and thermal expansion properties of biocomposites based on microfibrillated cellulose. Cellulose 2008, 15: 555-559.

[40] Nakagaito AN, Fujimura A, Sakai T, Hama Y, Yano H. Production of microfibrillated cellulose (MFC)-reinforced polylactic acid (PLA) nanocomposites from sheets obtained by a papermaking-like process. Compos Sci Technol 2009; 69:1293-1297.

[41] Zou Y, Hsieh J. Review of microfibrillated cellulose for papermaking. http://www.tappi.org/Downloads/Conference-Papers/2007/07NAN/07NAN18.aspx, 2007, Accessed November 2011.

[42] Huang X, Netravali AN. Biodegradable green composites made using bamboo micro/nano-fibrils and chemically modified soy protein resin. Compos Sci Technol 2009; 69: 1009-1015.

[43] Stenstad P, Andresen M, Tanem BS, Stenius P. Chemical surface modifications of microfibrillated cellulose. Cellulose 2008, 15: 35-45.

[44] Nakagaito AN, Yano H. The effect of morphological changes from pulp fiber towards nano-scale fibrillated cellulose on the mechanical properties of high-strength plant fiber based composites. Appl Phys A-Mater 2004; 78: 547-552.

[45] Nakagaito AN, Yano H. Novel high-strength biocomposites based on microfibrillated cellulose having nano-order-unit web-like network structure. Appl Phys A-Mater 2005; 80: 155-159.

[46] Nakagaito AN, Iwamoto S, Yano H. Bacterial cellulose: the ultimate nano-scalar cellulose morphology for the production of high-strength composites. Appl Phys A-Mater 2005; 80: 93-97.

[47] Liu M, Guo B, Du M, Jia D. Drying induced aggregation of halloysite nanotubes in polyvinyl alcohol/halloysite nanotubes solution and its effect on properties of composite film. Appl Phys A-Mater 2007; 88: 391-395.

[48] Joussein E, Petit S, Churchman J, Theng B, Righi D, Delvaux B. Halloysite clay minerals-a review. Clay Miner 2005; 40: 383-426.

[49] Rathi P. Soy protein based nanophase reins for green composites. Ithaca, NY: A project report, Cornell University 2007. p. 13-18.

[50] Endres JG. Soy protein products: Characteristics, nutritional aspects and utilization (revised and expanded Ed). Champaign, Illinois: AOCS Press 2001. p. 4-18.

[51] Martin H, Laswai H, Kulwa K. Nutrient content and acceptability of soybean based complementary food. Afr J Food Agric Nutr Dev 2010; 10(1): 2040-2049.

[52] Kim JT, Netravali AN. Mechanical, thermal, and interfacial properties of green composites with ramie fiber and soy resins. J Agric Food Chem 2010; 58:5400-5407.

[53] Solaro R, Corti A, Chiellini E. Biodegradation of poly (vinyl alcohol) with different molecular weight and degree of hydrolysis. Polym Adv Technol 2000; 11 (8-12): 873-878.

[54] Chiellini E, Corti A, D'Antone S, Solaro R. Biodegradation of poly (vinyl alcohol) based materials. Prog Polym Sci 2003; 28: 963-1014.

[55] Hong F, Qiu K. An alternative carbon source from konjac powder for enhancing production of bacterial cellulose in static cultures by a model strain *Acetobacter aceti subsp. xylinus* ATCC 23770. Carbohyd Polym 2008; 72 (3): 545-549.

[56] Saddler JN, Gregg DJ. Ethanol production from the forest product waste. In*:* Bruce A, Palfreyman JW. Forest product biotechnology. London: Taylor & Francis Ltd. 1998. p. 183-195.

[57] Ramana KV, Tomar A, Singh L. Effect of various carbon and nitrogen sources on cellulose synthesis by *Acetobacter xylinum*. World J Microbiol Biotechnol 2000; 16: 245-248.

[58] Tarr HLA, Hibbert H. Studies on reactions relating to carbohydrates and polysaccharides. XXXV. Polysaccharides synthesis by the action of *Acetobacter xylinus* on carbohydrates and related compounds. Can J Res 1931; 4: 372-388.

[59] Kaushal R, Walker TK. Formation of cellulose by certain species of *Acetobacter*. Biochem J 1951; 48: 618-621.

[60] Ishihara M, Matsunaga M, Hayashi N, Tišler V. Utilization of d-xylose as carbon source for production of bacterial cellulose. Enzyme Microb Technol 2002; 31 (7): 986-991.

[61] Hestrin S, Schramm M. Synthesis of cellulose by *Acetobacter xylinum*. Biochem J 1954; 58: 345-352.

[62] Keshk S, Sameshima K. The utilization of sugar cane molasses with/without the presence of lignosulfonate for the production of bacterial cellulose. Appl Microbiol and Biotechnol 2006; 72 (2): 291-296.

[63] Keshk S, Razek T, Sameshima K. Bacterial cellulose production from beet molasses. Afr J Biotechnol 2006; 5(17): 1519-1523.

[64] Goelzer FDE, Faria-Tischer PCS, Vitorino JC, Sierakowski Maria-R, Tischer CA. Production and characterization of nanospheres of bacterial cellulose from Acetobacter xylinum from processed rice bark. Mater Sci Eng C 2009; 29(2): 546-551.

[65] Giannoccaro E, Wang Y J, Chen P. Comparison of two HPLC systems and an enzymatic method for quantification of soybean sugars. Food Chem 2008; 106: 324-330.

[66] Yang YK, Park SH, Hwang JW, Pyun YR, Kim YS. Cellulose production by *Acetobacter xylinum* BRC5 under agitated conditions. J Ferment Bioeng 1998; 85(3): 312-317.

[67] Wang YC, Yu RC, Yang HY, Chou CC. Sugar and acid contents in soymilk fermented with lactic acid bacteria alone or simultaneously with bifidobacteria. Food Microbiol 2003; 20(3): 333-338.

[68] Alexandre M, Dubois P. Polymer layered silicate nanocomposites: preparation, properties and use of a new class of materials. Mater Sci Eng R: Rep 2000; 28: 1-63.

[69] Bordes P, Pollet E, Averous L. Nano-biocomposites: biodegradable polyester/nanoclay systems. Pro Polym Sci 2009; 34: 125-155.

[70] Pavlidoua S, Papaspyrides CD. A review on polymer-layered silicate nanocomposites. Prog Polym Sci 2008; 33: 1119-1198.

[71] Thermo Scientific. Thermo scientific pierce-crosslinking technical handbook, http://www.piercenet.com/files/1601673_Crosslink_HB_Intl.pdf, Accessed November 2011.

[72]. Yeom CK, Lee KH. Pervaporation speration of water-acetic acid mixtures through poly (vinyl alcohol) membranes crosslinked with glutaraldehyde. J Membrane Sci 1996; 109: 257-265.

[73] Zhang Y, Zhu PC, Edgren D. Crosslinking reaction of poly(vinyl alcohol) with glyoxal. J Polym Res 2010; 17 (5): 725-730.

[74] BASF. Glyoxal as a cellulose crosslinker. http://www.intermediates.basf.com/chemicals/glyoxal/crosslinker-for-cellulose, Accessed November 2011.

[75] Chabba S, Matthews GF, Netravali AN. 'Green' composites using crosslinked soy flour and flax yarns. Green Chem 2005; 7 (8): 576-581.

[76] Gent AN. Engineering with rubber: how to design rubber component (2nd Ed.) Munich; Hanser; Cincinatti: Hanser Gardner 2001; p. 19-29.

[77] Khan MA, Bhattacharia SK, Kader MA, Bahari K. Preparation and characterization of ultra

violet (UV) radiation cured bio-degradable films of sago starch/PVA blend. Carbohyd Polym 2006; 63 (4): 500-506.

[78] McCaig MS, Paul DR. Effect of UV crosslinking and physical aging on the gas permeability of thin glassy polyarylate films. Polymer 1999; 40 (26): 7209-7225.

[79] Huang X. Preparation and investigation of soy protein based environmentally friendly plastics and composites. Ithaca, NY: PhD dissertation, Cornell University 2007; p. 18-41.

[80] MSDS. http://www.msdsonline.com, Accessed November 2011.

[81] Weiner N. Malonic acid. Org Synth 1943; Collective 2: 376.

[82] Jian S, Ming SX. Crosslinked PVA-PS thin-film composite membrane for reverse osmosis. Desalination 1987; 62: 395-403.

[83] Majumdar S, Adhikari B. Polyvinyl alcohol: A taste sensing material. Sensors Actuators B-Chem 2006; 114: 747-755.

[84] Zammarano M, Krämer RH, Harris R, Ohlemiller TJ, Shields JR, Rahatekar SS, Lacerda S, Gilman JW. Flammability reduction of flexible polyurethane foams via carbon nanofiber network formation. Polym Adv Technol 2008; 19: 588-595.

[85] Morgan AB, Gilman W. Characterization of polymer layered silicate (clay) nanocomposites by transmission electron microscopy and X-ray diffraction. J Appl Polym Sci 2003; 87: 1329-1338.

[86] Li YC, Schulz J, Mannen S, Delhom C, Condon B, Chang SC, Zammarano M, Grunlan JC. Flame retardant behavior of polyelectrolyte-clay thin film assembiles on cotton fabric. ACS Nano 2010; 4 (6): 3325-2227.

[87] Zammarano M, Maupin PH, Sung LP, Gilman JW, McCarthy ED, Kim YS, Fox DM. Revealing the interface in polymer nancomposites. ACS Nano 2011; 4 (4): 3391-3399.

[88] Bohlmann GM. General characteristics, processability, industrial applications and market evolution of biodegradable polymers. In: Bastioli C. Handbook of biodegradable polymers. Shawbury, UK: Rapra Tech Ltd 2005. p. 183-218.

[89] Lemm W, Krukenberg T, Regier G, Gerlach K, Bucherl ES. Biodegrdation of some biomaterials after subcutaneous implantation. Proc Eur Sco Artif Org 1981; 8:71-75.

[90] Potts JE, Clendinning RA, Ackart WB, Neigisch WD. The biodegradability of synthetic polymers. In; Guillet J. Polymers and ecological problems. New York: Plenum Press 1973. p. 61-80.

[91] Swift G. Biodegrdable polymers in the environment: are they really biodegradable? Pro ACS Div Polym Mater Sci Eng 1992; 66: 403-404.

[92] Ratner BC, Gladhill KW, Horbett TA. Analysis of *in vitro* enzymatic and oxidative degradation of polyurethane. J Biome Mater Res 1988; 22: 509-527.

[93] Hergenrother RW, Wabers HD, Cooper SL. The effect of chain extenders and stabilizers on the in vivo stability of polyurethanes. J Appl Biomater 1992; 3: 17-22.

[94] Reich L, Stivala SS. Elements of polymer degradation. New York: McGraw-Hill 1971.

[95] Kronenthal RL. Biodegradable polymers in medicine and surgery. In: Kronenthal RL, Oser Z, Martin E. Polymers in medicine and surgery. New York: Plenum Press 1975. p. 119-133.

[96] Gilding DK. Biodegradable polymers. In: Williams DF. Biocompatibility of clinic implant materials. Boca Raton, FL: CRC Press 1981. p. 209-232.

[97] Tokiwa Y, Suzuki T. Hydrolysis of polyesters by rhizopus delemar lipase. Agric Biol Chem 1978; 42: 1071-1072.

[98] Tokiwa Y, Suzuki T. Hydrolysis of copolyesters containing aromatic and aliphatic ester blocks by lipase. J Appl Polym Sci 1981; 26: 441-448.

[99] Tokiwa Y, Suzuki, T, Ando T. Synthesis of copolyamide-esters and some aspects involved in their hydrolysis by lipase. J Appl Polym Sci 1979; 24: 1701-1711.

[100] Tokiwa Y, Calabia BP, Ugwu CU, Aiba S. Biodegradability of plastics. Int J Mol Sci 2009; 10: 3722-3742.

[101] Cho Daehwan, Netravali AN, Joo YL. Mechanical properties and biodegradability of electronspun soy protein isolate/PVA hybrid nanofibers. Polym Degrad Stab 2012; 97: 747-754.

[102] Luo S, Netravali AN. A study of physical and mechanical properties of poly(hydroxybutyrate-co-hydroxyvalerate) during composting. Polym Degrad Stab 2003; 80: 59-66.

[103] Lodha P, Netravali AN. Effect of soy protein isolate resin modifications on their biodegradation in a compost medium. Polym Degrad Stab 2005; 87: 465-477.

[104] Corti A, Solaro R, Chiellini E. Biodegradation of poly (vinyl alcohol) in selected mixed microbial culture and relevant culture filtrate. Polym Degrad Stab 2002; 75 (3): 447-458.

[105] Lodha P. Fundamental approaches to improving performance of soy protein isolate based 'green' plastics and composites. Ithaca, NY: PhD Dissertation, Cornell University 2004; p. 101-129.

[106] Semenov SA, Gumargalieva KZ, Zaikov GE. Biodegrdation and durability of materials under the effect of microorganisms. Boston, MA: VSP BV, 2003.

[107] Han SI, Lim JS, Kim DK, Kim MN, Im SS. In situ polymerized poly (butylene succinate)/silica nancomposites: physical properties and biodegradation. Polym Degrad Stab 2008; 93: 889-895.

[108] Yang HS, Yoon JS, Kim MN. Dependence of biodegradability of plastics in compost on the shape of specimens. Polym Degrad Sta 2005; 87: 131-135.

[109] Ray SS, Okamoto M. Biodegradable polylactide and its nancomposites; opening a new dimension for plastics and composites. Macromol Rap Comm 2003; 24: 815-840.

[110] Fukuda N, Tsuji H, Ohnishi Y. Physical properties and enzymatic hydrolysis of poly (-latide)-$CaCO_3$ composites. Polym Degrad Stab 2002; 78, 119-127.

[111] Quynh TM, Mitomo H, Nagasawa N, Wada Y, Yoshii F, Tamada M. Properties of crosslinked polylactides (PLLA & PDLA) by radation and its biodegradability. Euro Polym J 2007; 43: 1779-1785.

[112] Solaro R, Corti A, Chiellini E. Biodegradation of poly (vinyl alcohol) with different molecular weight and degree of hydrolysis. Polym Adv Technol 2000; 11 (8-12): 873-878.

[113] Watanabe Y, Morita M, Hamada N, Tsujisaka Y. Formation of hydrogen peroxide by a polyvinyl alcohol degrading enzyme. Agric Biol Chem 1975; 39: 2447-2448.

[114] Suzuki T, Ichihara Y, Yamada M, Tonomura K. Some characteristics of *Pesudomonas* O-3 which utilize polyvinyl alcohol. Agric Biol Chem 1973; 37: 747-756.

[115] Sakai K, Hamada N, Watanabe Y. Studies on the poly(vinyl alcohol)-degrading enzyme. Part VI. Degradation mechanism of poly(vinyl alcohol) by successive reactions of secondary alcohol oxidase and β-diketone hydrolase from *Pseudomonas* sp. Agric Biol Chem 1986; 50: 989-996.

[116] Jecu L, Grosu E, Raut I, Ghiurea M, Constantin M, Stoica A, Stroescu M, Vasilescu G. Fungal degradation of polymeric materials: morphological aspects. http://www.inginerie-electrica.ro/acqu/2011/P_1_Fungal_degradation_of_polymeric_materials_Morfological_aspects.pdf. Accessed 2012.

[117] Larking DM, Crawford RJ, Christie GBY, Lonergan GT. Enhanced degradation of polyvinyl alcohol by *Pysnoporus cinnabarinus* after pretreatment with Fenton's reagent. Appl Environ Microbiol 1999; 65 (4): 1798-1800.

[118] Chiellini E, Corti A, Solaro R. Biodegradation of poly (vinyl alcohol) based blown films under different environmental conditions. Polym Degrad Stab 1999; 64: 305-312.

[119] Jayasekara R, Harding I, Bowater I, Christie GBY, Lonergan GT. Biodegradation by composting of surface modified starch and PVA blended films. J Polym Environ 2003; 11 (2): 49-56.

[120] Solaro R, Corti A, Chiellini E. A new respirometric test simulating soil burial conditions for the evaluation of polymer biodegradation. J Environ Polym Degrad 1998; 6: 203-208.

[121] Matsumura S, Tanaka T. Novel malonate-type copolymers containing vinyl alcohol blocks as biodegradable segments and their builder performance in detergent formulation. J Environ Polym Degrad 1994; 2: 89-97.

[122] Diaz LF, Savage GM, Eggerth LI, Golueke CG. Composting and recycling-municipal solid waste. Boca Raton, FL: Lewis Publishers, 1993.

[123] Tensile property testing of plastics - MatWeb

http://www.matweb.com/reference/tensilestrength.aspx. Accessed June 2011

[124] Netravali AN, Qiu K. Bacterial Cellulose Based 'Green' Composites. International patent 2010; International Publication No.: WO 2010/135234 A2.

Chapter 2 'Green' composites based on bacterial cellulose produced using novel low cost carbon source and soy protein resin

Kaiyan Qiu, Anil N. Netravali*
Fiber Science Program, Cornell University, Ithaca, NY 14853-4401

2.1 Abstract

A novel low cost carbon source, soy flour extract (SFE), was developed from defatted soy flour (SF) to culture bacterial cellulose (BC). The enriched protein remaining after extracting sugars was used as resin to form BC based thin membrane-like 'green' composites. The results of this study showed that SFE consists of five sugars; fructose, glucose, sucrose, raffinose and stachyose. Further the study indicated that *Acetobacter xylinum*, the bacteria used in this study, metabolized sugars in the following order: fructose and glucose, sucrose, raffinose and stachyose during the culture process. However, the consumption rates of raffinose and stachyose were extremely low. Results also indicated that autoclaving process resulted in hydrolyzing sucrose to fructose and glucose. Based on the same concentration of sugars, BC yield achieved using SFE medium (based only on the concentration of fructose, glucose and sucrose) was close to or even higher than the yields obtained using expensive conventional carbon sources such as fructose, mannitol and glucose. Modified soy four (MSF), the residual protein after removing sugars from SF, was successfully used as a resin to fabricate 'green' BC-MSF membrane-like thin composites. These composites had excellent tensile and thermal properties that were better than the BC-SF resin composites. This is primarily due to the higher protein content in MSF compared to SF. The sugars in SF also plasticized it thus reducing its modulus and increasing the fracture strain.

Keywords:

Acetobacter xylinum; bacterial cellulose; low-cost carbon source; soy flour extract; BC-MSF resin 'green' composite

2.2 Introduction

Bacterial cellulose (BC) produced by *Acetobacter xylinum*, is a promising, sustainable and biodegradable nanofibrous material that has the same chemical structure as the plant-based cellulose. However, BC fibers have diameters in the range of a few nanometers and display many unique characteristics including high purity, high degree of polymerization, high crystallinity, high tensile strength, high modulus and strong biological adaptability [1-5]. The BC material is already being used in many applications including artificial skin and blood vessel, binding agent for fibers and other materials, loud speaker diaphragms, high quality paper, foods, textiles, composite membranes, etc. [5-10]. Many pure sugars such as glucose, sucrose, fructose, etc. and sugar alcohols such as mannitol, xylitol, sorbitol, etc. have been used as carbon source for BC culture [11-15]. Among them glucose, fructose and mannitol are the most common and have shown excellent results in terms of BC production [11-17]. However, cost of these sugars or sugar alcohols is high and hence they are not considered to be ideal for large scale, inexpensive BC production. As a result, many attempts have been made to obtain higher BC yields as well as to reduce the cost of the carbon sources. Some of these efforts have been successful. For example, konjac powder hydrolyzate [11], sugarcane molasses [18], beet molasses [19] and processed rice bark [20] have been found to be useful in BC production. While some of these sources may be used for industrial BC production in the near future, there is significant scope to further reduce the cost of BC production by using inexpensive waste

products and expand its use in many mass volume applications. This paper describes a novel and inexpensive source derived from soybeans for BC production.

Defatted soy flour (SF) is obtained as a by-product after extracting oil from the soybeans. It is commercially available and consists mainly of protein (52-54%), sugars (30-32%), dietary fiber (2-3%), minerals and ash (3-6%) and moisture (6-8%). SF is also very inexpensive, about $0.25/lb. The soybean is a legume species native to East Asia and is classified as an oilseed. It is an annual and economic crop and has been abundantly produced and used in many countries for over 5,000 years [21]. Currently, it is an important global crop and provides major amount of edible oil and protein [22]. Soybeans contain decent amount of sugars, including fructose, glucose, sucrose, raffinose and stachyose [23]. Fructose, glucose and sucrose have been used routinely as carbon sources for BC production [24]. It has also been reported that raffinose and stachyose can be metabolized by lactic acid bacteria [25]. To obtain higher protein content from SF, the sugars are removed in the form of soy flour extract (SFE), a by-product. The present research discusses the use of SFE, a mixture of five sugars mentioned earlier, as an inexpensive carbon source to produce BC.

Because of excellent mechanical properties of BC, some research on fabrication of BC based composites with petroleum based resins has already been reported [26, 27]. High strength composites using BC sheet impregnated with phenolic resin or acrylic resin have been developed [24, 25]. Although useful, these resins are not biodegradable and as a result, composites are not biodegradable or environment-friendly. It should, however, be possible to fabricate completely degradable BC based ‘green’ composites using sustainable and biodegradable resins.

As mentioned earlier, SF contains sugars and protein. It is possible to dissolve and extract water soluble sugars from SF, termed as soy flour extract (SFE). After removing SFE, the

residual protein product, termed as MSF, has higher protein content of 65-70%. MSF based resin has been shown to have better tensile properties than those of SF resin [28]. MSF resin also has higher interfacial bonding with ramie fiber compared to SF resin [28]. As a result, composites using MSF resin could be expected to have much better mechanical properties than those using SF resin.

In the present research the sugar-containing SFE has been successfully developed for BC production as a high-yield and low cost carbon source [29]. The consumption of different sugars by *Acetobacter xylinum* and the compositional changes of sugars in the SFE medium during autoclaving were analyzed as well. The residual insoluble protein, after SFE extraction, termed MSF, was successfully used as resin to fabricate BC based 'green' composite. Thus both fibers and resins were produced from defatted soy flour as the sole feedstock. The tensile and thermal properties of the composites were characterized and were found to be comparable or even better than those of traditional plastic materials.

2.3 Materials and methods

2.3.1 Microorganism and culture media

Acetobacter xylinum, ATCC 23769, obtained from the American Type Culture Collection (ATCC, Manassas, VA), was used as the model strain and maintained on agar plates containing 25 g/L D-mannitol, 5 g/L yeast extract and 5 g/L tryptone and 20 g/L agar. The SFE medium used for BC production consisted of 5 g/L yeast extract, 5 g/L tryptone and the autoclaved SFE as the sole carbon source [29]. Other culture media used for comparison of BC yields consisted of 25 g/L carbon sources raffinose, glucose, sucrose, fructose and mannitol, individually, and 5 g/L yeast extract and 5 g/L tryptone, which have the similar function for BC production as Hestrin–Schramm (HS) medium [17].

2.3.2 Soy flour powder treatment

The soy flour, SF, (7B) powder obtained from ADM Co. (Decatur, IL) was mixed with deionized water to get SFE. SF powder was initially soaked in deionized water in a ratio of 3:17 and the pH of the mixture was adjusted to 4.5, its isoelectric point, by adding hydrochloric acid. The mixture was kept at 50 ℃ in a water bath for 1 hr. After that, the mixture was filtered to remove the solid content (MSF), mostly the insolubilized protein. Part of the filtrate, containing the soluble sugars (SFE), was then allowed to evaporate to obtain the desired sugar concentration for BC culture [29].

2.3.3 Sugar consumption of SFE medium during culture

The concentrations of sugars in the SFE, including fructose, glucose, sucrose, raffinose and stachyose were determined before and after autoclaving using high performance liquid chromatography (HPLC) (UltiMate 3000 LC system, Dionex, Sunnyvale, CA) attached with the refractive index (RI) detector (RI-101, Ecom, Purage, Czech Republic). Autoclaving of the SFE was carried out at 121 ℃ and about 0.1 MPa pressure in a sterilizer (Market forge, Alfa Medical, Westbury, NY) for 25 min. After autoclaving, the SFE was filtered to remove the remaining solid protein deposits and used for BC culture. Sugar concentrations in the SFE during 10 days of culture were determined on a daily basis using HPLC to obtain a quantitative measure of the sugar consumption by the bacteria. After filtering the SFE culture media samples through a polytetrafluoroethylene (PTFE) filter (0.45 μm pore size) and removing tiny BC fibrils and other impurities, concentration for each sugar was analyzed using a SUPELCOSIL LC-NH_2 column (25 cm x 4.6 mm ID & 5 μm particles, Supelco, Bellefonte, PA) and the RI detector. The HPLC column was used at 30 ℃ temperature. The mobile phase was the mixture of acetonitrile and deionized water (3:1, v/v) and was kept at a flow rate of 1 mL/min. It is important to note that

while all sugar concentrations were determined individually, it was not possible to measure the fructose and glucose concentrations separately and hence was measured together and reported as 'fructose plus glucose' [29].

2.3.4 BC Production

The acetobacter strain was inoculated into a conical flask containing the prepared SFE culture medium as the seed culture. The initial pH value of the medium was adjusted to 5.0 and was not regulated during the culture. The seed culture was incubated at 30 ℃ and 130 rpm on a rotary shaker for 2 days, and 6 mL of this was inoculated into a 100 mL culture medium in 600 mL conical flask for production of BC. The cultivation was carried out initially at pH of 5.0 and 30 ℃ in a static incubator for 10 days. Samples of the culture medium and BC were extracted every day during the 10-day culture period to measure individual consumption of sugars and BC yields. The BC pellicles taken out from the medium were washed successively with water and 1% (w/v), aqueous NaOH at 90 ℃ for 15 min, and then washed by deionized water to remove all microbial product contaminants. The purified cellulose pellicles were finally dried at 105 ℃ on a Teflon® plate until constant weight was reached [29].

In another set of experiments BC pellicles produced using other culture media containing individual sugars mentioned in section 2.1 were harvested every day. The BC pellicles were then washed and dried using the same procedure mentioned earlier. BC pellicles cultured in SFE medium and other culture media mentioned in section 2.1 were compared for their yields. Dried BC specimens were conditioned at ASTM conditions of 21^{o}C and 65% relative humidity (RH) for 3 days before tensile testing [29].

2.3.5 Preparation of SF and MSF resin sheets

The SF powder and MSF obtained during SFE production were initially mixed with deionized water in a weight ratio of 1:15, respectively. Glycerol was added (15% by weight) as a plasticizer, pH value of both solutions were adjusted to 10 by addition of sodium hydroxide [22]. The solutions were maintained at 75 ℃ while stirring continuously for 30 min to obtain precured SF resin and MSF resin. This 'precuring' process helps denature the globular protein by opening up the molecules. Precured SF resin and MSF resin were cast on a Teflon® coated glass plate and dried in a 35 ℃ air circulated drying oven for 16 hr, respectively. Dried SF resin sheet and MSF resin sheet were cured using Carver Hydraulic hot press (model 3981-4PROA00, Wabash, IN) at 120^{o}C for 25 min under a pressure of 7 MPa. The thickness of all resin sheets was in the range of 0.2 mm. The cured SF and MSF resin sheets were conditioned at ASTM conditions for 3 days prior to characterizing their tensile properties.

2.3.6 Fabrication of BC based 'green' composites with SF and MSF resins

BC based membrane-like 'green' composites with SF resin and MSF resins were produced by using BC pellicles and impregnating them with precured SF and MSF resins, individually. Resin impregnation into the BC pellicle was achieved using ultrasonication for 30 min. The wet BC-SF and BC-MSF resin composites were dried in an air circulating oven at 35 ℃ for 8 hr to obtain prepregs. The BC content in the BC-SF resin composite and BC-MSF resin composite was kept around 50% in order to achieve tensile properties that are comparable to traditional non-biodegradable plastics. While the BC content in both composites could be easily adjusted by varying the resin concentration, it was difficult to obtain uniform distribution of resin with higher BC concentration. The prepregs were then cured by hot pressing at 120^{o}C under a pressure of 7 MPa. The thickness of all composites was in the range of 0.2 mm. The cured

composites were conditioned at ASTM conditions for 3 days prior to characterizing their tensile properties.

2.3.7 Characterization

Freeze dried specimens of BC and BC-MSF resin composites were sputter coated with gold and their surface topographies were observed with scanning electron microscope (SEM, LEO 1550 FESEM) at an accelerating voltage of 15 kV.

Tensile testing was performed using an Instron tensile testing machine (Instron, model 5566). The test specimens were prepared by cutting the BC membranes and green composites into 10 mm wide and 60 mm long strips using a precise cutter. Young's moduli of the specimens were determined from the tensile test results conducted according to ASTM D-882-02. Two ends of the specimens were placed between the upper and lower jaws of Instrton, leaving a gauge length of 30 mm. Crosshead speed during the tensile tests was maintained at 0.6 mm/min to obtain a strain rate of 0.02 min^{-1}.

Thermogravimetric analysis (TGA, TA instrument Model No. 2050) was carried out to analyze the thermal properties of both BC-SF and BC-MSF resin composites. TGA runs were performed using aluminum pans between 25 and 600^{o}C under nitrogen environment. The scanning rate was 20^{o}C/min and the nitrogen purge flow rate was maintained at 10 mL/min.

2.4 Results and discussion

2.4.1 Influence of autoclaving on the SFE medium

The HPLC analysis of the as obtained SFE used in this study showed that it consisted of 1.92 g/L fructose and glucose (combined), 21.21 g/L sucrose, 1.59 g/L raffinose, 11.92 g/L stachyose, water and other components including proteins. The concentration of total sugars was over 36 g/L. After autoclaving (sterilizing) at 121 ℃ and pressure of 0.1 MPa for 25 min, however, the

HPLC analysis showed a slightly different composition of sugars in the SFE medium. Therefore, the influence of autoclaving on the SFE medium was further explored.

It has been reported that sucrose is prone to partial hydrolysis during autoclaving and hence the sucrose-containing media sterilization will result in a mixture of D-glucose, D-fructose and sucrose [30]. In another study it was shown that 15 to 25% of the sucrose may hydrolyze to glucose and fructose during autoclaving at the elevated temperature [31, 32].

Table 2.1 presents the HPLC data of various sugar concentrations in SFE before and after autoclaving. Table 2.1 also gives adjusted values for all sugars after taking into consideration the water evaporation during autoclaving. Before autoclaving, the freshly made SFE medium had concentrations of 1.92 g/L for fructose plus glucose, 21.21 g/L for sucrose, 1.59 g/L for raffinose, and 11.92 g/L for stachyose. After the autoclaving the concentrations changed to 7.54 g/L for fructose plus glucose, 17.54 g/L for sucrose, 1.58 g/L for raffinose and 9.92 g/L for stachyose. The concentration of total sugars was 36.58 g/L and the concentration of three traditional carbon sources (fructose, glucose and sucrose) for BC production was approximately 23-25 g/L which was almost the same as the regular concentration of carbon source used for BC production by others [11]

Table 2.1 Effect of autoclaving on the concentrations of various sugars in the SFE medium

	Concentrations of sugars in SFE medium				
	Fructose + Glucose (g/L)	Sucrose (g/L)	Raffinose (g/L)	Stachyose (g/L)	Total Sugars (g/L)
SFE before autoclaving	1.92	21.21	1.59	11.92	36.64
SFE after autoclaving	7.54	17.54	1.58	9.92	36.58
SFE after autoclaving (adjusted data by considering water evaporation)	7.16	16.66	1.50	9.42	34.74

The data in Table 2.1 clearly indicate that there was a significant (about 20%) decrease in sucrose concentration and an almost equivalent increase in the fructose plus glucose concentration after autoclaving. As a result, there was no significant change in the combined concentration of fructose, glucose and sucrose which remained in the range of 23-25 g/L, before and after autoclaving. As discussed earlier, this was mainly due to the degradation of sucrose [30-32]. During the autoclaving process, our data also indicated a small decrease in the concentrations of both stachyose and raffinose (Table 2.1). While the reasons for this are not well understood, this may be either due to hydrolysis of raffinose and stachyose similar to that of sucrose, or due to side reactions such as caramelization or maillard reaction [33]. The splitting of sucrose into glucose and fructose is, in fact, better as it will be seen later that the *Acetobacter Xylinum* bacteria metabolize glucose and fructose much more easily than sucrose.

2.4.2 Sugar consumption in SFE medium during the culture

Our preliminary study had indicated that all five sugars in SFE, fructose, glucose, sucrose, raffinose and stachyose, could be used as carbon sources separately for BC culture by *Acetobacter xylinum* and different sugars had different effectiveness for BC yields. Detailed

discussion of this is presented later in this paper. To measure the actual consumption of individual sugars in the SFE culture medium, specimens were analyzed for the sugar content every day.

Figure 2.1 shows plots of changes in the concentrations of all five sugars as a function of culture time in days. As can be seen from the plots, fructose plus glucose concentration decreased steadily and almost linearly until day 7. During that period concentrations of the other three sugars remained more or less stable. After the sixth day the sucrose concentration started to decrease. This suggests that when fructose plus glucose concentration decreased to an extremely low value (around 1.09 g/L) from initial 7.54 g/L, the *Acetobacter xylinum* started to consume sucrose. These results indicate that the *Acetobacter xylinum* preferred to consume fructose and glucose before the other three sugars present in the SFE medium. During the entire 10-day culture time, very little or no raffinose and stachyose were consumed and, as a result, no significant change was noticed in their concentrations.

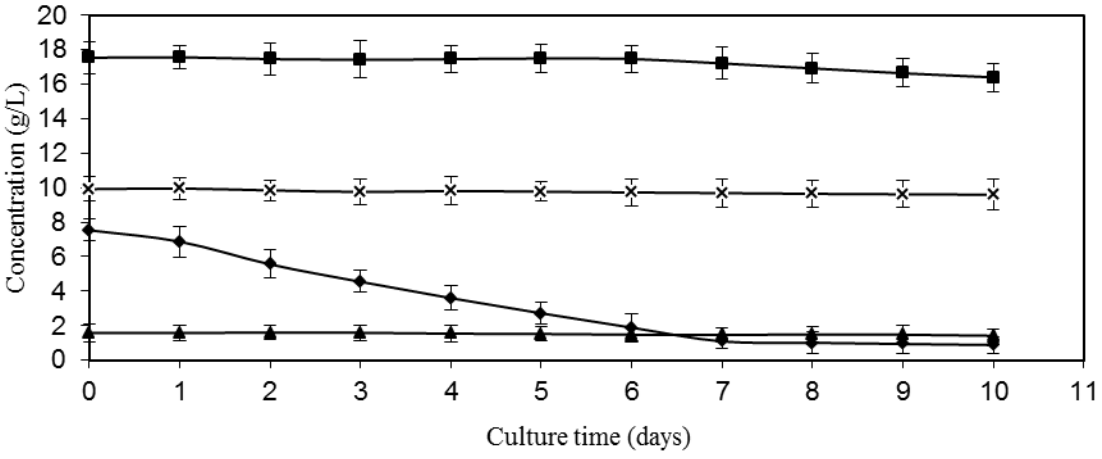

Figure 2.1 Consumption of sugars in SFE medium during BC culture by *Acetobacter xylinum* as a function of time in days
Symbols: ♦, fructose plus glucose; ■, sucrose; ▲, raffinose; ×, stachyose

2.4.3 BC yield in SFE medium

It has been reported that BC yield in fructose or glucose media was higher than in sucrose medium [24]. Based on our preliminary experiments, fructose and glucose were better carbon sources for BC production compared to a combination of sucrose, raffinose and stachyose, if the pH value of the media were kept constant. As mentioned earlier, after autoclaving, the concentration of fructose plus glucose in the SFE medium reached 7.54 g/L from the initial concentration of 1.92 g/L. This higher fructose plus glucose concentration was obviously beneficial for BC culture. It is important to note that the total concentration of the three sugars (fructose, glucose and sucrose) in the SFE medium, that *Acetobacter xylinum* mainly consumed during the 10-day culture, was around 25 g/L which was almost the same concentration of conventional carbon sources used by other researchers for BC production [11].

Figure 2.2 shows plots of BC yields in SFE (blue), fructose (brown), mannitol (green), glucose (purple) and sucrose (light blue) media as a function of culture time in days. As seen in Figure 2.2 BC yield in SFE medium increased dramatically during the initial 3-4 days and then the yield growth significantly decreased after 7 days of culture. The main reason for this was that the preferred carbon sources, fructose and glucose, were used up almost fully at this time. BC yield, however, continued to increase during the period of 7 to 10 days but with a relatively lower rate partially because *Acetobacter xylinum* started to consume sucrose and other sugars which were not as suitable or metabolizable as fructose and glucose for BC production. The results in Figure 2.2 also indicate BC yield in SFE medium can reach 255 mg after 10 days of culture which is close to or even better than BC yields obtained with other conventional carbon sources under similar culture conditions [34, 11]. According to comparison diagrams shown in Figure 2.2, BC yields in mannitol and fructose media have almost same diagrams as in SFE

medium at the beginning 7 days of culture. However, the BC yield rates in mannitol and fructose media were slightly higher than in SFE medium during the period of 7 to 10 days. This further confirms that preferred carbon sources, fructose and glucose were at low concentrations during this time. BC yields in glucose and sucrose media have diagrams with consistent lower values during culture time.

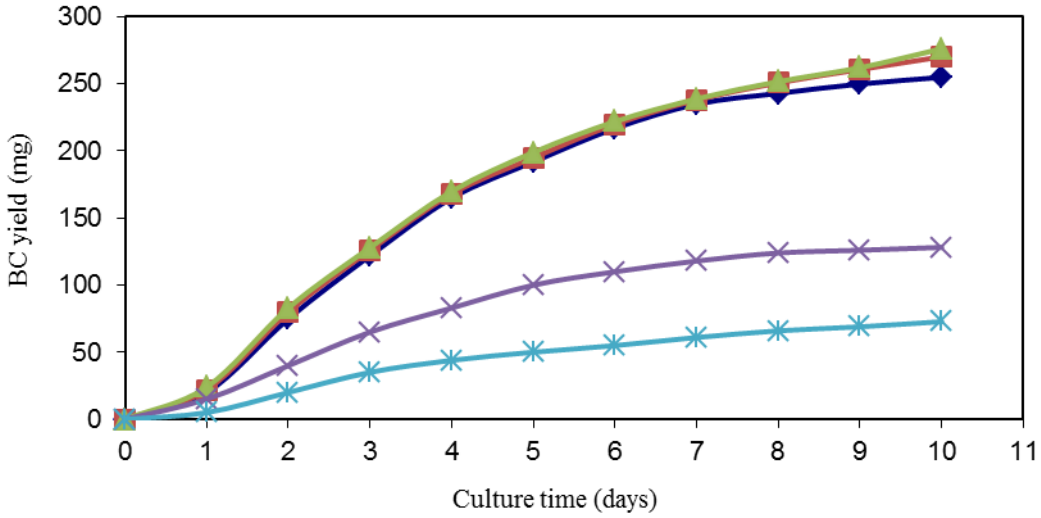

Figure 2.2 BC yields in SFE (♦), fructose (■), mannitol (▲), glucose (×) and sucrose (*) media as a function of culture time

Figure 2.3 compares BC yields obtained using different carbon sources individually after 10 days of culture. BC yield of 255 mg in SFE medium was almost as high as those using fructose (270.3 mg) and mannitol (276.3 mg) media which have been regarded as two excellent carbon sources for BC production. Based on these data it may be concluded that SFE could be used as an excellent but one of the least expensive carbon sources for BC production. BC yield in SFE medium was also significantly higher than those obtained in raffinose (29.7 mg), sucrose (72.8 mg) and glucose (128.2 mg) media, individually. Glucose has also been reported as an excellent carbon source for BC production [34]. However, in our trial carried out with pure glucose medium, under same conditions, the yield was lower because the pH value of the medium was

not regulated and gluconic acid generated by glucose during the culture caused the pH value to change to less than 3.5 which was not suitable for BC production. However, glucose in SFE medium still could be used as a good carbon source because pH value in SFE medium did not change significantly during the culture. The reason might be that relatively low amount of gluconic acid formed during culture was not able to change the pH of the medium. Also, other sugars present in SFE created a buffer effect in the SFE medium. Since sucrose partially hydrolyzed into glucose and fructose during autoclaving as seen in our results as well as by others [30-32], BC yield obtained in sucrose medium was from the combined presence of sucrose, fructose and glucose.

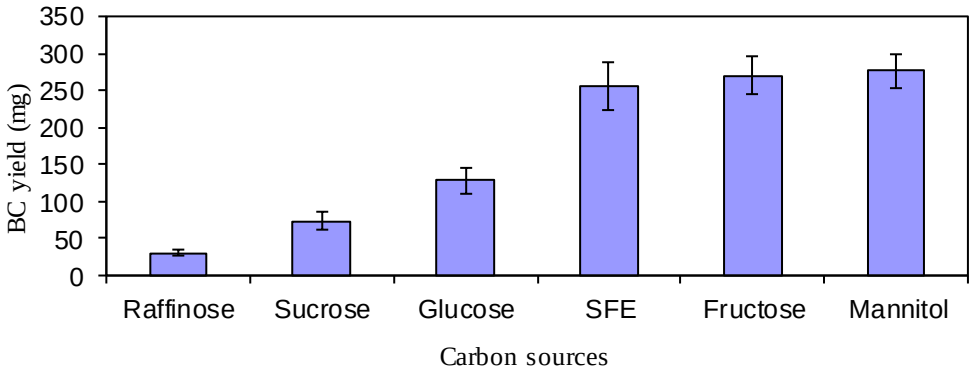

Figure 2.3 BC yields obtained for different carbon sources

The BC yield in SFE medium (255 mg) was also higher than previously reported BC yields obtained using konjac powder hydrolyzate (212 mg, *Acetobacter xylinum*-ATCC 23770, 8 days) and processed rice bark (242 mg, *Acetobacter xylinum*-ATCC 23769, 10 days) [11, 20].

In addition, the cost of carbon source, one of the major expenses for BC culture, is indeed reduced largely because the SFE is a by-product obtained from the soy protein production process. The cost of SFE is almost nothing. Therefore, based on rough calculation, the cost for BC production can be reduced by more than 30%.

2.4.4 Microstructure of BC-soy resin composite and its fabrication mechanism

The photographs of BC-SF resin and BC-MSF resin composites are shown in Figure 2.4A (a) and 2.4A (b), respectively. Both of these thin membrane-like composites had fairly smooth surfaces. This indicates that both SF resin and MSF resin are fully embedded into BC to fabricate corresponding composites.

Figure 2.4B shows SEM images of freeze dried BC pellicle and BC-MSF resin composite. Both specimens were not hot pressed prior to SEM observations. In Figure 2.4B (a), the BC network and porous structure can be observed clearly at the surface of the membrane. Since these specimens were freeze dried, the porous structure has been maintained. The mean diameter BC-nanofibers is less than 100 nm and the pore diameters range from several dozens to several hundred nanometers. Figure 2.4B (b) shows the structure of BC-MSF resin composite. MSF resin penetrated into the BC network structure and filled in most of pores of BC. Again, since the specimen was freeze dried, the porous structure was partially maintained. The spread of the MSF resin in between the BC-nanofibers and their embedment in the resin can be clearly seen. If this resin containing membrane is hot pressed, the gaps are fully filled as a result of the resin flow and consolidation, forming a thin membrane-like composite. The SEM of BC-SF resin composite and BC-MSF resin composite specimens shown in Figure 2.4B (a) and (b), respectively, look identical.

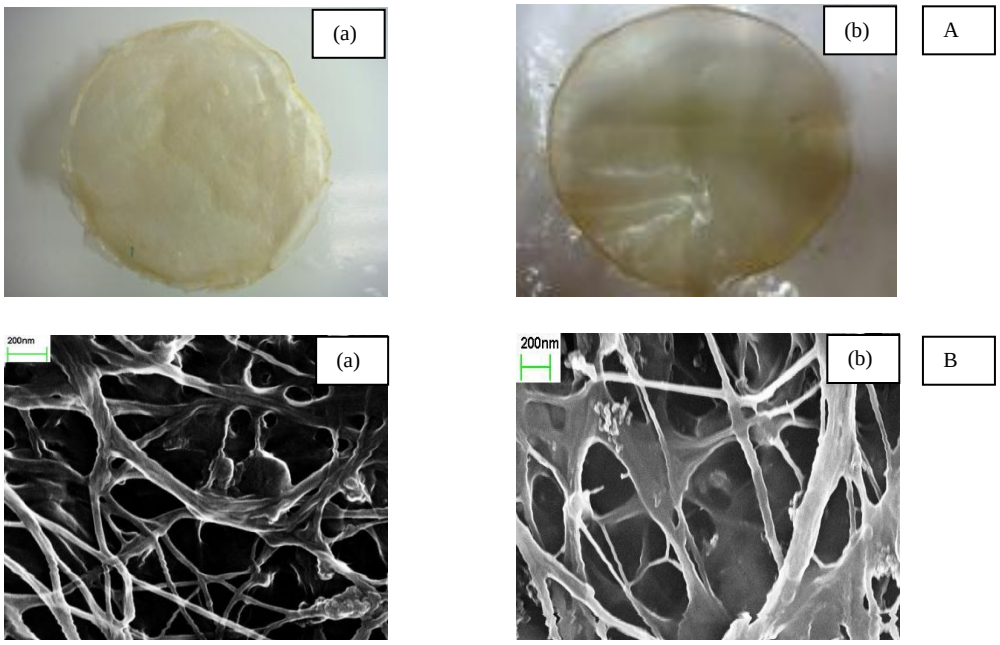

Figure 2.4 A: Images of (a) BC-SF resin composite and (b) BC-MSF resin composite;
B: SEM images of (a) freeze dried BC and (b) freeze dried BC-MSF resin composite

MSF resin infiltration into the BC pellicle is facilitated by the ultrasonication process. When the wet pellicle is immersed into the resin solution, there exists a big concentration difference between water inside of BC network structure and MSF resin outside of BC. The mass transfer was driven by the concentration gradient resulting in MSF resin penetrating into the BC network structure. Since BC is hydrophilic and the resin is water based, the diffusion is easy, though assisted by the ultrasonication. The equilibrium could be achieved until there is no concentration gradient between the resin inside of BC and outside of BC. Once the MSF resin infiltrates the BC pellicle the wet BC-MSF resin composite is achieved. It is then dried and hot pressed to form strong composite. This composite fabrication procedure was also used for SF resin as well.

2.4.5 Tensile properties of resins and green composites

Table 2.2 presents the tensile test results for BC, SF resin, MSF resin as well as BC-SF resin composites and BC-MSF resin composites. The soy resin content in both composites was around 50% by wt.

The Young's modulus value for BC with randomly organized and entangled nanofibers (Fig. 4B a) was 2493 MPa while the value for the MSF resin was 104.3 MPa. The Young's modulus values for BC-MSF resin composite was 1231 MPa which was between the modulus values of MSF resin and BC.

The tensile strength at the break of BC was 78.9 MPa and for MSF resin it was 8.1 MPa. The tensile strength value for BC-MSF resin composite was around 47.7 MPa, which was between those of BC and MSF resin.

Both the modulus and tensile strength values of BC-MSF resin composite are close or even higher than many traditional plastic materials, including polyethylene (modulus: 800 MPa; tensile strength: 15 MPa), polypropylene (modulus: 1900 MPa; tensile strength: 40 MPa), and Nylon 6 (modulus: 1800 MPa; tensile strength: 70 MPa) [35]. The BC-MSF resin composites may be easily protected from water by applying varnish or other water-resistant coatings to increase their durability. They have the potential to replace traditional non-biodegradable plastic materials in many applications, including racket frame, ski pole, circuit board, automobile inside etc.

It should be noted that the BC nanofiber Young's modulus has been estimated to be up to 78 GPa or even to 114 GPa [36, 37]. However, the nanofibers in the pellicles are not unidirectionally oriented but instead are highly entangled as a result of the random path travelled by the *Acetobacter xylinum* (Figure 2.4B (a)). Their strength, like the Young's modulus, is reduced significantly. This is reflected in the composite strength as well.

The fracture strain value for MSF resin was 23.4%, which was much higher than the value of 5.7% obtained for BC. The fracture strain of BC-MSF resin composite, however, was only 3.1%. Although the fracture strain is controlled by the BC, both BC and resin being hydrophilic in

nature, the fiber/resin bonding is expected to be good. Better bonding allows the resin to lock the fibers in place reducing the fracture strain of the composite.

The SF resin and BC-SF resin composites were fabricated and used for comparison. The results presented in Table 2.2 indicate that MSF resin and BC-MSF resin composites have higher Young's modulus and tensile strength than those of SF resin and BC-SF composites, respectively. The higher MSF resin properties are due to high protein content in the MSF resin compared to SF [28]. Also, the SF resin contains low molecular weight sugars (up to 35% by wt.) which plasticize the resin. As mentioned earlier these sugars were removed to obtain MSF. This is evident in the higher fracture strain and lower Young's modulus obtained for SF. The higher properties of the MSF resin get reflected in the BC-MSF composite properties as can be expected, though the difference of tensile properties between BC-MSF resin composites and BC-SF resin composites in the manuscript is not significant, only 5-10%. This is because the tensile values of MSF and SF resins are an order of magnitude lower than BC and both composites have 50 wt% BC content, the tensile values of the composites are dominated by BC properties. However, both experimental and theoretical values shown in Table 2.2 indicate BC-MSF resin composites have better tensile properties than BC-SF resin composites. This conclusion was further confirmed by composites with 10 wt% BC content for the two resins in our preliminary experiments.

Table 2.2 also presents theoretically calculated values for Young's modulus and tensile strength values calculated using the rule of mixture [38]. The densities of cellulose and soy resins were 1.52 g/cc and 1.30 g/cc, respectively [39], and the weight ratio of BC and resin is 1 to 1 in the composites. It is clear that the theoretical and experimental Young's modulus values are very close but the experimental strength values are slightly lower which is controlled by the defects in the specimens.

Table 2.2 Tensile properties of BC, MSF resin and BC-soy resin composites

	Young's modulus (MPa)	Theoretical Young's modulus (MPa)	Tensile strength (MPa)	Theoretical tensile strength (MPa)	Tensile strain (%)
BC	2493 (9.6)*		78.9 (13.7)		5.7 (17.5)
SF resin	62.3 (31.9)		7.5 (4.0)		110.7 (28.4)
MSF resin	104.3 (22.0)		8.1 (11.1)		23.4 (25.2)
BC-SF resin composite (50 wt% BC)	1178 (2.4)	1183	43.3 (5.3)	40.4	3.4 (2.9)
BC-MSF resin composite (50 wt% BC)	1231 (2.6)	1206	47.7 (9.3)	40.8	3.1 (41.9)

**: values in the parentheses are % coefficient of variation values.*

2.4.6 Thermal stability of BC-SF and BC-MSF resin composites

TGA studies were conducted to obtain information on the thermal decomposition behavior of BC-SF and BC-MSF resin composites. Figure 2.5 shows typical TGA thermograms obtained for the two composites. These curves confirm that the BC-MSF resin composite has better thermal stability than that of BC-SF resin composite as can be expected. The degradation temperature, T_d, for BC-SF resin composites was found to be around 205 ℃ compared the 220 ℃ obtained for BC-MSF composites. This was, again, due to the higher protein content in the MSF resin than that in SF resin after removing sugars. The sugars start to degrade at much earlier temperatures. Our preliminary experiments had shown that, fructose, glucose and sucrose start to degrade around 160 ℃, 170 ℃ and 200 ℃, respectively, much earlier than the degradation temperatures of proteins and cellulose. These results confirm that BC-MSF resin composite is thermally slightly more stable than the BC-SF resin composite and hence may be used at slightly higher temperatures or would be more durable at the same temperature.

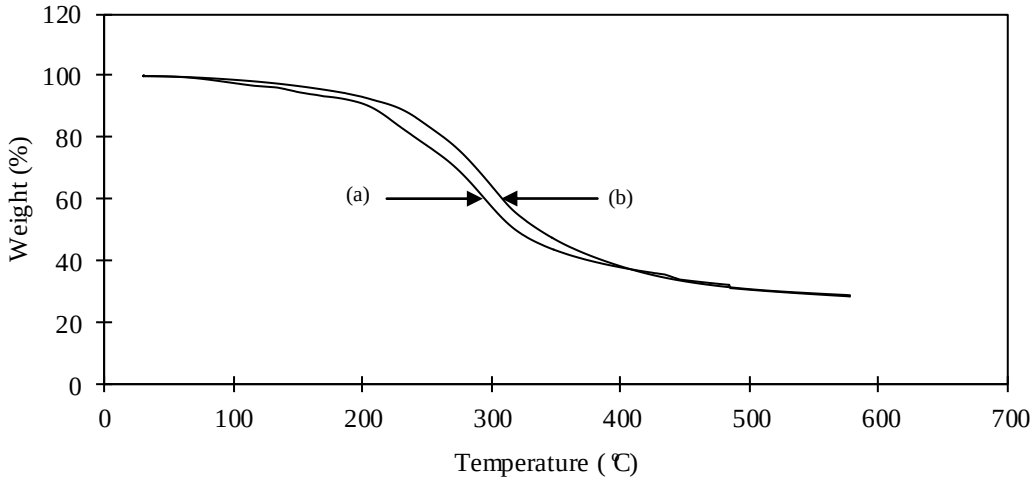

Figure 2.5 TGA of (a) BC-SF resin composite and (b) BC-MSF resin composite

2.5 Conclusions

The present study has shown for the first time that the SFE can be an excellent carbon source for BC production. The BC yield obtained with the new carbon source (SFE) was high and close to or even better than those obtained with other expensive conventional carbon sources. The cost of SFE carbon source can be very low because it is a by-product of soy flour processing and is produced in abundance throughout the world.

The study also showed that SFE contains at least five sugars and three of them, fructose, glucose and sucrose, can be utilized as an excellent carbon source for BC production. In addition, the study confirmed that autoclaving process can hydrolyze higher sugars in SFE.

The results further indicated that *Acetobacter xylinum* prefers to consume fructose and glucose before sucrose and other higher sugars such as raffinose and stachyose during the culture. Importantly, the results show that the rate of BC production is much higher when the concentration of fructose and glucose is high.

The study successfully developed membrane-like ‘green’ composites using BC produced by SFE and MSF resin produced by residual protein product after SFE extraction. BC-MSF resin composite showed better tensile and thermal properties than the BC-SF resin composite. These composites could provide a ‘green’ choice to replace many traditional plastic materials.

2.6 Acknowledgments

This work was partly supported by the National Textile Center (NTC) and the Wallace Foundation. The authors would like to thank Prof.s Dan Luo, Antje Baeumner and Jocelyn Rose of Cornell University for allowing the use of their facilities. We would also like to acknowledge Dr. Jun Tae Kim for his help in SFE process and useful discussions about the HPLC data.

References

[1] Iguchi M, Yamanaka S, Budhiono A. Bacterial cellulose - a masterpiece of Nature's arts. J Mater Sci 2000; 35(2): 261-270.

[2] Baeckdahl H, Helenius G, Bodin A, Nannmark U, Johansson BR, Risberg B, Gatenholm P. Mechanical properties of bacterial cellulose and interactions with smooth muscle cells. Biomaterials 2006; 27(9): 2141-2149.

[3] Klemm D, Schumann D, Udhardt U, Marsch S. Bacterial synthesized cellulose - artificial blood vessels for microsurgery. Prog Polym Sci 2001; 26(9): 1561-1603.

[4] Klemm D, Heublein B, Fink HP, Bohn A. Cellulose: Fascinating biopolymer and sustainable raw material. Angew Chem Int Ed 2005; 44(22): 3358-3393.

[5] Fink HP, Weigel P, Purz HJ, Ganster J. Structure formation of regenerated cellulose materials from NMMO-solutions. Prog Polym Sci 2001; 26(9): 1473-1524.

[6] Wan Y, Hong L, Jia S, Huang Y, Zhu Y, Wang Y, Jiang H. Synthesis and characterization of hydroxyapatite - bacterial cellulose nanocomposites. Compos Sci Technol 2006; 66(11-12): 1825-1832.

[7] Fontana JD, De Souza, AM, Fontana CK, Torriani IL, Moreschi JC, Gallotti BJ, De Souza, SJ, Narcisco GP, Bichara JA, Farah LFX. Acetobacter cellulose pellicle as a temporary skin substitute. Appl Biochem Biotechnol 1990; 24-25: 253-264.

[8] Shibazaki H, Kuga S, Onabe F, Usuda M. Bacterial cellulose membrane as separation medium. J Appl Polym Sci 1993; 50(6): 965-969.

[9] Svensson A, Nicklasson E, Harrah T, Panilaitis B, Kaplan DL, Brittberg M, Gatenholm P. Bacterial cellulose as a potential scaffold for tissue engineering of cartilage. Biomaterials 2005; 26(4): 419-431.

[10] Westland JA (Bothell, WA), Stephens SR (Auburn, WA), Johnston Jr., WC (Puyallup, WA), Rosenkrans HJ (Seattle, WA). Bacterial cellulose binding agent. United States, Weyerhaeuser Company (Tacoma, WA) 1993; 5207826. http://www.freepatentsonline.com/5207826.html. Accessed June 2011

[11] Hong F, Qiu K. An alternative carbon source from konjac powder for enhancing production of bacterial cellulose in static cultures by a model strain *Acetobacter aceti subsp. xylinus* ATCC 23770. Carbohyd Polym 2008; 72 (3): 545-549.

[12] Saddler JN, Gregg DJ. Ethanol production from the forest product waste. In*:* Bruce A, Palfreyman JW. Forest product biotechnology. London: Taylor & Francis Ltd. 1998. p. 183-195.

[13] Ramana KV, Tomar A, Singh L. Effect of various carbon and nitrogen sources on cellulose synthesis by *Acetobacter xylinum*. World J Microbiol Biotechnol 2000; 16: 245-248.

[14] Tarr HLA, Hibbert H. Studies on reactions relating to carbohydrates and polysaccharides. XXXV. Polysaccharides synthesis by the action of *Acetobacter xylinus* on carbohydrates and related compounds. Can J Res 1931; 4: 372-388.

[15] Kaushal R, Walker TK. Formation of cellulose by certain species of *Acetobacter*. Biochem J 1951; 48: 618-621.

[16] Ishihara M, Matsunaga M, Hayashi N, Tišler V. Utilization of d-xylose as carbon source for production of bacterial cellulose. Enzyme Microb Technol 2002; 31 (7): 986-991.

[17] Hestrin S, Schramm M. Synthesis of cellulose by *Acetobacter xylinum*. Biochem J 1954; 58: 345-352.

[18] Keshk S, Sameshima K. The utilization of sugar cane molasses with/without the presence of lignosulfonate for the production of bacterial cellulose. Appl Microbiol and Biotechnol 2006; 72 (2): 291-296.

[19] Keshk S, Razek T, Sameshima K. Bacterial cellulose production from beet molasses. Afr J Biotechnol 2006; 5(17): 1519-1523.

[20] Goelzer FDE, Faria-Tischer PCS, Vitorino JC, Sierakowski Maria-R, Tischer CA. Production and characterization of nanospheres of bacterial cellulose from Acetobacter xylinum from processed rice bark. Mater Sci Eng C 2009; 29(2): 546-551.

[21] Endres JG. Soy protein products: Characteristics, nutritional aspects and utilization (revised and expanded Ed). Champaign, Illinois: AOCS Press 2001. p. 4-18.

[22] Martin H, Laswai H, Kulwa K. Nutrient content and acceptability of soybean based complementary food. Afr J Food Agric Nutr Dev 2010; 10(1): 2040-2049.

[23] Giannoccaro E, Wang Y J, Chen P. Comparison of two HPLC systems and an enzymatic method for quantification of soybean sugars. Food Chem 2008; 106: 324-330.

[24] Yang YK, Park SH, Hwang JW, Pyun YR, Kim YS. Cellulose production by *Acetobacter xylinum* BRC5 under agitated conditions. J Ferment Bioeng 1998; 85(3): 312-317.

[25] Wang YC, Yu RC, Yang HY, Chou CC. Sugar and acid contents in soymilk fermented with lactic acid bacteria alone or simultaneously with bifidobacteria. Food Microbiol 2003; 20(3): 333-338.

[26] Nakagaito AN, Iwamoto S, Yano H. Bacterial cellulose: the ultimate nano-scalar cellulose morphology for the production of high-strength composites. Appl Phys A-Mater 2005; 80 (1): 93-97.

[27] Ifuku S, Nogi M, Abe K, Handa K, Nakatsubo F, Yano H. Surface Modification of Bacterial Cellulose Nanofibers for Property Enhancement of Optically Transparent Composites: Dependence on Acetyl-Group DS. Biomacromolecules, 2007; 8 (6): 1973-1978.

[28] Kim JT, Netravali AN. Mechanical, thermal, and interfacial properties of green composites with ramie fiber and soy resins. J Agric Food Chem 2010; 58: 5400-5407.

[29] Netravali AN, Qiu K. Bacterial Cellulose Based 'Green' Composites. International patent 2010; International Publication No.: WO 2010/135234 A2.

[30] Dobbs JH, Roberts LW. Experiments in plant tissue culture, 3rd edition. Cambridge, UK: Cambridge Press 1995. p. 53.

[31] Ball E. Hydrolysis of Sucrose by Autoclaving Media, a Neglected Aspect in the Technique of Culture of Plant Tissues. Bull Torrey Bot Club 1953; 80(5): 409-411.

[32] Schenk N, Hsiao KC, Bornman CH. Avoidance of precipitation and carbohydrate breakdown in autoclaved plant tissue culture media. Plant Cell Rep 1991; 10(3): 115-119.

[33] Berrios JDeJ, Morales P, Cámara M, Sánchez-Mata MC. Carbohydrate composition of raw and extruded pulse flours. Food Res Int 2010; 43: 531-536.

[34] Keshk S, Sameshima K. Evaluation of different carbon sources for bacterial cellulose production. Afr J Biotechnol 2005; 4(6): 478-482.

[35] Tensile property testing of plastics - MatWeb http://www.matweb.com/reference/tensilestrength.aspx. Accessed June 2011

[36] Guhados G,Wan W, Hutter JL. Measurement of the elastic modulus of single bacterial cellulose fibers using atomic force microscopy. Langmuir 2005; 21: 6642-6646.

[37] Hsieh YC, Yano H, Nogi M, Eichhorn SJ. An estimation of the Young's modulus of bacterial cellulose filaments. Cellulose 2008; 15: 507-513.

[38] Warner SB. Fiber Science. Upper Saddle River, NJ: Prentice Hall; 1995. p. 205-206.

[39] Lodha P. Fundamental approaches to improving performance of soy protein isolate based 'green' plastics and composites. Ithaca, NY: PhD Dissertation, Cornell University 2004; p. 101.

Chapter 3 Bacterial cellulose based membrane-like biodegradable composites using cross-linked and noncross-linked polyvinyl alcohol

Kaiyan Qiu, Anil N. Netravali*
Fiber Science Program, Cornell University, Ithaca, NY 14853-4401

3.1 Abstract

Bacterial cellulose (BC) based membrane-like biodegradable composites were produced by immersing wet BC pellicles in polyvinyl alcohol (PVA) solution. The BC content in the BC-PVA composites can be adjusted by varying the concentration of PVA solution. Chemical cross-linking of PVA was carried out using glutaraldehyde (GA) to increase the mechanical properties of the composites as well as to make the PVA partially to highly water-insoluble. Examination by scanning electron microscopy (SEM) indicated that the PVA not only penetrated the BC network, but also filled the pores within the BC pellicle. Attenuated total reflectance-Fourier transform infrared (ATR-FTIR) spectroscopy showed that acetal linkages could be formed in the BC-PVA composites by a cross-linking reaction. Sol-gel results indicated that cross-linking reaction increasingly made PVA insoluble in water resulting in higher gel (cross-linked fraction) content in the PVA. Wide-angle X-ray diffraction (WXRD) results showed decreased crystallinity in cross-linked BC and PVA, as was expected. It was also found that crystal size was smaller in PVA after cross-linking. The BC-PVA composites had excellent tensile properties and cross-linking increased these properties further. Thermogravimetric analysis (TGA) showed higher thermal stability for BC-PVA composites compared to PVA. The cross-linked specimens, especially the highly cross-linked ones, showed even higher thermal stability. The methods developed in this study make it possible to control the PVA content in the composites as well as the cross-linking level of PVA. These composites could be good candidates for replacing

traditional non-biodegradable plastics.

Keywords: Bacterial cellulose (BC); BC-poly (vinyl alcohol) (PVA) composite; Biodegradable composite; Cross-linking; Tensile properties; Thermal stability

3.2 Introduction

The past several decades have seen rapid development of advanced composites with excellent mechanical properties that have replaced metals in many applications. Most of these composites are made using petroleum-derived non-degradable fibers, such as carbon, aramid and polymers/resins such as polyetheretherketone (PEEK) and epoxy. These composites are difficult to recycle or reuse and hence pose a serious solid waste disposal problem due to decreasing landfill space, widespread litter and pollution of land, air and marine environments [1-3]. As a result, significant interest has been generated in developing fully biodegradable bio-based composites in the past few years [4-10].

Bacterial cellulose (BC) is a promising biodegradable green material with excellent potential as reinforcement for composites. BC is a specific cellulose primarily produced by *Acetobacter xylinum*, a Gram-negative, obligately aerobic bacterium, in a nutritional fermentation medium at 30 ℃. The medium requires carbon sources (mannitol, sucrose, fructose or others) and nitrogen sources (peptone, typtone, yeast extract, etc.), with optimum pH of 5.0. BC has the same chemical structure as other plant-based cellulose and is produced as fibers with diameters in the range of 70-90 nanometers. It displays many unique properties including higher purity, higher degree of polymerization, higher crystallinity, higher tensile strength and modulus and stronger biological adaptability [11-15]. The BC material is already being used in many applications

including artificial skin and blood vessels, binding agent for fibers and other materials, loud speaker diaphragms, high quality paper, foods, textiles, composite membranes, etc. [15-20].

Polyvinyl alcohol (PVA) is a thermoplastic, biocompatible, and biodegradable polymer. With hydroxyl groups in its structure, it is hydrophilic and expected to form hydrogen bonds and acetal linkages with other materials, such as cellulose and aldehydes [21, 22]. Therefore, BC-PVA is an excellent reinforcement and resin combination for fabricating biodegradable composites. BC-PVA based composites have been developed previously [21-25]. Hydrogen bonds formed between hydroxyl groups on BC and PVA have been shown to facilitate fabrication of homogenous composites [21]. However, BC content in those composites was low and as a result the properties were not ideal to replace most of the traditional plastic materials. If the desired mechanical properties are achieved, such composites can have great potential for applications as articular cartilage [22] and aortic heart valve prosthesis [23, 24].

Both cellulose and PVA have been studied in the past and shown to be fully biodegradable [26-28]. As a result, their composites made using the two are also biodegradable. However, biodegradation investigation experiments involving BC-PVA composites, particularly those using cross-linked PVA are currently ongoing in our lab and will be the subject of our next paper.

Research in chemical cross-linking of PVA and cellulose fabrics has been reported earlier [29-36]. PVA can be cross-linked using glutaraldehyde (GA) in the presence of a strong acid [29-34]. PVA contains hydroxyl groups that form acetal linkages with aldehyde groups in the GA [29-34]. Cotton fibers (cellulose) and cellulose nanofibers from softwood which are chemically identical have also been cross-linked using GA to modify their properties [35, 36]. Recently, some research for crosslinking bacterial cellulose and bacterial cellulose/fibrin using glyoxal or GA has also been reported [37, 38]. However, effects of cross-linking of membrane-

like BC-PVA composites have not been investigated yet.

In the present study, three types of thin membrane-like BC based biodegradable composites; BC-PVA composites and partially and highly cross-linked BC-PVA composites were developed and characterized. The BC content in these composites could be easily controlled as desired, by varying the concentration of PVA solution. A simple immersion method was used to cross-link the BC-PVA composites. Further, the extent of cross-linking could be controlled. The membrane-like composites prepared had smooth surfaces, and their tensile and thermal properties were excellent, especially those that were highly cross-linked.

3.3 Materials and methods

3.3.1 Microorganism and culture media

Acetobacter xylinum, ATCC 23769, obtained from the American Type Culture Collection (ATCC, Manassas, VA) was used as the model strain and maintained on agar plates containing 25 g/L D-mannitol, 5 g/L yeast extract and 5 g/L tryptone and 20 g/L agar. The mannitol culture medium used for BC production consisted of 25 g/L D-mannitol, 5 g/L yeast extract and 5 g/L tryptone.

3.3.2 Preparation of BC pellicles

The strain from the agar plate was inoculated into a conical flask containing mannitol culture medium as the seed culture. The initial pH value of the medium was adjusted to 5.0 and was not regulated during the culture. The seed culture was incubated at 30^{o}C and 130 rpm on a rotary shaker for 2 days, and 9 mL of this seed culture was inoculated into a 150-mL culture medium in 1000-mL conical flask for production of BC. The cultivation was carried out at initial pH 5.0 and 30^{o}C in a static incubator for 10 days. After incubation, the BC pellicles produced on the surface of mannitol culture medium were harvested and washed successively with water and 1%

(w/v), aqueous NaOH at 90^{o}C for 15 min, and then washed with deionized water to remove all microbial product contaminants and obtain purified pellicles.

3.3.3 Preparation of BC-PVA composites

PVA powder (M_w 31,000-50,000, 98-99% hydrolyzed, Aldrich, St. Louis, MO) was added to deionized water in 3.2 w/v% concentration, and the mixture was then stirred at 80^{o}C for 30 min to form the PVA solution. The purified BC pellicles were immersed into the PVA solution and kept in a water bath at 80^{o}C for 2 hr, and were then allowed to remain in the PVA solution at room temperature for 12 hr. The PVA containing BC pellicles were then transferred into deionized water for 30 min to remove superfluous PVA on the surface of the BC pellicles to obtain BC-PVA prepregs. The BC-PVA prepregs were dried on a Teflon® plate in an oven at 45^{o}C for 12 hr until the weights of the BC-PVA composites remained constant. The BC content in these composites was in the range of 50%. The percentage BC content mentioned in the manuscript has been calculated on dry weight basis. The BC-PVA composites with varying BC content could be obtained, if desired, by simply adjusting the concentration of the PVA solution. BC mass was weighed after removing PVA from the BC-PVA composites by hot water washing. BC content in the composites was calculated using PVA and BC dry weights. BC and PVA were prepared by drying BC pellicles and casting PVA solution as control, for comparison. All composites, BC and PVA specimens prepared in this study were thin, membrane-like. The PVA solution concentrations used and the resulting BC content obtained in BC-PVA composites are presented in Table 3.1.

Table 3.1 BC content in BC-PVA composites

Concentrations of PVA solution for BC pellicle treatment (w/v%)	BC content in BC-PVA composites (wt%)
1.5%	75 ±4
3.2%	50 ±4
6.0%	25 ±3

3.3.4 Preparation of cross-linked BC-PVA composites

Partially cross-linked BC-PVA composites were prepared by immersion method using GA-acetone solution. The BC-PVA composites with 50% BC content were initially immersed into the GA-acetone solution which contained 10% by volume GA solution (Glutaraldehyde, 25% solution in water, Aldrich, St. Louis, MO) and 90% by volume acetone (Mallinckrodt Baker, Phillipsburg, NJ). The pH of the GA-acetone solution was adjusted to around 1.0 by hydrochloric acid to trigger the cross-linking reaction. The reason for using acetone as a solvent was to prevent the PVA from dissolving in water during the cross-linking reaction [30]. After carrying the cross-linking reaction for 12 hr at room temperature, the partially cross-linked specimens (prepregs) were taken out from the GA-acetone solution and rinsed with water to remove the residual GA and acetone. The partially cross-linked BC-PVA composites were then dried in an oven at 45^{o}C for 12 hr until their weights stabilized. Same process was used to partially cross-link BC and PVA specimens individually, to compare their properties.

Highly cross-linked BC-PVA composites were prepared in GA-water solution using similar method described above. The BC-PVA prepregs initially were partially dried at room temperature for 8 hr before immersing into the GA-water solution and water content in the partially dried specimens was around 50%. The partially dried BC-PVA prepregs were then immersed into the GA-water solution containing 10% by volume GA solution (Glutaraldehyde, 25% solution in water, Aldrich, St. Louis, MO) and 90% by volume deionized water. The pH

value of the GA-water solution was adjusted to around 1.0 using hydrochloric acid to trigger the cross-linking reaction. The incomplete drying of BC-PVA prepregs was to make sure the GA-water solution penetrated into the inner structures of BC-PVA prepregs and triggered the cross-linking reaction to as complete as possible. Our preliminary test results had indicated that the completely dried BC lost a majority of its porous structure as the individual nanofibers stuck to each other reducing the penetration of the GA-water solution. After 12 hr of cross-linking reaction at room temperature, the highly cross-linked BC-PVA prepregs were taken out from the GA-water solution and rinsed with deionized water to remove the residual GA. The highly cross-linked BC-PVA prepregs were then dried between two steel plates, to retain their flatness, in an oven at 45^{o}C for 12 hr until the weights stabilized. Highly cross-linked BC specimens and highly cross-linked PVA films were also prepared using the same method to compare their properties.

3.3.5 Characterization

3.3.5.1 SEM analysis

Freeze dried BC and freeze dried BC-PVA composites (50% BC) were sputter coated with gold and their surface topographies were observed with scanning electron microscope (SEM, LEO 1550 FESEM, Oberkochen, Germany) at an accelerating voltage of 15 kV.

3.3.5.2 ATR-FTIR spectroscopy

The BC-PVA composites, the partially cross-linked BC-PVA composites and the highly cross-linked BC-PVA composites were characterized using an FTIR spectrophotometer (Nicolet Magna-IR 560, Thermo Scientific, Waltham, MA). Attenuated total reflection (ATR) FTIR spectra were taken in the range of 4000-800 cm^{-1} wavenumbers using a split pea accessory. Each scan was an average of 64 scans obtained at a resolution of 4 cm^{-1}. BC content in all the

composite specimens was in the range of 50% and the specimens were dried in an oven at 45^{o}C for 12 hr prior to the spectroscopy. Reproducibility was confirmed for each type of specimen by repeating the experiment 3 times.

3.5.3. Sol-gel analysis

The cross-linked PVA, either in the form of cross-linked PVA film or the cross-linked BC-PVA composites (50% BC), was dried in a moisture-meter (CW Brabender Instruments, Inc., South Hackensack, NJ) at 105^{o}C for 12 hr prior to conducting the sol-gel test. The specimens were weighed to obtain their initial dry weights and then immersed in distilled water in 150 mL glass bottles. The mixtures in the glass bottles were then placed on a shaker table (MAXQ 4450, Thermo Scientific, Waltham, MA) at 80^{o}C and 175 rpm for 12 hr. The solid contents for all specimens were then washed three times and filtered using a Whatman® filter paper (Number 4, 20-25 μm pore size, qualitative) to obtain final residues. The water-soluble portion (sol) and particles smaller than the pore size of the filter paper were removed. The final residues of the cross-linked PVA, either in the cross-linked PVA or the cross-linked BC-PVA composites, were kept in the moisture-meter at 105^{o}C for 12 hr again to obtain their final dry weights (gel). Ratios of the gel weights of the cross-linked PVA to their corresponding initial dry weights were used to determine the PVA gel (cross-linked) percentages. The BC weights in the cross-linked BC-PVA composites were regarded as constant values before and after the test.

3.3.5.4 X-ray diffraction studies

Wide angle X-ray diffraction (WXRD) was used to evaluate the crystallinity and/or crystal sizes of the BC, the PVA, the highly cross-linked BC and the highly cross-linked PVA. All specimens were dried in an oven at 45^{o}C for 12 hr before WXRD studies. The general area detection diffraction system (GADDS, Bruker-AXS, Inc., Madison, WI) was used at 45 KV and

40 mA. The X-ray diffraction patterns of all the specimens were obtained using a Scintag theta-theta powder diffractometer (PAD X, Scintag, Inc., Cupertino, CA) with a solid-state intrinsic germanium detector. All specimens were scanned from 2^o to 30^o at 3^o/min employing the Cu K_α X-ray radiation with a wavelength of 1.54 Å.

3.3.5.5 Tensile property characterization

Tensile tests of various specimens were performed using an Instron tensile testing machine (Instron, model 5566, Canton, MA). The specimens for BC, PVA, BC-PVA composites and their corresponding cross-linked specimens at different levels of cross-linking were cut into 10 mm wide and 60 mm long strips using a precise cutter. Young's moduli of all specimens were determined from the tensile test results conducted according to ASTM D-882-02. Two ends of the specimens were placed between the upper and lower grips of the Instron, leaving a gauge length of 30 mm. The strain rate of 0.02/min was maintained for all specimens. All specimens were conditioned at 21 ℃ and 65% RH for 3 days prior to tensile test.

3.3.5.6 Thermogravimetric analysis

Thermogravimetric analysis (TGA, TA instrument, Model No. 2050) was used to analyze the thermal properties of BC, PVA, BC-PVA composites (50% BC) and their corresponding cross-linked specimens at different levels of cross-linking. All specimens were dried in an oven at 45^oC for 12 hr prior to conducting the test. All TGA analyses were performed between 25 and 600^oC, and at a ramp rate of 20^oC/min under a nitrogen atmosphere by maintaining a flow rate of 10 ml/min.

3.4 Results and discussion

3.4.1 SEM images of BC and BC-PVA composites

Figure 3.1 (a and b) show the SEM images of freeze dried BC and freeze dried BC-PVA

composite (50% BC) specimens, respectively. Both specimens were not hot pressed to preserve their structure. In Figure 3.1 (a), the porous BC network structure is clearly visible. Since these specimens were freeze dried, the porous structure has been maintained. Based on the diameter measurements of 100 BC-nanofibers and 100 pores in the SEM image of the BC, the mean diameter of BC-nanofibers was found to be less than 100 nm and the pore diameters ranged from several dozens to several hundred nanometers. It is clear from Figure 3.1 (b) that the PVA penetrated the BC network structure and filled many of the pores. The diameters of the BC-nanofibers became larger since they were covered by the PVA. Many BC-nanofibers were embedded within the PVA layers, thus forming uniform composite structures with excellent properties. Similar surface topography of BC-polyethylene glycol (PEG) composite reported previously showed that PEG not only coated the surface of BC pellicles but also penetrated into the BC fiber network [39]. It has also been reported that structural modification can occur as the water surrounding polyglucosan chains are displaced and hydrogen bonds are formed between the hydroxyl groups of BC and PEG and of BC and PVA [21, 40, 41].

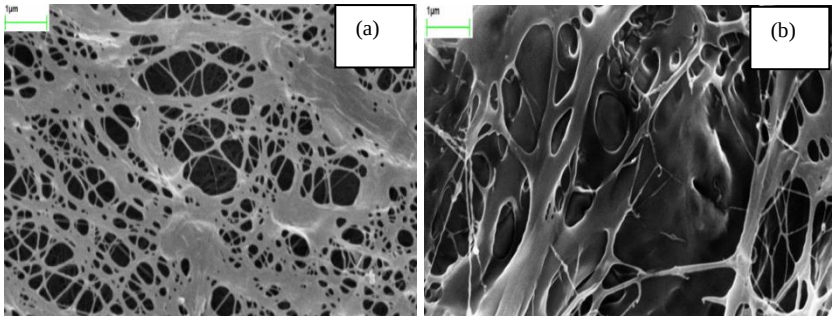

Figure 3.1 SEM images of freeze dried BC (a) and freeze dried BC-PVA composite (b)

3.4.2 ATR-FTIR analysis of BC-PVA composites and cross-linked BC-PVA composites

Figure 3.2 shows the ATR-FTIR spectra of the BC-PVA composites (50% BC) and BC-PVA composites cross-linked to different levels. All spectra were normalized based on bands observed at 1058 cm^{-1} wavenumber associated with C-O stretching. ATR-FTIR spectrum 3.2 (a)

is for the BC-PVA composite. ATR-FTIR spectrum 3.2 (b) is for the partially cross-linked BC-PVA composite, using the GA-acetone solution, while spectrum 3.2 (c) is for the highly cross-linked BC-PVA composite, using the GA-water solution. As mentioned earlier the BC content in all three specimens was around 50%. A broad band at 3200-3550 cm^{-1}, wavenumber seen in all 3 spectra, is a result of the hydroxyl (O-H) stretching vibration resulting from the strong hydrogen bonds of intra-molecular and inter-molecular type [31, 32]. The absorption band observed between 2820 and 3000 cm^{-1} wavenumber is due to the stretching of aliphatic C-H bond [32]. Compared to spectrum 3.2 (a), the absorbance intensity at 3200-3500 cm^{-1} band in the spectrum 3.2 (b) is much lower. The normalized absorbance intensity ratio of bands for O-H to C-H decreased from 1.60 for spectrum 3.2 (a) to 1.20 for spectrum 3.2 (b). In the spectrum 3.2 (c), the absorbance intensity ratio of bands for O-H to C-H decreased even further, to 0.83. This spectral change indicates reduction in the O-H groups on the specimens as a result of cross-linking reaction with the GA [32]. Normalized absorbance of bands at 1700-1750 cm^{-1} in the spectra 3.2 (a) and 3.2 (b) were 0.13 and 0.20 respectively. While they are not sharp, they still demonstrate the presence of carbonyl (C=O) group in the composites from the remaining non-hydrolyzed vinyl acetate group of the PVA [31, 42]. In spectrum 3.2 (c), however, a significantly sharp absorption (normalized absorbance of 0.57) observed at 1700-1750 cm^{-1} wavenumber indicates stronger stretching vibration of C=O in the composites. This means that in addition to the remaining non-hydrolyzed vinyl acetate groups, some residual aldehyde groups from the GA also existed in the highly cross-linked BC-PVA composites, both of them contributing to the stronger C=O absorption. This confirms the earlier observation that the GA-water solution can penetrate into the inner cavities of the BC-PVA composites network and part of the residual GA may still be trapped in the highly cross-linked BC-PVA composites even after wash. This is very

likely when only one aldehyde group from GA reacts and the other end remains unreacted. The absorption at 1050-1150 cm^{-1} wavenumber seen in spectrum 3.2 (a) is due to the presence of C-O stretching vibration from the acetate group [31, 32, 42]. The same absorption band for C-O stretching vibration was much broader in spectrum 3.2 (b) than in spectrum 3.2 (a), resulting from the formation of the acetal linkages upon reaction of the PVA with the GA. In the spectrum 3.2 (c), the band of C-O stretching vibration became the broadest one in three spectra due to the high cross-linking level and the formation of more acetal linkages.

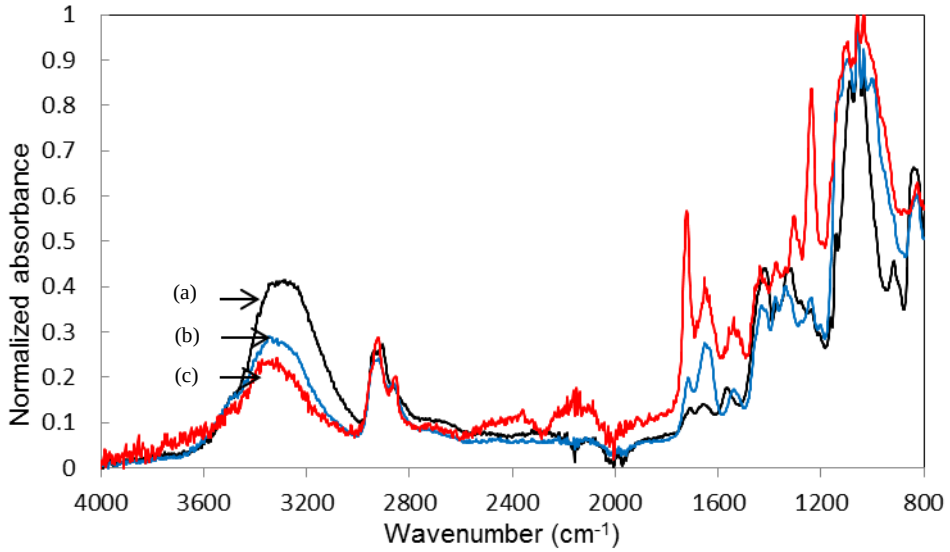

Figure 3.2 ATR-FTIR spectra for BC-PVA composites (a), partially cross-linked BC-PVA composites (b) and highly cross-linked BC-PVA composites (c)

Overall, the ATR-FTIR results indicate that the BC-PVA composites were partially or highly cross-linked based on the decreased intensity of bands for O-H stretching vibration combined with the increased intensity of bands for C-O stretching vibration. Our preliminary ATR-FTIR study had shown that both BC and PVA are able to be cross-linked using either GA-acetone or GA-water solutions. The cross-linking reactions can occur between hydroxyl groups of the BC, between hydroxyl groups of the PVA, or between BC and PVA. These results also confirm that a higher cross-linking level can be achieved for BC-PVA composites with GA-water solution.

This is mainly because the GA-acetone solution can hardly penetrate into the fully dried BC-PVA composites, whereas the GA-water solution has the ability to penetrate the BC-PVA prepregs well and trigger a cross-linking reaction inside the BC-PVA prepregs and form highly cross-linked BC-PVA composites.

3.4.3 Sol-gel analysis of cross-linked PVA and BC-PVA composites

Sol-gel analysis was performed for PVA as well as for the resin in BC-PVA composites that were cross-linked to different levels. Table 3.2 presents the sol-gel test results for partially and highly cross-linked PVA (the resins from partially and highly cross-linked BC-PVA composites) as well as control PVA. The results indicate that the gel (cross-linked) percentage of the partially cross-linked PVA was about 10%. The values were close in both the partially cross-linked PVA and the resin present in the partially cross-linked BC-PVA composites. Approximately 90% of the PVA was noncross-linked and thus could be dissolved in deionized water during the sol-gel test. The results of this test confirm that the cross-linking reaction using the GA-acetone solution occurred mostly on the surfaces of the PVA and the BC-PVA composites. This was mainly because the GA-acetone solution could not penetrate into the PVA with a sufficient quantity to trigger the cross-linking reaction inside the PVA. The results also indicate that the gel (cross-linked) percentage of the highly cross-linked PVA could be over 90%. The levels of cross-linking were also close in both the highly cross-linked PVA and the resin in the highly cross-linked BC-PVA composites. While both resin and composite specimens were swollen after being exposed to water, they remained intact. The results of this test further demonstrate that the cross-linking reaction with the GA-water solution occurred on the surface as well as inside of the specimens as a result of easy penetration of the GA-water solution into the PVA.

Table 3.2 Sol-gel test results of PVA at different levels of cross-linking

Specimens	PVA	Partially cross-linked PVA	PVA in partially cross-linked BC-PVA composites	Highly cross-linked PVA	PVA in highly cross-linked BC-PVA composites
Gel percentage in specimens (%)	0	10.8	9.6	90.2	88.9

3.4.4 WXRD of BC, PVA and their highly cross-linked specimens

WXRD was used to evaluate the crystallinity and the crystal sizes of the BC, the PVA and their corresponding highly cross-linked specimens. The crystallinity (%) values for individual specimens were calculated using a ratio of crystalline area to the combined crystalline and amorphous areas in the WXRD patterns [43]. The crystal sizes (d-spacing) were calculated using the WXRD patterns using analysis software (Scintag, Inc., Cupertino, CA) based on Scherrer Equation.

Figure 3.3A (a) and (b) illustrate WXRD patterns obtained for BC and highly cross-linked BC, respectively. Both WXRD patterns showed distinct peaks at 2θ values of 5.5^{o}, 14.5^{o} and 22.5^{o}. Figure 3.3A also shows that the crystallinity of the BC decreased from 62.5% (Figure 3.3A (a)) to 12.7% (Figure 3.3A (b)) after the cross-linking reaction. The reduction in the crystallinity is mainly because the cross-linking within the BC that changes the morphology and destroys the crystallites.

Figure 3.3B shows WXRD patterns of the control PVA (a) and highly cross-linked PVA (b). Both the WXRD patterns show a distinct peak at 2θ values of 20^{o}. Figure 3.3B indicates that the crystallinity of the PVA decreased from 61.7% (Figure 3.3B (a)) to 4.9% (Figure 3.3B (b)) after cross-linking and the average crystal size of the PVA at 20^{o} decreased from 45 Å (Figure 3.3B (a)) to 14 Å (Figure 3.3B (b)). It should be noted that the transparency of highly cross-linked PVA was slightly higher than the noncross-linked PVA further confirming the reduction in

crystallinity after cross-linking. The lower crystallinity is largely because of the cross-links formed in the PVA that restrict crystallization. The cross-links are also known to play the role of defect centers impeding the folding of the macromolecular chains and, thus, decrease the size of the crystals [44, 45].

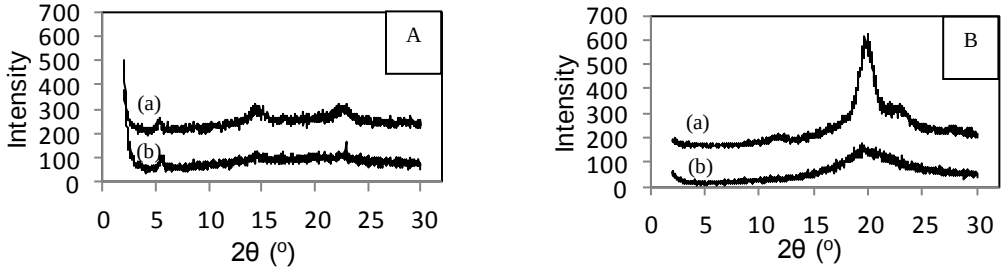

Figure 3.3 WXRD patterns **A:** BC (a) and highly cross-linked BC (b); **B:** PVA (a) and highly cross-linked PVA (b)

3.4.5 Tensile properties of BC, PVA, BC-PVA composites and their corresponding cross-linked specimens

Table 3.3 presents the tensile test results for BC, PVA and BC-PVA composites with varying BC contents (25%, 50 % and 75%). For comparison, theoretical values calculated, using the rule of mixture, for Young's modulus and fracture stress are also presented in Table 3.3. The Young's modulus of the BC membrane was 3424 MPa while the Young's modulus of the PVA was 12.8 MPa. The Young's modulus values of the BC-PVA composites were between those obtained for BC and PVA as can be expected. With the increase in BC content (or decrease in PVA content), the Young's modulus of the BC-PVA composites increased as well. For composites with BC content of 25%, the Young's modulus was only around 731.6 MPa and when the BC content increased to 50% and 75% the Young's modulus values increased to 1590 MPa and 2473 MPa, respectively. The fracture stress values for BC and PVA were 63.7 MPa and 5.4 MPa, respectively. It is clear that BC-PVA composite fracture stress values are between those of BC and PVA and increase as the BC content in the composites increases. This is again as can be

expected. While the fracture stress values for composites increased with the BC content, they did not show a direct correlation with BC content as the modulus values did. This is due to the decreased fracture strain of the composites with increase in BC content. The fracture stress values ranged from 22.9 MPa for composites with BC content of 25% to 44.6 MPa when the BC content was 75%. For the fracture strain, the value of the PVA was 234.3%, which was much higher than BC's fracture strain of 5.8%. However, most fracture strain values of the BC-PVA composites were close to or even lower than that obtained for BC. This is likely due to the two components in composites having extremely good bonding resulting in a brittle composite [46, 47].

Table 3.3 Tensile properties for BC, PVA and BC-PVA composites with varying BC content

Specimens	Young's modulus (MPa)	Rule of mixture (MPa)	Fracture stress (MPa)	Rule of mixture (MPa)	Fracture strain (%)
BC	3424 (8.2)*		63.7 (50.4)		5.8 (44.7)
PVA	12.8 (36.3)		5.4 (3.4)		234.3 (14.4)
BC-PVA composites (25% BC)	731.6 (1.1)	754.8	22.9 (6.5)	18.1	3.7 (1.6)
BC-PVA composites (50% BC)	1590 (12.0)	1565	32.6 (10.9)	31.9	2.4 (26.1)
BC-PVA composites (75% BC)	2473 (5.2)	2449	44.6 (13.3)	47.0	2.0 (18.9)

**: values in the parentheses are % coefficient of variation values*

Table 3.4 presents tensile test results for BC, PVA, BC-PVA composites (50% BC) and their corresponding cross-linked specimens at different cross-linking levels. The Young's modulus values of partially cross-linked BC and highly cross-linked BC increased to 4243 MPa and 5107 MPa, respectively, from 3424 MPa obtained for BC. The Young's modulus values of partially cross-linked and highly cross-linked PVA increased to 54.1 MPa and 270.1 MPa, respectively,

from 12.8 MPa obtained for the control (noncross-linked) PVA. The Young's modulus values of the partially cross-linked and highly cross-linked BC-PVA composites increased to 1875 MPa and 2429 MPa, respectively, from 1590 MPa obtained for the BC-PVA composites. While the increase in Young's modulus values is due to the cross-linked structure and increased molecular weight in the case of PVA, the cross-linking of BC makes the structure rigid when cross-linked [48]. The reduction in moisture content from 9.1% of the PVA to a lower range of 3.8-6.0% for the cross-linked specimens may also partially contribute to the increased Young's modulus. As is expected, higher cross-linking level leads to higher modulus. From data presented in Table 3.4, it is clear that with increased cross-linking, all three specimens, PVA, BC and the composites, become brittle with lower fracture strain values. This affects their fracture stress values which do not show a correlation seen for Young's modulus. For example, cross-linking reduces the fracture stress of BC whereas cross-linking increases the fracture stress of PVA and for the BC-PVA composites, there is almost no effect.

Table 3.4 Tensile properties for BC, PVA, BC-PVA composites at different levels of cross-linking

Specimens	Young's modulus (MPa)	Rule of mixture (MPa)	Fracture stress (MPa)	Rule of mixture (MPa)	Fracture strain (%)
BC	3424		63.7		5.8
	(8.2)*		(50.4)		(44.7)
Partially cross-linked BC	4243		61.6		1.9
	(14.6)		(17.5)		(27.9)
Highly cross-linked BC	5107		43.8		1.0
	(11.2)		(37.6)		(41.1)
PVA	12.8		5.4		234.3
	(36.3)		(3.4)		(14.4)
Partially cross-linked PVA	54.1		7.9		59.6
	(15.8)		(9.2)		(11.1)
Highly cross-linked PVA	270.1		19.2		19.9
	(19.6)		(5.1)		(22.9)
BC-PVA composites (50% BC)	1590	1565	32.6	31.9	2.4
	(12.0)		(10.9)		(26.1)
Partially cross-linked BC-PVA composites (50% BC)	1875	1938	31.9	32.3	2.0
	(15.2)		(30.4)		(34.2)
Highly cross-linked BC-PVA composites (50% BC)	2429	2471	31.6	30.4	1.5
	(4.7)		(14.3)		(39.3)

**: values in the parentheses are % coefficient of variation values*

Tables 3.3 and 3.4 also present theoretical values for Young's modulus and fracture stress values calculated using the rule of mixtures [49]. The densities of cellulose and PVA used were 1.52 g/cc and 1.27 g/cc, respectively [50], and the BC content in the BC-PVA composites varied from 25% to 75% by weight. It is clear that the theoretical values and the experimentally obtained values for both Young's modulus and fracture stress are very close to each other.

Figure 3.4 shows typical stress vs strain plots of BC-PVA composites (a) and partially (b) and highly cross-linked (c) BC-PVA composites. The BC content in all the three specimens is around 50% by weight. Figure 3.4 (a) for BC-PVA composite shows an initial elastic behavior followed by a plastic yielding. The yielding may be due to PVA's high ductility and breaking of some BC nanofibers that are in the stress direction and possible alignment of the remaining

nanofibers. Once that process was over, BC-PVA composites showed elastic behavior until the fracture point. Figures 3.4 (b) and 3.4 (c) indicate no obvious yielding for partially or highly cross-linked BC-PVA composites. Once the PVA becomes cross-linked it loses its ductility. As can be expected, Figure 3.4 also indicates that higher cross-linking level leads to higher modulus and lower fracture strain values.

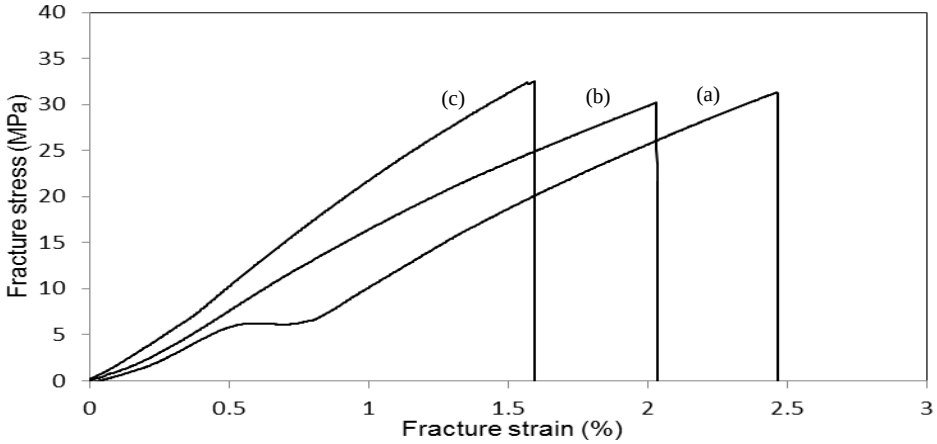

Figure 3.4 Stress vs Strain plots for BC-PVA composites (a), partially cross-linked BC-PVA composites (b) and highly cross-linked BC-PVA composites (c)

It is interesting to note that both Young's modulus and fracture stress values for the BC-PVA composites and the cross-linked BC-PVA composites are close or higher than many traditional plastic materials, including polyethylene (Young's modulus: 800 MPa; fracture stress: 15 MPa), polypropylene (Young's modulus: 1900 MPa; fracture stress: 40 MPa), and nylon 6 (Young's modulus: 1800 MPa; fracture stress: 70 MPa) [51]. As a result, the BC-PVA composites, both cross-linked and noncross-linked, have the potential to replace these traditional non-biodegradable plastic materials in many applications, including racket frame, ski pole, circuit board, automobile inside etc. These degradable composites may be easily protected from water by applying varnish or other water-resistant coatings to increase their durability.

3.4.6 TGA of BC, PVA, BC-PVA composites and their corresponding cross-linked specimens

Figure 3.5A presents typical TGA thermograms of BC, partially cross-linked BC and highly cross-linked BC specimens. Thermogram 3.5A (a), the TGA thermogram for BC, shows the onset decomposition temperature (T_d) at 260^{o}C. Weight losses for BC were 30% at 284^{o}C, 50% at 303^{o}C and 80% at 600^{o}C. It has been reported that two competing reaction pathways, low-temperature pathway and high-temperature pathway (>300^{o}C), occur simultaneously during the thermal degradation of cellulose [52]. The low-temperature pathway is mainly responsible for the water loss. The primary reaction in the high-temperature pathway is depolymerization, as the cellulose structure can absorb enough energy to activate the cleavage of the glycosidic linkages to produce glucose, which is dehydrated to levoglucosan and oligosaccharides. The production of volatile compounds is complete when the temperature reaches around 450^{o}C. The continuing weight loss is due to degradation when all other elements are driven off and the char (carbon) remains [52]. The thermogram for the BC indicates that the weight loss of cellulose is the result of a combination of both low-temperature and high-temperature pathways. Thermogram 3.5A (b), for partially cross-linked BC, showed a T_d at 285^{o}C. Weight losses for the partially cross-linked BC were 30% at 309^{o}C, 50% at 334^{o}C and about 83% at 600^{o}C. Thermogram 3.5A (c) for highly cross-linked BC showed a T_d at 315 ℃ with weight losses of 30% at 329^{o}C, 50% at 346^{o}C and about 80% at 600^{o}C. These results indicate that the cross-linking makes the BC thermally more stable.

Figure 3.5B presents typical TGA thermograms for PVA and partially and highly cross-linked PVA. Thermogram 3.5B (a) for the PVA shows two decomposition onset temperatures, T_{d1} and T_{d2}, at 255^{o}C and 400^{o}C, respectively. Weight loss for the PVA was 30% at 267^{o}C, 50%

at 279^{o}C and up to 93% at 600^{o}C. Two-step degradation of PVA has been reported earlier [50]. A likely explanation for this is that PVA first degrades into small-molecular-weight polymer at approximately 250^{o}C and then further degrades into carbon char at temperatures above 350^{o}C. These results confirm the earlier findings of Peng and Kong [53]. Thermogram 3.5B (b) for partially cross-linked PVA shows a single T_d at 325^{o}C. Weight losses observed were 30% at 340^{o}C, 50% at 364^{o}C and about 97% at 600^{o}C. Thermogram 3.5B (c), for highly cross-linked PVA, shows T_d at 330^{o}C. Weight losses observed for highly cross-linked PVA were 30% at 348^{o}C, 50% at 370^{o}C and about 97% at 600^{o}C. The two-step degradation pattern was not so obvious in the thermograms for partially and highly cross-linked PVA.

Figure 3.5C presents typical TGA thermograms for BC-PVA composites and partially cross-linked and highly cross-linked BC-PVA composites. As mentioned earlier BC content in all the BC-PVA composites was around 50%. Thermogram 3.5C (a) for BC-PVA composites shows two decomposition temperatures, T_{d1} and T_{d2} at 257^{o}C and 380^{o}C, respectively. Weight losses observed were 30% at 273^{o}C, 50% at 283^{o}C and about 90% at 600^{o}C. When thermograms for BC and BC-PVA composites are compared, it is clear that BC reinforcement is able to increase the thermal stability of the PVA. Two distinct and well-separated degradation onsets can be seen in thermogram 3.5C (a) for BC-PVA composites. As a result, this degradation can also be regarded as a two-step-degradation and could be a result of the PVA. Thermogram for partially cross-linked BC-PVA composites presented in 3.5C (b) shows much better thermal stability than the BC-PVA composites. The T_d for the partially cross-linked BC-PVA composites was at 307^{o}C and the weight losses were 30% at 331^{o}C, 50% at 352^{o}C and about 94% at 600^{o}C. Thermogram 3.5C (c) obtained for highly cross-linked BC-PVA composites showed the highest thermal stability among the three BC-PVA composites, as can be expected. The T_d for the highly cross-

linked BC-PVA composites was 313°C and weight losses were 30% at 337°C, 50% at 372°C and about 90% at 600°C. The two-step-degradation pattern was not obvious in the thermograms for partially and highly cross-linked BC-PVA composites.

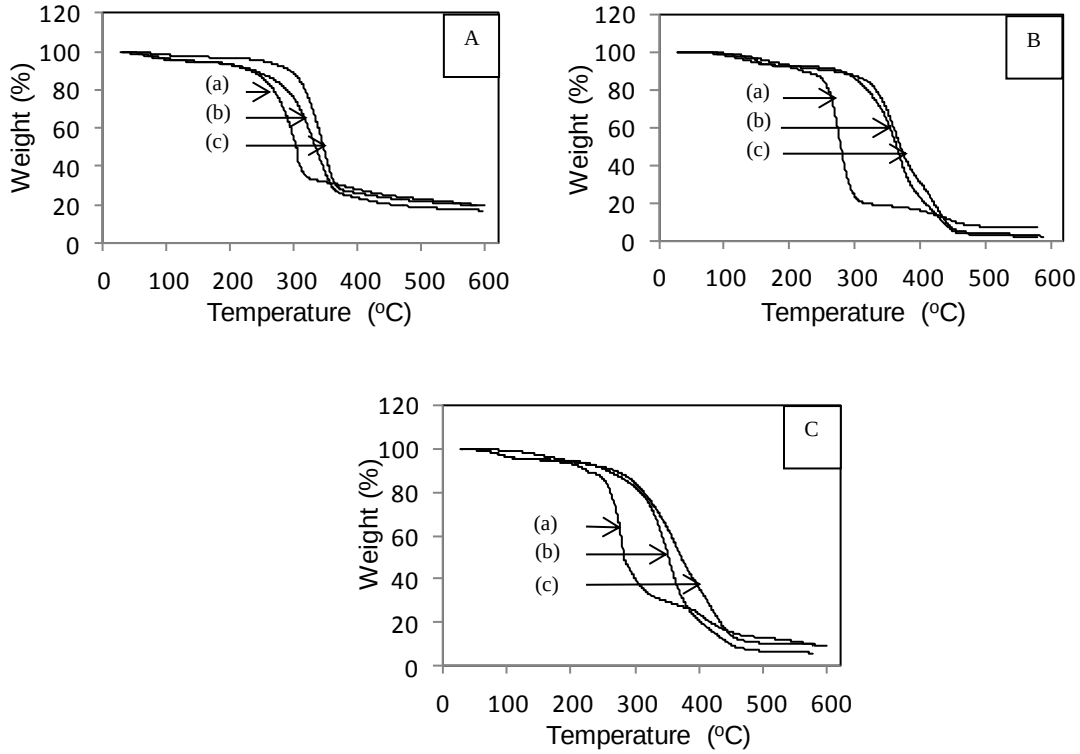

Figure 3.5 TGA thermograms A: BC (a), partially cross-linked BC (b) and highly cross-linked BC (c); B: PVA (a), partially cross-linked PVA (b) and highly cross-linked PVA (c); **C:** BC-PVA composite (a), partially cross-linked BC-PVA composite (b) and highly cross-linked BC-PVA composite (c)

These results clearly indicate that cross-linking can increase the thermal stability of BC, PVA and BC-PVA composites. Other researchers have obtained similar results for soy flour, collagen and chitosan after cross-linking [54-56]. These results also confirm that the BC-PVA composites and their cross-linked specimens, particularly the highly cross-linked ones, can exhibit excellent thermal stability in addition to their high tensile properties. The final char weights of the cross-linked specimens in TGA tests were slightly less than those of the specimens without cross-linking treatments. The lower char weight of the cross-linked specimens is probably due to

volatilization of the residual GA trapped in the cross-linked specimens during the TGA test.

3.5 Conclusions

The biodegradable membrane-like BC-PVA composites with differing BC contents were produced by simple immersion methods. The SEM images indicated that the PVA not only penetrated into the BC network, but also filled in the pores present within the BC nanofiber membrane. The ATR-FTIR results showed acetal linkages were formed in the BC-PVA composites after a cross-linking reaction. The sol-gel results showed cross-linked PVA to be water-insoluble, and a good correlation between cross-linking level and insolubility was observed. The WXRD results indicated a reduction in crystallinity as a result of cross-linking for BC and PVA as well as a reduction in the crystal size of the PVA. The tensile test results showed good mechanical properties for BC-PVA composites indicating the ability of the BC to reinforce the PVA. The TGA showed higher thermal stability for the BC-PVA composites than the PVA. This was because the BC itself is thermally more stable. Cross-linking of PVA was shown to increase the Young's modulus and thermal stability of the BC-PVA composites. At the same time the fracture strain decreased significantly with cross-linking. The methods developed in this study make it possible to control the PVA content in the composites as well as the cross-linking level of PVA.

3.6 Acknowledgments

This work was partly supported by the National Textile Center (NTC) and the Wallace Foundation. The authors would like to thank Prof.s Dan Luo, John March and Antje Baeumner of Cornell University for allowing the use of their laboratory facilities. The authors also thank the Cornell Center for Materials Research (CCMR) for the use of their facilities.

References

[1] Chou TW, Frank KK. Composite materials series, 3, Textile structural composites. New York: Elsevier Science Publishers 1989. pp 1-26.

[2] Mohanty AK, Khan MA, Hinrichsen G. Surface modification of jute and its influence on performance of biodegradable jute - fabric/Biopol composites. Compos Sci Technol 2000; 60 (7): 1115-1124.

[3] Stevens ES. Green plastics: an introduction to the new science of biodegradable plastics. Princeton, NJ: Princeton University 2001. pp. 15-30.

[4] Netravali AN, Huang X, Mizuta K. Advanced 'green' composite. Adv Compos Mater 2007; 16 (4): 269-282

[5] Netravali AN, Chabba S. 'Composites get greener'. Mater Today 2003; 6 (4): 22-29.

[6] Kim JT, Netravali AN. Mechanical and thermal properties of sisal fiber-reinforced green composites with soy protein-gelatin blend resins. J Biobased Mater Bioenergy 2010; (4): 338-345.

[7] Nakamura R, Goda K, Noda J, Netravali AN. Elastic properties of green composites reinforced with ramie twisted yarn. J Solid Mech and Mater Eng 2010; 4 (11): 1605-1614.

[8] Huang X, Netravali AN. Biodegradable green composites made using bamboo micro/nano-fibrils and chemically modified soy protein resin. Compos Sci Technol 2009; 69: 1009-1025.

[9] Huang X, Netravali AN. Characterization of flax yarn and flax fabric reinforced nano-clay modified soy protein resin composites. Compos Sci Technol 2007; 67: 2005-2014.

[10] Lodha P, Netravali AN. Characterization of Phytagel® modified soy protein isolate resin and unidirectional flax yarn reinforced 'green' composites. Polym Compos 2005; 26 (5): 647-659.

[11] Iguchi M, Yamanaka S, Budhiono A. Bacterial cellulose - a masterpiece of Nature's arts. J Mater Sci 2000; 35(2): 261-270.

[12] Baeckdahl H, Helenius G, Bodin A, Nannmark U, Johansson BR, Risberg B, Gatenholm P. Mechanical properties of bacterial cellulose and interactions with smooth muscle cells. Biomaterials 2006; 27(9): 2141-2149.

[13] Klemm D, Schumann D, Udhardt U, Marsch S. Bacterial synthesized cellulose - artificial blood vessels for microsurgery. Prog Polym Sci 2001; 26(9): 1561-1603.

[14] Klemm D, Heublein B, Fink HP, Bohn A. Cellulose: Fascinating biopolymer and sustainable raw material. Angew Chem Int Ed 2005; 44(22): 3358-3393.

[15] Fink HP, Weigel P, Purz HJ, Ganster J. Structure formation of regenerated cellulose materials from NMMO-solutions. Prog Polym Sci 2001; 26(9): 1473-1524.

[16] Wan Y, Hong L, Jia S, Huang Y, Zhu Y, Wang Y, Jiang H. Synthesis and characterization of hydroxyapatite - bacterial cellulose nanocomposites. Compos Sci Technol 2006; 66(11-12): 1825-1832.

[17] Fontana JD, De Souza, AM, Fontana CK, Torriani IL, Moreschi JC, Gallotti BJ, De Souza, SJ, Narcisco GP, Bichara JA, Farah LFX. Acetobacter cellulose pellicle as a temporary skin substitute. Appl Biochem Biotechnol 1990; 24-25: 253-264.

[18] Shibazaki H, Kuga S, Onabe F, Usuda M. Bacterial cellulose membrane as separation medium. J Appl Polym Sci 1993; 50(6): 965-969.

[19] Svensson A, Nicklasson E, Harrah T, Panilaitis B, Kaplan DL, Brittberg M, Gatenholm P. Bacterial cellulose as a potential scaffold for tissue engineering of cartilage. Biomaterials 2005; 26(4): 419-431.

[20] Westland JA (Bothell, WA), Stephens SR (Auburn, WA), Johnston Jr., WC (Puyallup, WA), Rosenkrans HJ (Seattle, WA) Bacterial cellulose binding agent. United States, Weyerhaeuser Company (Tacoma, WA) 1993; 5207826. http://www.freepatentsonline.com/5207826.html. Accessed June 2011

[21] Wang J, Gao C, Zhang Y, Wan Y. Preparation and in vitro characterization of BC/PVA hydrogel composite for its potentisl use as artificial corena biomaterial. Mater Sci and Eng C 2010; 30: 214-218.

[22] Millon LE, Oates CJ, Wan WK. Compression properties of polyvinyl alcohol-bacterial cellulose nanocomposite. Journal of Biomedical Materials Research B Appl Biomater 2009; 90B (2): 922-929.

[23] Millon LE, Wan WK. The polyvinyl alcohol-bacterial cellulose system as a new nanocomposite for biomedical applications. J Biomed Mater Res B App Biomater 2006; 79B (2): 245-253.

[24] Mohamadi H, Boughner D, Millon LE, Wan WK. Design and simulation of a poly(vinyl alcohol)-bacterial cellulose nanocomposite mechanical aortic heart valve prosthesis. Proc Inst Mech Eng H J Eng Med 2009; 223: 697-711.

[25] Ghiciudean TG, Stoica A, Dobre T, Tooren MV. Synthesis and characterization of poly(vinyl alcohol)-bacterial cellulose nanocomposite. U.P.B. Sci Bull B 2011; 73 (2): 17-30.

[26] Yang HS, Yoon JS, Kim MN. Effects of storage of a mature compost on its potential for biodegradation of plastics. Polym Degrad Stabil 2004; 84: 411-417.

[27] Chiellini E, Corti A, Antone SD, Solaro R. Biodegradation of poly (vinyl alcohol) based materials. Prog Polym Sci 2003; 28: 963-1014.

[28] Chen L, Imam SH, Cordon SH, Greene RV. Starch-polyvinyl alcohol crosslinked film-

performance and biodegradation. J Environ Polym Degr 1997; 5 (2): 111-117.

[29] Kim KJ, Lee SB, Han NW. Kinetics of crosslinking reaction of PVA membrane with glutaraldehyde. Korean J Chem Eng 1994; 11(1): 41-47.

[30] Yeom CK, Lee KH. Pervaporation speration of water-acetic acid mixtures through poly (vinyl alcohol) membranes crosslinked with glutaraldehyde. J Membr Sci 1996; 109: 257-265.

[31] Gohil JM, Bhattacharya A, Ray P. Studies on the cross-linking of poly (vinyl alcohol). J Polym Res 2006; 13: 161-169.

[32] Mansur HS, Sadahira CM, Souza AN, Mansur AAP. FTIR spectroscopy characterization of poly (vinyl alcohol) hydrogel with different hydrolysis degree and chemically crosslinked with glutaraldehyde. Mater Sci Eng C 2008; 28: 539-548.

[33] Tang C, Saquing CD, Hardiing JR, Khan SA. In Situ cross-linking of electronspun poly (vinyl alcohol) nanofibers. Macromolecules 2010; 43: 630-637.

[34] Wang Y, Hsieh Y. Cross-linking of polyvinyl alcohol (PVA) fibrous membranes with glutaraldehyde and PEG diacylchloride. J Appl Polym Sci 2010; 116: 3249-3255.

[35] Yang CQ, Wei W. Evaluating glutaraldehyde as a nonformaldehyde durable press finishing agent for cotton fabrics. Text Res J 2000; 70 (3): 230-236.

[36] Mathew AP, Oksman K, Pierron D, Harmad MF. Crosslinked fibrous composites based on cellulose nanofibers and collagen with in situ pH induced fibrillation. Cellulose 2012; 19: 139-150.

[37] Quero F, Nogi M, Lee KY, Poel GV, Bismarck A, Mantalaris A, Yano H, Eichhorn SJ. Cross-linked bacterial cellulose networks using glyoxalization. ACS Appl Mater Interfaces 2011; 3: 490-499.

[38] Brown EE, Laborie MPG, Zhang J. Glutaraldehyde treatment of bacterial cellulose/fibrin

composites: impact on morphology, tensile and viscoelastic properties. Cellulose 2012; 19:127-137.

[39] Cai Z, Kim J. Bacterial cellulose/poly (ethylene glycol) composite: Characterization and first evaluation of biocompatibility. Cellulose 2010; 17: 83-91.

[40] Alberto S, Giovanni T, Anna MB, Erinestina DP, Elena S, Bruni M. Characterization of native cellulose/poly(ethylene glycol) films. Macromol Mater Eng 2001; 286 (9): 524-538.

[41] Brown EE, Laborie MG. Bioengineering bacterial cellulose/poly (ethylene oxide) nanocomposites. Biomacromolecules 2007; 8: 3074-3081.

[42] Kim JH, Moon EJ, Kim CK. Composite membranes prepared from poly (m-animostyrene-co-vinyl alcohol) copolymers for the reverse osmosis process. J Membr Sci 2003; 216: 107-120

[43] Young RJ, Lovell PA. Introduction to polymers, 3rd edn. Boca Raton, FL: CRC Press 2011. pp 591-622.

[44] Mtshali TN, Krupa I, Luyt AS. The effect of cross-linking on the thermal properties of LDPE/wax blends. Thermalchim Acta 2001; 380: 47-54.

[45] Kim JH, Kim JY, Lee YM, Kim KY. Properties and swelling characteristics of cross-linked poly (vinyl alcohol)/chitosan blend membrane. J Appl Polym Sci 1992; 45 (10): 1711-1717.

[46] Chamis CC (1974) Mechanics of load transfer at the *interface.* In: Pluddemann EP (ed) Interfaces in polymer matrix composites. New York: Academic Press 1974. pp 31-77.

[47] Netravali AN, Henstenburg R, Phoenix SL, Schwartz P. Interfacial shear strength studies using the single-filament-composite test I: experiments on graphite fibers in an epoxy. Polym Compos 1989; 10: 226-241.

[48] Zhang L, Chen P, Huang J, Yang G, Zheng L. Way of strengthening biodegradable soy-dreg plastics. J Appl Polym Sci 2003; 88: 422-427.

[49] Warner SB. Fiber Science. Upper Saddle River, NJ: Prentice Hall 1995. pp 205-206.

[50] Lodha P, Netravali AN. Characterization of stearic acid modified soy protein isolate resin and ramie fiber reinforced 'green' composites. Compos Sci Technol 2005; 65: 1211-1225.

[51] Tensile property testing of plastics - MatWeb 2011. http://www.matweb.com/reference/tensilestrength.aspx. Accessed June 2011

[52] Schniewind AP. Concise encyclopedia of wood & wood-based materials, 1st edn. Elmsford, NY: Pergamon Press 1989. pp 271-273.

[53] Peng Z, Kong LX. A thermal degradation mechanism of polyvinyl alcohol/silica nanocomposites. Polym Degrad Stab 2007; 92: 1061-1071.

[54] Chabba S, Matthews GF, Netravali AN. 'Green' composites using cross-linked soy flour and flax yarns. Green Chem 2005; 7: 576-581.

[55] Rodrigues FT, Martins VCA, Plepis AMG. Porcine skin as a source of biodegradable matrices: alkaline treatment and glutaraldehyde crosslinking. Polimeros 2010; 20 (2): 92-97.

[56] Liu BS, Yao CH, Fang SS. Evaluation of a non-woven fabric coated with a chitosan Bi-layer composite for wound dressing. Macromol Biosci 2008; 8 (5): 432-440.

Chapter 4 Fabrication and characterization of biodegradable composites based on microfibrillated cellulose and polyvinyl alcohol

Kaiyan Qiu, Anil N. Netravali*
Fiber Science Program, Cornell University, Ithaca, NY 14853-4401

4.1 Abstract

Microfibrillated cellulose (MFC) based thin membrane-like fully biodegradable composites were produced by blending MFC suspension with polyvinyl alcohol (PVA). Desired MFC content in the composites could be easily obtained by varying the PVA solution concentration. Chemical crosslinking of PVA was carried out using glyoxal to increase the mechanical and thermal properties of the composites as well as to make the PVA partially water-insoluble. Examination of composite surfaces and fracture topographies indicated that the MFC fibrils were well bonded to PVA and uniformly distributed. Infrared spectroscopy showed that acetal linkages could be formed in the MFC-PVA composites by a glyoxal crosslinking reaction. Sol-gel and swelling results indicated that crosslinking reaction made PVA partially insoluble and reduced its swelling ability. The MFC-PVA composites had excellent tensile properties which were further enhanced by crosslinking. Thermogravimetric analysis (TGA) showed higher thermal stability for MFC-PVA composites compared to PVA. The crosslinked MFC-PVA composites showed even higher thermal stability. Differential scanning calorimetry (DSC) indicated that crosslinking increased the glass transition temperature and reduced melting temperature and crystallinity of PVA in MFC-PVA composites. Results also indicated that nano- and micro-fibrils in MFC inhibit the crystallization of PVA. These composites could be good candidates for replacing today's traditional non-biodegradable plastics.

Keywords: A. Nano composites, A. Polymer-matrix composites (PMCs), B. Mechanical properties, D. Differential scanning calorimetry (DSC), B. Infrared (IR) spectroscopy

4.2 Introduction

Polymers with broad range of properties play a significant role in our everyday life [1]. However, with increased use of polymeric products, there are increased concerns on the impact these polymers have on the environment [2]. Most traditional polymers are produced using fossil feed-stocks and are non-biodegradable. Over 30 million and 15 million tons of plastic waste, in the US and western Europe, respectively, are generated each year [2]. At the end of their life majority of the conventional plastics and composites are disposed of in landfills where they may stay as is for several decades without degrading making that land unusable. About 6-7% of the petroleum produced today is used for making polymers, fibers and other chemicals. It is estimated that we are currently consuming petroleum at an 'unsustainable' rate, 100,000 times faster than the nature can create it [3]. At the current rate of consumption, it is estimated that the current petroleum reserves will last for only 50-60 years [2].

These concerns have forced the development of environmentally friendly, sustainable and biodegradable polymers and composites in recent years [2-4]. Biodegradable polymers are generally defined as those that decompose in natural aerobic (composting) and anaerobic (landfill) environments [2]. Biodegradation of biodegradable polymers can be achieved by enabling microorganisms in the environment to metabolize the polymer to produce an inert humus-like material that is less harmful to the environment and can get easily blended with the natural soil. They may be composed of either biopolymers, whose components are derived from renewable raw materials, or biodegradable petroleum-based polymers [2-4].

Microfibrillated cellulose (MFC) can be obtained by mechanical treatment, primarily shearing, of pulp cellulose fibers to small diameter fibrils through refining and high-pressure homogenization processes [5-8]. Since the widths of the fibrils in MFC are in submicron range, they are considered as nanofibers [5, 6, 9-11]. However, being cellulose, MFC is biodegradable. The MFC has high aspect ratio and high tensile properties as a result of high orientation and crystallinity. Their modulus is estimated at 140 GPa and tensile strength between 2 and 6 GPa [12]. Most efforts until now have been focused on fabrication of MFC based composites using nonbiodegradable phenolic and other resins [5, 9-11]. Such composites, although greener, are not fully biodegradable and still need to be disposed of in landfills at the end of their life.

Polyvinyl alcohol (PVA) is a thermoplastic and biocompatible petroleum based polymer. It is also one of the rare polymers with a carbon-carbon single bond backbone that is fully biodegradable [2]. Because of the hydroxyl (-OH) groups on alternating carbon atoms PVA is strongly hydrophilic and soluble in water, which helps to promote its degradation through hydrolysis [2]. Besides, hydroxyl groups in PVA are expected to form hydrogen bonds and acetal linkages with other materials such as cellulose and aldehydes when put together [13, 14].

MFC contains very short fibers while PVA has relatively lower stiffness and strength [5-14]. Fabricating biodegradable MFC reinforced PVA composite may be a potential way to address the application limitations of MFC and PVA. Such composites should have excellent mechanical properties because of strong hydrogen bonding between MFC and PVA. MFC-PVA composites have been reported earlier but without any PVA modifications [15].

Crosslinking has been commonly used to improve the mechanical and thermal properties as well as solubility of polymers. When used as resin, crosslinked polymers can also improve composite properties. Crosslinking is the process of chemically joining two or more molecules

at different locations along the length by covalent bonds. Crosslinkers are commonly selected on the basis of their chemical reactivities with the functionalities present on the polymers [16]. Glyoxal is the smallest dialdehyde which has the ability to crosslink a wide range of polymer, including cellulose and PVA [17, 18]. Glyoxal and gluteraldehyde have been shown to crosslink both cellulose and PVA, separately [9, 18, 19]. However, glyoxal is also readily biodegradable and less toxic than glutaraldehyde [17-20].

Both PVA and MFC are fully biodegradable and as a result composites made using the two are also are expected to be biodegradable [2, 5-11]. However, biodegradation investigation experiments involving MFC-PVA composites and glyoxal crosslinked PVA are currently ongoing in our lab and will be reported when the study is complete.

In the present study, two types of thin membrane-like MFC reinforced biodegradable composites: MFC-PVA composites and glyoxal crosslinked MFC-PVA composites have been fabricated and characterized. The MFC content in these composites could be easily controlled as desired. The membrane-like composites had smooth surfaces and their tensile and thermal properties were excellent. The crosslinked composites had significantly better properties.

4.3 Materials and methods

4.3.1 Preparation of PVA and crosslinked PVA using glyoxal

PVA powder (M_w 31,000-50,000, 98-99% hydrolyzed, Aldrich, St. Louis, MO) was added to the deionized water at a weight ratio of 1:9 to form PVA solution kept in a water bath at 80^{o}C and stirred for 30 min. Glyoxal solution (Glyoxal, 25 wt% solution in water, Aldrich, St. Louis, MO) was added to the PVA solution. The glyoxal:PVA weight ratio was 3:100. The pH of the mixture was adjusted to 3 using phosphoric acid (85 wt% solution in water, Mallinckrodt Baker, Phillipsburg, NJ). The mixture was stirred at 80^{o}C for 1 hr for precuring. The precured mixture

was then cast on Teflon® coated glass plates and dried at RT to form flat precured crosslinked PVA film. The precured film was cured in an oven at 100°C for 1 hr and hot pressed at 80°C under a pressure of 4 MPa for 30 min to form cured crosslinked PVA film. The PVA film was prepared by casting PVA solution without the addition of glyoxal as control, for comparison. Thicknesses of all specimens were about 0.2 mm.

4.3.2 Preparation of MFC suspension

MFC in water (KY-100G) was obtained from Daicel Chemical Industries, Japan. The MFC was added into deionized water at a weight ratio of 1:199. The mixture was stirred using mechanical stirrer at 80°C for 1 hr and followed by ultrasonication (Branson Ultrasonics, Model 2510, Mumbai, India) at 65°C for 1 hr to form MFC suspension and to separate the fibrils.

4.3.3 Fabrication of MFC-PVA composites

The PVA powder was added to the MFC suspension at desired weight ratios. The MFC suspension and PVA powder mixtures were stirred at 80°C for 1 hr and ultrasonicated at 65°C for 1 hr. The mixtures were cast on Teflon® glass plate and slowly dried at RT to form MFC-PVA composites (5, 10, 15, 20, 30, 40 and 50% MFC contents (by wt) in the composites). The MFC-PVA composites were hot pressed at 80°C and 4 MPa for 30 min to form the final composites. As mentioned previously the specimen thicknesses were about 0.2 mm.

4.3.4 Fabrication of crosslinked MFC-PVA composites using glyoxal

The PVA powder was added to the MFC suspension at desired weight ratios. The mixtures of MFC suspension and PVA powder, at desired ratios, were stirred at 65°C for 1 hr and ultrasonicated at 65°C for 1 hr. Glyoxal solution (25 wt% solution) was then added to the MFC suspension and PVA mixture to obtain the wt ratio of glyoxal to PVA and MFC of 3:100. The pH values of all the mixtures were adjusted to 3 using phosphoric acid. The mixtures were

stirred at 80^{o}C for 1 hr for precuring (partial crosslinking). The precured mixtures were then cast on Teflon® coated glass plates and dried at RT to form precured crossliked MFC-PVA composites. The precured composites were cured in an oven at 100^{o}C for 30 min and hot pressed at 80^{o}C and 4 MPa for 30 min to form cured, crosslinked MFC-PVA composites. The MFC content in crosslinked MFC-PVA composites was controlled at 10 (by wt) for comparison with corresponding noncrosslinked MFC-PVA composites. The specimen thicknesses again were about 0.2 mm.

4.3.5 Characterization

4.3.5.1 SEM analysis

MFC-PVA composites (10% MFC) were sputter coated with gold and their surface and fracture topographies were observed with scanning electron microscope (SEM Leica 440, Leica Microsystems, Cambridge, UK) at an accelerating voltage of 15 kV.

4.3.5.2 ATR-FTIR spectroscopy

Chemical analysis of MFC-PVA composites (10% MFC) and its glyoxal crosslinked specimens was carried out using an FTIR spectrophotometer (Nicolet Magna-IR 560, Thermo Scientific, Waltham, MA) in attenuated total reflection (ATR) mode using a split pea accessory. Spectra, averaged over 64 scans, were taken in the range of 4000-800 cm^{-1} wavenumber at a resolution of 4 cm^{-1}. All composite specimens were dried prior to conducting the spectroscopy.

4.3.5.3 Sol-gel and swelling analyses

PVA and glyoxal crosslinked PVA specimens (crosslinked PVA film and the crosslinked MFC-PVA composites, 10% MFC) were fully dried at 105^{o}C for 12 hr prior to conducting the sol-gel test. The specimens were weighed to obtain their initial dry weights and then immersed in distilled water in 150 mL glass bottles. The mixtures in the glass bottles were then placed on a

shaker table (MAXQ 4450, Thermo Scientific, Waltham, MA) at 65°C and 150 rpm until the control (noncrosslinked) PVA was completely dissolved. The solid contents for all crosslinked specimens were then washed three times and filtered using a Whatman® filter paper (Number 4, 20-25 μm pore size) to obtain final residues. The water-soluble portion (sol) and particles smaller than the pore size of the filter paper were removed. The final residues of the crosslinked PVA and the crosslinked MFC-PVA composites, were dried at 105°C for 12 hr to obtain their dry wt (gel). Ratios of the gel wt of the crosslinked PVA to their corresponding initial dry wt were used to determine the PVA gel (crosslinked) percentages. The MFC wt in the crosslinked MFC-PVA composites were regarded as constant before and after the test.

PVA and glyoxal crosslinked PVA specimens (crosslinked PVA film or crosslinked MFC-PVA composite, 10% MFC) were dried at 105°C for 12 hr prior to conducting the swelling test. The specimens were weighed to obtain their initial dry wt and then immersed in distilled water in 150 mL glass bottles at RT for 24 hr. The surface water from the swollen specimens was wiped using Kimwipe® paper tissue to remove excess water weighed again to obtain the swollen wt. Ratios of the wt of absorbed water by the specimens to their corresponding initial dry wt were used to determine the swelling powers of the control and crosslinked PVA. The MFC wt in the crosslinked MFC-PVA composites was regarded as constant, before and after the test.

4.3.5.4 Tensile properties and moisture content

The tensile tests were performed using an Instron universal testing machine (model 5566). The specimens for PVA, MFC-PVA composites (5, 10, 15, 20, 30, 40 and 50% MFC), glyoxal crosslinked PVA and glyoxal crosslinked MFC-PVA composites (10% MFC) were cut to 10 mm x 60 mm strips. Tensile properties of all specimens were measured from the tests conducted as per ASTM D-882-02. Specimen gauge length of 30 mm and strain rate of 0.02 were used for all

specimens. Specimens were conditioned at 21 ℃ and 65% RH for 3 days prior to testing.

Percent moisture content (MC%) of all conditioned specimens were measured as per ASTM D 2654-89a. To obtain the MC% values specimens were dried at 105^{o}C until their wt stabilized. The MC% values were calculated using the dry wt and corresponding conditioned wt.

4.3.5.5 Thermogravimetric analysis (TGA)

Thermogravimetric analysis (TGA Model Q500, TA Instrument, New Castle, DE) was used to analyze the thermal properties of all specimens. Specimens were dried in an oven at 45^{o}C for 12 hr prior to conducting the tests. All TGA tests were performed under a nitrogen atmosphere by keeping the flow rate of 60 ml/min, between 25 and 800^{o}C and at a scanning rate of 10^{o}C/min.

4.3.5.6 Differential scanning calorimetry (DSC)

Differential scanning calorimetry (DSC, Model Q2000, TA Instrument, New Castle, DE) was used to analyze the glass transition temperature (T_g), melting temperature (T_m), enthalpy of fusion (ΔH_f) and crystallinity of PVA, MFC-PVA composites (10% MFC) and their glyoxal crosslinked specimens. All specimens were dried in an oven at 105^{o}C for 12 hr prior to conducting the test. All DSC analyses were performed under a nitrogen atmosphere by keeping the flow rate of 50 ml/min, between -20 and 250^{o}C and at a scanning rate of 10^{o}C/min.

4.4 Results and discussions

4.4.1 SEM images of MFC-PVA composite surface and fracture topographies

Figure 4.1 shows typical SEM images of MFC-PVA composite (noncrosslinked, 10% MFC), surface topography (A) that shows the MFC distribution and facture surface (B) after tensile testing. From Figure 4.1 (A), it can be clearly seen that the MFC fibrils are randomly organized but uniformly distributed within PVA and some of them are just at the surface of the composite. Figure 4.1 (B) clearly shows the MFC fibrils protruding out from the PVA at the facture surface.

However, the protruding fibril lengths are very short. This indicates that the PVA-MFC bonding is strong. The MFC fibrils also seem to be distributed uniformly within the PVA at the facture surface. This is expected since both PVA and MFC have hydroxyl groups and can mix and disperse easily and also form hydrogen bonds at multiple locations. In addition, the fibrils also look oriented in the direction of the stress. This is due to the high fracture strain of the noncrosslinked composites which allows orientation during the tensile test.

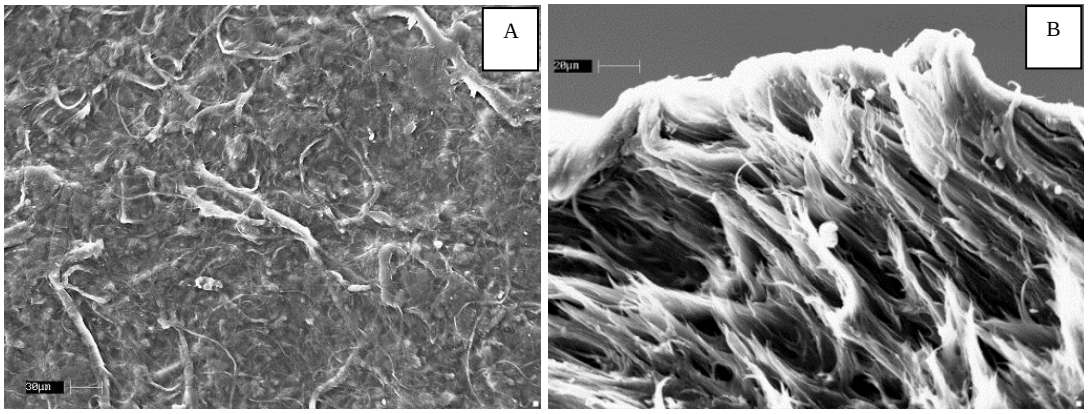

Figure 4.1 Typical SEM images A: Surface topography of the MFC-PVA composites; B: Fracture surface of the MFC-PVA composite. Both specimens contain 10% MFC

4.4.2 ATR-FTIR analysis of crosslinked and noncrosslinked MFC-PVA composites

Figure 4.2A shows typical crosslinking of glyoxal with PVA or MFC. In the present case three possible crosslinking reactions can occur; between the PVA molecules, between the MFC fibrils and between PVA and MFC.

Figure 4.2B shows the ATR-FTIR spectra for control MFC-PVA composites (a) and glyoxal crosslinked MFC-PVA composites (b). A broad band at 3550-3200 cm^{-1}, wavenumber seen in both spectra, is a result of the hydroxyl (O-H) stretching vibration resulting from the strong intra-molecular and inter-molecular hydrogen bonds [21, 22]. The absorption band observed between 3000 and 2820 cm^{-1} wavenumbers is due to the stretching of aliphatic C-H bond [22]. The absorbance intensity ratio of bands for O-H to C-H showed a decrease from 1.81 for spectrum (a)

to 1.28 for spectrum (b). This lower absorption clearly indicates a reduction in the O-H groups due to crosslinking by glyoxal [22]. Absorption at 1750-1700 cm^{-1} (stretching of C=O) for noncrosslinked specimen (spectrum (a)) was weak (intensity ratio of C=O to C-H = 0.35) and indicates the presence of carbonyl (C=O) in the composites from the non-hydrolyzed acetate group remaining in the PVA, confirming the results obtained by Gohil et al. [21] and Mansur et al. [22]. In spectrum (b), however, a sharp absorption (intensity ratio of C=O to C-H = 0.63) observed at 1750-1700 cm^{-1} wavenumber indicates strong presence of C=O in the crosslinked resin of the composites. This shows that in addition to the non-hydrolyzed vinyl acetate groups, some residual unreacted aldehyde groups from glyoxal also exist in the crosslinked MFC-PVA composites, both contributing to the stronger C=O absorption. Glyoxal may exist as half (one group) reacted or fully unreacted. The absorption at 1150-1050 cm^{-1} wavenumber in spectrum (a) is due to C-O stretching vibration from the acetate group [21-23]. The intensity of absorption band for C-O stretching vibration was stronger in spectrum (b) (intensity ratio of C-O to C-H = 3.38) than in spectrum (a) (intensity ratio of C-O to C-H = 2.72), resulting from the formation of the acetal linkages (shown in Figure 2A) upon reaction of the composites with the glyoxal.

Overall, the ATR-FTIR results indicate that the MFC-PVA composites were crosslinked based on the decreased intensity of bands for O-H stretching vibration combined with the increased intensity of bands for C=O and C-O stretching vibrations. As mentioned earlier, the crosslinking reactions can occur between the MFC fibrils or the PVA resin or between MFC and PVA.

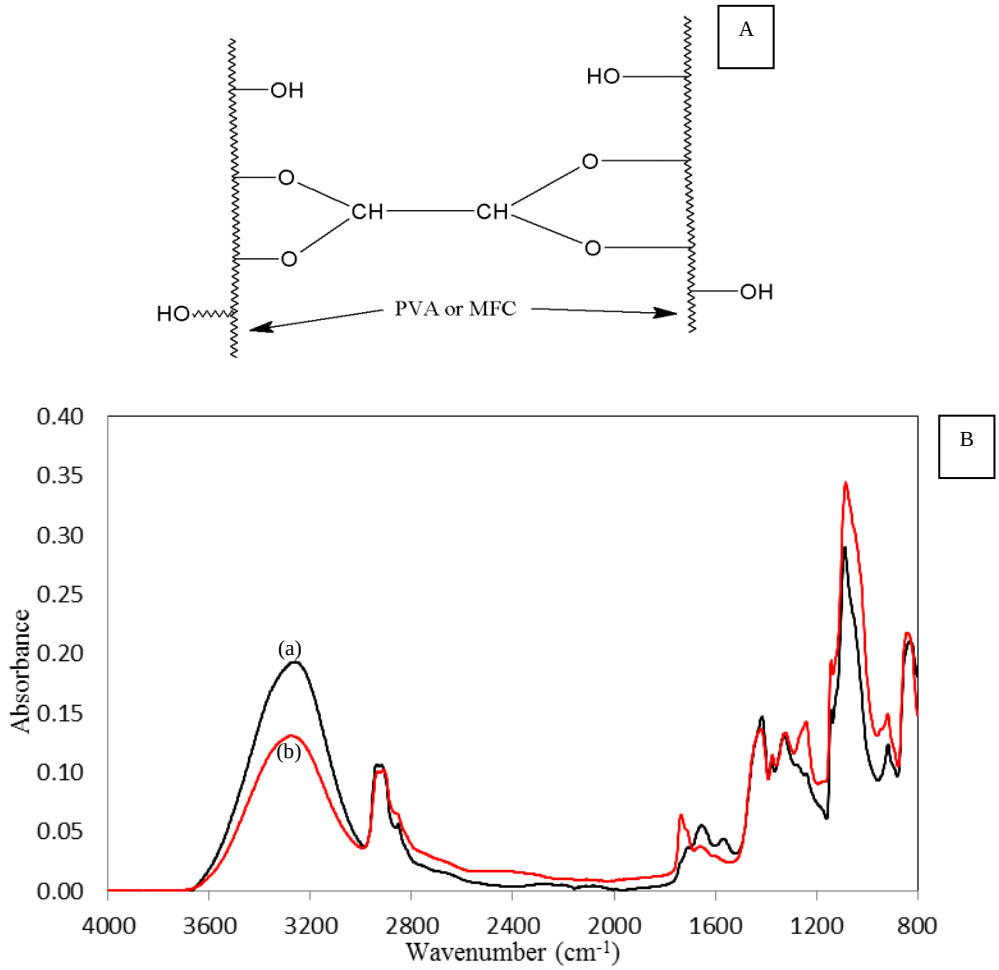

Figure 4.2 A: Schematic of the acetal linkage in glyoxal crosslinked PVA or MFC structure; B: FTIR spectra of MFC-PVA composites (a: 10% MFC) and glyoxal crosslinked MFC-PVA composites (b: 10% MFC)

4.4.3 Sol-gel and swelling analyses

Sol-gel and swelling analyses were performed for noncrosslinked (control) and crosslinked PVA, as well as for the crosslinked MFC-PVA composites to evaluate the crosslinking levels. Table 4.1 presents the sol-gel and swelling results for crosslinked PVA as well as control PVA. The results show that the PVA gel (crosslinked) percentages of the crosslinked PVA and the resin in the crosslinked MFC-PVA composites were 7.0% and 6.6%, respectively, while the control PVA dissolved completely during the sol-gel test. The low gel percentage suggests that the PVA was only partially crosslinked. The results also show that the swelling powers of crosslinked

PVA and the resin in the crosslinked MFC-PVA composites were 78.3% and 75.1% respectively, much lower than control PVA (105.6%), confirming the crosslinking, though only partial.

Table 4.1 Sol-gel and swelling power results of PVA and glyoxal crosslinked PVA

Tests	PVA	Crosslinked PVA	PVA in crosslinked MFC-PVA composites
Gel percentage (%)	0	7.0 (8.3)*	6.6 (10.3)
Swelling power (%)	105.6 (5.5)	78.3 (2.7)	75.1 (8.8)

**: values in the parentheses are % coefficient of variation values*

4.4.4 Tensile properties and moisture content

Table 4.2 presents the tensile test and moisture content results for pure (control) PVA and noncrossllinked MFC-PVA composites with MFC contents from 5 to 50%. The Young's modulus of the control PVA was 248 MPa. The Young's modulus of the MFC-PVA composites were significantly higher than for PVA and increased with the MFC content, as can be expected. For composites with 5 and 10% MFC content, the Young's moduli were 687 MPa and 1033 MPa, respectively. When the MFC content increased to 50% the Young's modulus increased to 3898 MPa, about 16 times that of control PVA. This is expected since the Young's modulus for MFC is much higher [12]. The facture stress for the control PVA was 34.1 MPa. The fracture stress values for MFC-PVA composites with 5 and 10%, MFC content were 43.3 MPa and 53.5 MPa, respectively, and increased to 89.9 and 84.9 MPa when the MFC content increased to 40 and 50%, respectively. This is again because the MFC has fracture stress is between 2 and 6 GPa [12]. The facture stress of MFC-PVA composites with 50% MFC, however, was lower than the composites with 40% MFC. This is due to the lower fracture strain (5.1%) of the composites with 50% MFC content compared to 8% obtained for composites with 40% MFC. Similar trend of increase in Young's modulus and fracture stress with increase in MFC content have been reported earlier by Lu et al. [15]. The fracture strain for control PVA was 331%. The facture

strains for the MFC-PVA composites were much lower than that obtained for PVA and decreased as the MFC content increased. This is due to the lower facture strain value of MFC. The moisture content for PVA was 9.1%, and the moisture content values for MFC-PVA composites were observed to be within a narrow range of 7.1% to 8.1%. This is because moisture content values of MFC and PVA are very close.

Table 4.2 Tensile properties for MFC-PVA composites with varying MFC content

Weight percentage of MFC content in MFC-PVA composites	Young's modulus (MPa)	Fracture stress (MPa)	Fracture strain (%)	Moisture content (%)
0 (PVA)	248 (22.9)	34.1 (13.3)	331 (15.4)	9.1 (4.2)
5	687 (10.3)	43.3 (4.6)	34.7 (13.4)	7.7 (5.5)
10	1033 (7.2)	53.5 (5.6)	25.2 (23.7)	7.4 (11.8)
15	1399 (13.6)	65.0 (8.0)	18.3(12.1)	7.3 (25.1)
20	1707 (8.0)	69.6 (8.3)	15.2 (12.4)	8.0 (1.0)
30	2538 (10.7)	81.6 (7.7)	8.9 (18.8)	8.1 (2.9)
40	3409 (9.4)	89.9 (13.5)	8.0 (26.2)	7.1 (12.6)
50	3898 (21.3)	84.9 (11.9)	5.1 (31.7)	7.7 (20.3)

**: values in the parentheses are % coefficient of variation values*

Table 4.3 presents tensile test and moisture content results for PVA, MFC-PVA composites (10% MFC) and their corresponding glyoxal crosslinked specimens. The Young's moduli of the crosslinked PVA and crosslinked MFC-PVA composites increased to 666 MPa and 1404 MPa, from 248 MPa for control PVA and 1033 MPa for MFC-PVA composites, respectively. It is obvious that the increase in Young's modulus for the PVA and MFC-PVA composites is due to the crosslinking of the PVA which makes the structure rigid [24]. In the case of the MFC-PVA composites, not only the PVA is crosslinked but the MFC fibrils can also get crosslinked between

themselves as well as with PVA. The reduction in moisture content from 9.1% for the PVA to 5.5% after crosslinking and from 7.4% for the MFC-PVA composites to 7.3% for the crosslinked MFC-PVA composites is also responsible, at least partially, for higher Young's modulus. From data in Table 4.3, it is also clear that after crosslinking, PVA fracture strain is significantly lower. However, MFC-PVA composites fracture strains did not change after crosslinking since this property is controlled by the MFC. While crosslinking increased the PVA fracture stress from 34.1 MPa to 47.7 MPa, MFC-PVA composites showed no significant change. This is because the crosslinked composites showed sharp yielding. And after the yielding, the stress remained the same. As a result, no change in the fracture stress was observed. Similar effect has also been observed in the case of bacterial cellulose reinforced PVA composites [25].

Table 4.3 Tensile properties for PVA, MFC-PVA composites and their glyoxal crosslinked specimens

Specimens	Young's modulus (MPa)	Fracture stress (MPa)	Fracture strain (%)	Moisture content (%)
PVA	248 (22.9)	34.1 (13.3)	331 (15.4)	9.1 (4.2)
Crosslinked PVA	666 (9.5)	47.7 (7.5)	184(16.3)	5.5 (28.5)
MFC-PVA (10 wt% MFC content)	1033 (7.2)	53.2 (5.6)	25.2 (23.7)	7.4 (11.8)
Crosslinked MFC-PVA (10 wt% MFC content)	1404 (9.4)	53.7 (7.1)	29.6 (16.8)	7.3 (1.7)

**: values in the parentheses are % coefficient of variation values*

It should be noted that tensile properties of MFC-PVA composites and crosslinked MFC-PVA composites are comparable or higher than many traditional polymers, including polyethylene (Young's modulus: 800 MPa; fracture stress: 15 MPa), polypropylene (Young's modulus: 1900 MPa; fracture stress: 40 MPa), and nylon 6 (Young's modulus: 1800 MPa; fracture stress: 70 MPa) [26]. In addition, fabrication process for the biodegradable MFC-PVA composites is

convenient and simple and the cost for raw materials is low. Therefore, both crosslinked and noncrosslinked MFC-PVA composites have the potential to replace traditional non-biodegradable plastic materials in many applications, including racket frame, ski pole, circuit board, automobile inside etc. These degradable composites may be easily protected from water by applying varnish or other water-resistant coatings to increase their durability. Also, their moisture sensitivity is lower after crosslinking, making them more useful.

4.4.5 Thermogravimetric analysis

Figure 4.3A presents typical TGA thermograms of PVA, MFC-PVA composites (10% and 40% MFC) and MFC. Thermogram 4.3A (a) for control PVA shows two decomposition onset temperatures, (T_{d1}) and (T_{d2}), at 257^{o}C and 400^{o}C, respectively. Weight losses for the PVA were 30% at 272^{o}C, 50% at 281^{o}C and up to 94% at 800^{o}C. Two-step-degradation of PVA has been reported earlier by Peng and Kong [26]. A likely explanation for this is that PVA first degrades into smaller molecular weight polymer at around 250^{o}C by chain scission and degrades further into carbon char at temperatures above 350^{o}C. Results of this study confirm the earlier findings [27]. Thermograms 4.3A (b) and 4.3A (c) for MFC-PVA composites with 10 and 40% MFC, respectively, also show two decomposition temperatures. Their T_{d1} and T_{d2} are very close to those observed for PVA, at 255^{o}C and 400^{o}C, respectively. Weight losses observed for the MFC-PVA composites (10% MFC) were 30% at 272^{o}C, 50% at 288^{o}C and 92% at 800^{o}C. Weight losses observed for the MFC-PVA composites (40% MFC) were 30% at 285^{o}C, 50% at 313^{o}C (both temperatures higher than those obtained for MFC-PVA composites with 10% MFC) and 92% at 800^{o}C. Thermogram 4.3A (d) for MFC showed a single decomposition onset temperature (T_{d}) at 315^{o}C. Weight losses observed for pure MFC were 30% at 326^{o}C, 50% at 340^{o}C and 85% at 800^{o}C, indicating higher thermal stability than PVA and close to the values

obtained by Quiévy et al. [28]. Thus it is obvious that MFC reinforcement is responsible for the higher thermal stability of the MFC-PVA composites. This conclusion is in agreement with the result in obtained in a previous study by Lu et al. [15].

Figure 4.3B presents typical TGA thermograms of PVA, MFC-PVA composites (10% MFC) and their corresponding glyoxal crosslinked specimens. Thermograms 4.3B (a) and 4.3B (b) are for PVA and MFC-PVA composites, respectively, and have been described in the last paragraph. Thermogram 4.3B (c), for crosslinked PVA, also shows a two-step degradation pattern with T_{d1} and T_{d2} observed at 370^{o}C and 410^{o}C, respectively. However, the steps are not as distinct compared to the control PVA. The weight losses observed were 30% at 303^{o}C, 50% at 368^{o}C and 91% at 800^{o}C. These temperatures are significantly higher than those obtained for control PVA indicating that the crosslinked PVA has significantly higher thermal stability as is the case for many polymers [29-31]. Similarly thermogram 4.3B (d) for crosslinked MFC-PVA composites also shows a two-step degradation pattern with T_{d1} and T_{d2} observed at 380^{o}C and 410^{o}C, respectively. Weight losses observed were 30% at 305^{o}C, 50% at 358^{o}C and 90% at 800^{o}C. As is expected these values are close to those obtained for the crosslinked PVA, the major constituent. These results clearly indicate that glyoxal crosslinking can increase the thermal stability of PVA and the MFC-PVA composites in addition to enhancing their tensile properties.

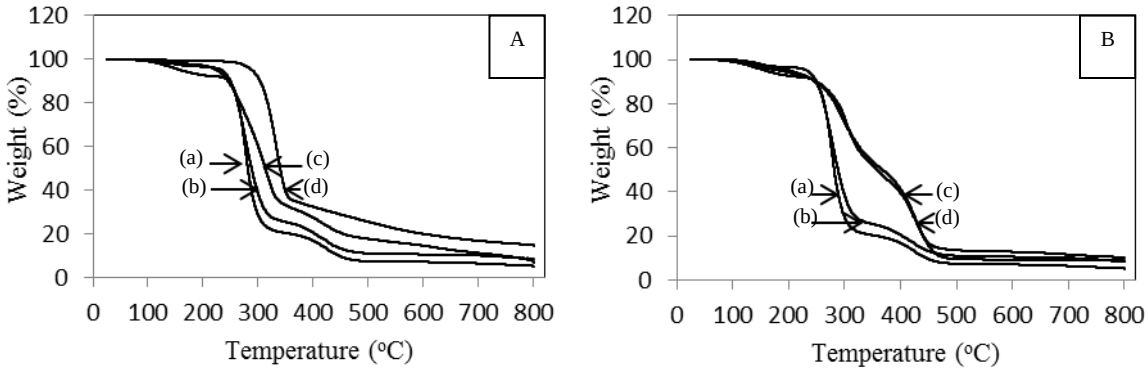

Figure 4.3 TGA thermograms A: PVA (a), MFC-PVA composites (b: 10% MFC), MFC-PVA composites (c: 40% MFC) and MFC (d); B: PVA (a), MFC-PVA composites (b: 10% MFC), glyoxal crosslinked PVA (c) and glyoxal crosslinked MFC-PVA composites (d: 10% MFC)

4.4.6 Differential scanning calorimetry

Typical DSC thermograms for PVA and glyoxal crosslinked PVA are presented in Figure 4.4A. Thermogram 4.4A (a) shows T_g and T_m of 92.1°C and 195.4°C, respectively, for PVA. The ΔH_f of 86.9 J/g, compared to 138.6 J/g for 100% crystalline PVA resulted in a crystallinity of 62.7% for control PVA [32-35]. Thermogram 4.4A (b) for the crosslinked PVA shows T_g and T_m of 110°C and 175.4°C, respectively. The ΔH_f and the crystallinity of the crosslinked PVA were 55.3 J/g and 39.9%, respectively. The lower ΔH_f and higher T_g further confirm that the PVA was partially crosslinked by glyoxal. The higher T_g and lower crystallinity after crosslinking due to restricted segmental motion, have been observed in most polymers [1, 32, 36, 37].

Figure 4.4B presents typical DSC thermograms of (a) MFC-PVA composites and (b) glyoxal crosslinked MFC-PVA composites. The T_g and T_m for the MFC-PVA composites were observed at 92.0°C and 197.5°C, respectively. These values are close to those obtained for PVA. While the T_g of cellulose is around 230°C, the MFC is highly crystalline and hence does not show any T_g. Also, no T_m for cellulose can be observed since it degrades prior to melting [38, 39]. As a result, the DSC thermogram mainly represents the PVA behavior. The conclusion here is in

agreement with the phenomenon observed by Lu et al. [15]. The ΔH_f and the crystallinity of the PVA in MFC-PVA composites were 61.4 J/g and 44.3%, respectively, which were much lower than 86.9 J/g and 62.7%, respectively, obtained for control PVA. It is likely that the nano- and micro-fibrils in the MFC can inhibit the crystallization of PVA, as they are well dispersed. The fibrils can suppress the free movement of polymeric chains restricting their ability to fold and thus lower the crystallinity [40]. Thermogram 4.4B (b) is for crosslinked MFC-PVA composites but mainly represents crosslinked PVA behavior. The T_g and T_m observed were 110.2^{o}C and 178.8^{o}C, respectively, and confirm that glyoxal crosslinking can increase T_g, decrease the T_m of PVA. These changed characteristics are reflected in the crosslinked MFC-PVA composites. The ΔH_f and crystallinity of PVA in crosslinked MFC-PVA composites were 50.5 J/g and 36.4%, respectively. These are lower than the PVA in MFC-PVA composites and slightly lower than those for the crosslinked PVA, showing the combined effect of crosslinking and the ability of the MFC to restrain the molecular motion needed for crystallization.

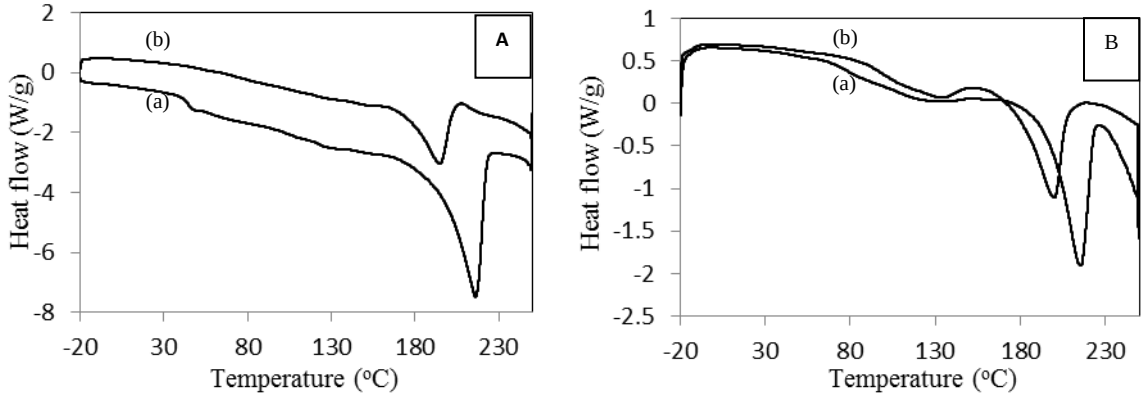

Figure 4.4 DSC thermograms A: PVA (a) and glyoxal crosslinked PVA (b); B: MFC-PVA composites (a: 10% MFC) and glyoxal crosslinked MFC-PVA composites (b: 10% MFC)

4.5 Conclusions

The biodegradable membrane-like MFC-PVA composites with differing MFC contents were produced using simple blending and casting method. The SEM images of surface and fracture

topographies indicated that MFC was uniformly distributed in PVA and the MFC-PVA bonding was strong. Crosslinks can be formed using glyoxal between PVA, MFC and MFC-PVA. Crosslinked PVA was partially water-insoluble with decreased swelling ability. PVA and MFC-PVA composites showed higher mechanical properties and thermal stability after crosslinking. MFC reinforcement also was responsible for higher thermal stability of the composites. At the same time the fracture strain decreased significantly with crosslinking. The DSC also showed higher T_g and lower T_m and lower crystallinity of the PVA in MFC-PVA composites as a result of glyoxal crosslinking.

4.6 Acknowledgements

This work was partly supported by the National Textile Center (NTC) and the Wallace Foundation. The authors also thank the Cornell Center for Materials Research (CCMR) for the use of their facilities.

References

[1] Young RJ, Lovell PA. Introduction to polymers, 3rd edition. CRC Press, Boca Raton, FL, 2011, pp. 591-622.

[2] Stevens ES. Green plastics: an introduction to the new science of biodegradable plastics, Princeton University Press, Princeton, NJ, 2002, pp.10-30.

[3] Netravali AN, Chabba S. 'Composites get greener'. Materials Today, 2003, 6 (4): 22-29.

[4] Georgia Tech Research Institute . 'Breaking down plastics: new standard specification may facilitate use of additives that trigger biodegradation of oil-based plastics in landfills'. http://gtresearchnews.gatech.edu/biodegradation-of-plastics/, Accessed November 2011.

[5] Nakagaito AN, Yano H. The effect of fiber content on the mechanical and thermal expansion properties of biocomposites based on microfibrillated cellulose. Cellulose, 2008, 15: 555-559.

[6] Nakagaito AN, Fujimura A, Sakai T, Hama Y, Yano H. Production of microfibrillated cellulose (MFC)-reinforced polylactic acid (PLA) nanocomposites from sheets obtained by a papermaking-like process. Composites Science and Technology, 2009, 69:1293-1297.

[7] Zou Y, Hsieh J. Review of microfibrillated cellulose for papermaking. http://www.tappi.org/Downloads/Conference-Papers/2007/07NAN/07NAN18.aspx, 2007, Accessed November 2011.

[8] Huang X, Netravali AN. Biodegradable green composites made using bamboo micro/nano-fibrils and chemically modified soy protein resin. Composites Science and Technology, 2009, 69: 1009-1015.

[9] Stenstad P, Andresen M, Tanem BS, Stenius P. Chemical surface modifications of microfibrillated cellulose. Cellulose, 2008, 15: 35-45.

[10] Nakagaito AN, Yano H. The effect of morphological changes from pulp fiber towards nano-scale fibrillated cellulose on the mechanical properties of high-strength plant fiber based composites. Applied physics A, 2004, 78: 547-552.

[11] Nakagaito AN, Yano H. Novel high-strength biocomposites based on microfibrillated cellulose having nano-order-unit web-like network structure. Applied physics A, 2005, 80: 155-159.

[12] Nakagaito AN, Iwamoto S, Yano H. Bacterial cellulose: the ultimate nano-scalar cellulose morphology for the production of high-strength composites. Applied Physics A, 2005, 80: 93-97.

[13] Wang J, Gao C, Zhang Y, Wan Y. Preparation and in vitro characterization of BC/PVA hydrogel composite for its potentisl use as artificial corena biomaterial. Material Science and Engineering C, 2010, 30: 214-218.

[14] Millon LE, Oates CJ, Wan WK. Compression properties of polyvinyl alcohol-bacterial cellulose nanocomposite. Journal of Biomedical Materials Research Part B: Applied Biomaterials, 2009, 90B (2): 922-929.

[15] Lu J, Wang T, Drzal LT. Preparation and properties of microfibrillated cellulose polyvinyl alcohol composite materials. Composites: Part A, 2008, 39, 738-746.

[16] Thermo Scientific. Thermo scientific pierce-crosslinking technical handbook, http://www.piercenet.com/files/1601673_Crosslink_HB_Intl.pdf, Accessed November 2011.

[17] BASF. Glyoxal-the sustainable solution for your business. http://worldaccount.basf.com/wa/NAFTA/Catalog/ChemicalsNAFTA/doc4/BASF/PRD/30037091/.pdf?title=Brochure&asset_type=pi/pdf&language=EN&urn=urn:documentum:eCommerce_sol_EU:09007bb2800475c8.pdf, Accessed November 2011.

[18] Zhang Y, Zhu PC, Edgren D. Crosslinking reaction of poly(vinyl alcohol) with glyoxal.

Journal of Polymer Research, 2010, 17 (5): 725-730.

[19] BASF. Glyoxal as a cellulose crosslinker. http://www.intermediates.basf.com/chemicals/glyoxal/crosslinker-for-cellulose, Accessed November 2011.

[20] MSDS. http://www.msdsonline.com, Accessed November 2011.

[21] Gohil JM, Bhattacharya A, Ray P. Studies on the cross-linking of poly (vinyl alcohol). Journal of Polymer Research, 2006, 13: 161-169.

[22] Mansur HS, Sadahira CM, Souza AN, Mansur AAP. FTIR spectroscopy characterization of poly (vinyl alcohol) hydrogel with different hydrolysis degree and chemically crosslinked with glutaraldehyde. Material Science and Engineering C, 2008, 28: 539-548.

[23] Kim JH, Moon EJ, Kim CK. Composite membranes prepared from poly (m-animostyrene-co-vinyl alcohol) copolymers for the reverse osmosis process. Journal of Membrane Science, 2003, 216: 107-120.

[24] Zhang L, Chen P, Huang J, Yang G, Zheng L. Way of strengthening biodegradable soy-dreg plastics. Journal of Applied Polymer Science, 2003, 88: 422-427.

[25] Qiu K, Netravali AN. Bacterial cellulose-based membrane-like biodegradable composites using cross-linked and noncross-linked polyvinyl alcohol. Journal of Material Science, 2012, 47 (16): 6066-6075.

[26] Tensile property testing of plastics - MatWeb. http://www.matweb.com/reference/tensilestrength.aspx, 2010, Accessed November 2011.

[27] Peng Z, Kong LX. A thermal degradation mechanism of polyvinyl alcohol/silica nanocomposites. Polymer Degradation and Stability, 2007, 92: 1061-1071.

[28] Qui évy N, Jacquet N, Sclavons M, Deroanne C, Paquot M, Devaux J. Influence of

homogenization and drying on the thermal stability of microfibrillated cellulose. Polymer Degradation and Stability, 2010, 95: 306-314.

[29] Chabba S, Matthews GF, Netravali AN. 'Green' composites using cross-linked soy flour and flax yarns. Green Chemistry, 2005, 7: 576-581.

[30] Rodrigues FT, Martins VCA, Plepis AMG. Porcine skin as a source of biodegradable matrices: alkaline treatment and glutaraldehyde crosslinking. Polimeros, 2010, 20 (2): 92-97.

[31] Liu BS, Yao CH, Fang SS. Evaluation of a non-woven fabric coated with a chitosan Bi-layer composite for wound dressing. Macromolecular Bioscience, 2008, 8 (5): 432-440.

[32] Warner SB. Fiber Science. Prentice Hall, Upper Saddle River, NJ, 1995, pp. 205-206.

[33] Blaine RL. Determination of polymer crystallnity by DSC. TA Instruments, www.tainstruments.com/library_download.aspx?file=TA123.PDF, Accessed December 2011.

[34] Sichina WJ. DSC as problem solving tool: measurement of percent crysallnity of thermoplastics. PerkinElmer Instruments, http://www.perkinelmer.com/Content/applicationnotes/app_thermalcrystallinitythermoplastics.pdf , Accessed December 2011.

[35] Guirguis OW, Moselhey MTH. Thermal and structural studies of poly (vinyl alcohol) and hydroxypropyl cellulose blends. Natural Science, 2012, 4 (1): 57-67.

[36] Kim JH, Kim JY, Lee YM, Kim KY. Properties and swelling characteristics of cross-linked poly (vinyl alcohol)/chitosan blend membrane. Journal of Applied Polymer Science, 1992, 45 (10): 1711-1717.

[37] Mtshali TN, Krupa I, Luyt AS. The effect of cross-linking on the thermal properties of LDPE/wax blends. Thermalchimica Acta, 2001, 380: 47-54.

[38] Gardner DJ, Oporto GS, Mills R, Samir MASA. Adhesion and surface issues in cellulose

and nanocellulose. Journal of Adhesion Science and Technology, 2008, 22: 545-567.

[39] Yan C, Zhang J, Lv Y, Yu J, Wu J, Zhang J, He J. Thermoplastic cellulose-graft-poly (L-lactide) copolymers homogeneously synthesized in an lonic liquid with 4-deimethylaminopyridine catalyst. Biomacromolecules, 2009, 10 (8): 2013-2018.

[40] Boudenne A, Ibos, L, Candau Y, Thomas S. Handbook of multiphase polymer systems. John Wiley & Sons Ltd, Chichester, West Sussex, UK, 2011, p. 455.

Chapter 5 Halloysite nanotube reinforced biodegradable nanocomposites using noncrosslinked and malonic acid crosslinked polyvinyl alcohol

Kaiyan Qiu, Anil N. Netravali*
Fiber Science Program, Cornell University, Ithaca, NY 14853-4401

5.1 Abstract

Halloysite nanotubes (HNTs) based thin membrane-like fully biodegradable nanocomposites were produced by blending individualized HNT dispersion with polyvinyl alcohol (PVA). Several separation techniques were applied, sequentially, to obtain stable individualized HNT dispersion. In addition, PVA was crosslinking using malonic acid (MA) as crosslinker and phosphoric acid as catalyst, to increase the mechanical and thermal properties of HNT-PVA nanocomposites. Crosslinking was also intended to make PVA water-insoluble, and hence more useful in commercial applications. Examination of the composites indicated that HNTs were uniformly dispersed in both PVA as well as crosslinked PVA. Excellent mechanical properties of the HNT-PVA nanocomposites were achieved. These nanocomposites could be composted easily and hence would be good candidates to\ replace some of today's traditional non-biodegradable plastics that end up in landfills.

Keywords: A. Nano-structures; A. Polymer-matrix composites (PMCs); B: Mechanical properties; B: Thermal properties; Biodegradable nanocomposites

5.2 Introduction

During the past decade or so polymer property modifications using nanoparticles and formation of nanocomposites has seen significantly increased interest. There are several reasons why nanoparticles with dimensions on the nanometer scale (10^{-9} m) are of interest. Nanoparticles with such small dimensions have been shown to improve not only the mechanical properties of the polymers but, in many cases, their functionalities as well [1-3]. In addition, only small loading of nanoparticles is sufficient to obtain significant property changes.

Halloysite nanotubes based on aluminosilicate clay nanosheets that are naturally rolled to form hollow tubular structures are mined from natural deposits [4, 5]. While the ideal unit formula for halloysite is $Al_2Si_2O_5(OH)_4$. n H_2O (n=0 for halloysite-(7Å) and n=2 for hydrated halloysite-(10Å)), the chemical composition is subject to variation due to the presence of impurities such as Fe oxides [5]. Halloysite has been found to occur widely throughout the world in weathered rocks as well as in soils and has been identified as having formed by the alternation of a wide variety of igneous and non-igneous rocks [4-6]. It is often intermixed with dickite, kaolin, montmorillonite and other clay minerals [6]. Since the dominant morphology of halloysite is tubular, it is commonly termed as halloysite nanotubes (HNTs) [5]. Unlike other nanostructured clays that must be exfoliated, HNTs naturally occur as cylinders with average diameters typically smaller than 100 nm and lengths ranging from 500 nm to over 1.2 μm [6]. HNTs have been used as bioreactor, time-release capsules, catalysts of polymer degradation, templates for depositing other nanoparticles, polymer filler or property modifier as well as in ceramic applications [4].

HNTs have been widely used during recent years to reinforcing the polymer matrices such as epoxy resin, polypropylene, polyamide, styrene rubber and ethylene propylene diene monomer rubber [7-16]. Such nanocomposites, although show good mechanical and thermal properties,

are not biodegradable and need to be disposed of in landfills at the end of their life [7-16]. In the case of biodegradable soy protein based nanocomposites the addition of HNTs was shown to improve their fire resistance [17].

Polyvinyl alcohol (PVA) is a thermoplastic and biocompatible petroleum based polymer. It is also one of the rare polymers with a carbon-carbon single bond backbone that is fully biodegradable [18]. Because of the hydroxyl (-OH) groups on alternating carbon atoms PVA is strongly hydrophilic and soluble in water, which helps to promote its degradation through hydrolysis [18]. However, PVA has relatively low strength and thermal stability for some applications. Fabricating biodegradable HNT-PVA nanocomposites may be a potential way to address some limitations of the PVA. Such nanocomposites can have excellent mechanical properties and thermal stability because the HNTs are stable even at very high temperatures. HNT-PVA nanocomposites have been reported earlier but without proper HNT individualization and any PVA modifications [19, 20]. The present research shows that HNT individualization together with crosslinking of PVA can achieve significantly better properties.

Crosslinking has been commonly used to improve the mechanical and thermal properties as well as solubility of many polymers [21-25]. When used as resin, crosslinked polymers can also improve composite properties. Crosslinking is the process of chemically joining two or more molecules at different locations along their length by covalent bonds. Crosslinkers are commonly selected on the basis of their chemical reactivities with the functionalities present on the polymers [21]. Glutaraldehyde and glyoxal are two universally used crosslinkers for polymers that contain amine groups such as proteins [22-24]. Although both of them are effective in crosslinking polymers, they are relatively toxic [25]. Therefore, less toxic

crosslinkers are of interest in the crosslinking reaction, particularly to maintain the biodegradability of the polymers.

Malonic acid (MA) is a dicarboxylic acid produced from chloroacetic acid and can be used as a crosslinker [26]. In terms of toxicity, it is a much better choice as a crosslinker than glutaraldehyde or glyoxal [25]. Some researchers have shown crosslinking of PVA using dicarboxylic acids, including MA, with sulphuric acid as catalyst to obtain esterification [27, 28]. However, the effectiveness of crosslinking has not been as good as expected and, importantly, the mechanical and thermal properties of PVA after crosslinking were not investigated in these studies.

In the present study, HNT clusters were individualized using several techniques and membrane-like biodegradable HNT-PVA nanocomposites were fabricated and their properties characterized. PVA and HNT-PVA nanocomposites were crosslinked using MA, with phosphoric acid as catalyst. High crosslinking levels of PVA and PVA in HNT-PVA nanocomposites were achieved making PVA water-insoluble. In addition, HNT loading in nanocomposites could be easily controlled as desired. These thin membrane-like nanocomposites had smooth surfaces and their tensile and thermal properties were excellent. The MA crosslinked HNT-PVA nanocomposites showed even better properties.

5.3 Materials and methods

5.3.1 Individualization of HNTs

HNT powder was initially added into deionized water at a weight ratio of 1:49. Tween® 80 (Sigma-Aldrich, St. Louis, MO) (HNT:Tween® 80 (w/w)=10:1) was then added into the mixture, as non-ionic surfactant, to help individualize the HNTs. The pH value of the mixture was adjusted to 10 to further avoid clustering of HNTs [6]. The mixture (at pH=10) was stirred using

mechanical stirrer (Polymix®, PX-SR 90 D, Kinematica Inc., Bohemia, NY) at 90°C and 1000 rpm for 1 hr and followed by ultrasonication (Branson Ultrasonics, Model 2510, Mumbai, India) at 65°C for 1 hr to form original HNT dispersion. The original HNT dispersion was kept standing for 2 days until it was stabilized. The supernatant of the HNT dispersion was used as final individualized HNT dispersion while the solution at the bottom with HNT deposition was removed. The HNT content in the final individualized HNT dispersion was 0.5% by wt.

5.3.2 Preparation of PVA and crosslinked PVA using MA

PVA powder (M_w 31,000-50,000, 98-99% hydrolyzed, Aldrich, St. Louis, MO) was added to the deionized water at a weight ratio of 1:9 to form PVA solution which was maintained in a water bath at 80°C and stirred for 30 min. MA powder (ReagentPlus®, 99%, Sigma-Aldrich, St. Louis, MO) was then added to the PVA solution. The weight ratio of MA and PVA was 1:10. The pH value of the mixture was adjusted to 1 by adding phosphoric acid (85 wt% solution in water, Mallinckrodt Baker, Phillipsburg, NJ). The mixture was stirred at 90°C for 1 hr for precuring. The precured mixture was then cast on Teflon® coated glass plates and slowly dried in an oven at 40°C to form flat precured crosslinked PVA film. The precured film was further hot pressed at 100°C under a pressure of 0.2 MPa for 60 min to form cured crosslinked PVA film. Carboxylic ester linkages are expected to form between hydroxyl group of PVA and carboxylic groups of MA at high temperature during the hotpressing [27, 28]. The cured (crosslinked) PVA film was then immersed into deionized water at RT for 12 hr until the system got stabilized in order to partially remove phosphoric acid, remaining MA and noncrosslinked PVA. The water-immersed and cured crosslinked PVA film was then dried at 40°C to form final crosslinked PVA film. The PVA film was prepared by casting PVA solution without the addition of MA as control, for comparison.

5.3.3 Fabrication of HNT-PVA nanocomposites

The PVA solution (10% by wt) was added to the final individualized HNT dispersion at desired PVA and HNT weight ratios. The HNT dispersion and PVA solution mixtures were stirred at 90^{o}C for 1 hr. The mixtures were cast on Teflon® coated glass plate and slowly dried in an oven at 40^{o}C to form HNT-PVA composite sheets (5, 10 and 20 HNT loading, by wt, in the composites). The HNT-PVA nanocomposite sheets were hot pressed at 100^{o}C and 0.2 MPa for 60 min to form the final nanocomposites.

5.3.4 Preparation of cross-linked HNT-PVA nanocomposites using MA

The 10% (by wt) PVA solution was added to the final individualized HNT dispersion at desired PVA and HNT weight ratios. The HNT dispersion and PVA solution mixtures were stirred at 90^{o}C for 1 hr and ultrasonicated at 65^{o}C for 1 hr. MA powder (ReagentPlus®, 99%, Sigma-Aldrich, St. Louis, MO) was then added to the mixtures. The weight ratio of MA to PVA was 1:10. The pH values of the mixtures were adjusted to 1 by adding crosslinking catalyst phosphoric acid (85 wt% solution in water, Mallinckrodt Baker, Phillipsburg, NJ). The mixtures were stirred at 90^{o}C for 1 hr for precuring. The precured mixtures were then cast on Teflon® coated glass plates and slowly dried in an oven at 40^{o}C to form flat precured crosslinked HNT-PVA nanocomposites (5, 10 and 20% HNT loading, by wt, in the nanocomposites). The precured composites were further hot pressed at 100^{o}C under a pressure of 0.2 MPa for 60 min to form crosslinked HNT-PVA nanocomposites as stated earlier. The crosslinked HNT-PVA nanocomposites were then immersed into deionized water at RT for 12 hr until the system got stabilized in order to partially remove phosphoric acid, remaining MA and noncrosslinked PVA. The water-immersed and cured crosslinked HNT-PVA nanocomposites then dried at 40^{o}C to form final crosslinked HNT-PVA nanocomposites with average thickness of 0.5 mm.

5.3.5 Characterization

5.3.5.1 TEM analysis

HNT-PVA nanocomposites (10% HNT loading) and MA crosslinked HNT-PVA nanocomposites (10% HNT loading) were initially frozen by liquid nitrogen and then cut into extremely thin sections (40-100 nm in thickness) using microtome (Leica EM UC7/FC7 Cryoultramicrotome, Leica Microsystems, Cambridge, UK) with diamond cutter. The slices of HNT-PVA nanocomposites were observed with transmission electron microscopy (FEI Tecnai™ F20 TEM, FEI Company, Hillsboro, OR). Copper grids with 300 mesh size were used to hold the specimens for TEM.

5.3.5.2 Sol-gel and swelling analyses

PVA and MA crosslinked PVA specimens (crosslinked PVA film and the crosslinked resin in HNT-PVA nanocomposites, 10% HNT loading) were fully dried at 105^{o}C for 12 hr prior to conducting the sol-gel test. The specimens were weighed to obtain their initial dry weights and then immersed in distilled water in 150 mL glass bottles. The glass bottles with the specimens were then placed on a shaker table (MAXQ 4450, Thermo Scientific, Waltham, MA) maintained at 80^{o}C and 150 rpm for 2 hr until the control (noncrosslinked) PVA was completely dissolved. The remaining solid contents for the crosslinked specimens were then washed three times with distilled water and filtered using a Whatman® filter paper (Number 4, 20-25 μm pore size) to obtain final residues. The water soluble portion (sol) and particles smaller than the pore size of the filter paper were removed. The final residues of the crosslinked PVA and the crosslinked HNT-PVA nanocomposites were dried at 105^{o}C for 12 hr to obtain their dry wt (gel). Ratios of the dry gel wt of the crosslinked PVA to their corresponding initial dry wt were used to determine the PVA gel (crosslinked) percentages. The HNT wt in the crosslinked HNT-PVA

nanocomposites were regarded as constant before and after the test.

PVA and MA crosslinked PVA specimens (crosslinked PVA film or the crosslinked resin in HNT-PVA nanocomposites, 10% HNT loading) were dried at 105^{o}C for 12 hr prior to conducting the swelling test. The specimens were weighed to obtain their initial dry wt and then immersed in distilled water in 150 mL glass bottles at RT for 24 hr. The surface water from the swollen specimens was wiped using Kimwipe® paper tissue to remove excess water weighed again to obtain the swollen wt. Ratios of the wt of absorbed water by the specimens to their corresponding initial dry wt were used to determine the swelling power of the control and crosslinked PVA. The HNT wt in the crosslinked HNT-PVA nanocomposites was regarded as constant, before and after the test.

5.3.5.3 ATR-FTIR spectroscopy

Chemical analysis of HNT-PVA nanocomposites (10% HNT loading) and its MA crosslinked specimens was carried out using FTIR spectrophotometer (Nicolet Magna-IR 560, Thermo Scientific, Waltham, MA) in attenuated total reflection (ATR) mode using a split pea accessory. Spectra, averaged over 64 scans, were taken in the range of 4000-800 cm^{-1} wavenumber at a resolution of 4 cm^{-1}. All nanocomposite specimens were dried in an air circulating oven at 40^{o}C for 12 hr prior to conducting the spectroscopy.

5.3.5.4 Tensile properties and moisture content

The specimens for PVA, HNT-PVA nanocomposites (5, 10 and 20% HNT loading) and their corresponding crosslinked specimens were cut to 10 mm x 60 mm strips and were tensile tested using an Instron universal testing machine (model 5566). These tests were conducted as per ASTM D-882-02. Specimen gauge length of 30 mm and strain rate of 0.02 were used for all specimens. Specimens were conditioned at 21 ℃ and 65% RH for 3 days prior to testing.

Percent moisture content (MC%) for all conditioned specimens were measured as per ASTM D 2654-89a. To obtain the MC% values specimens were dried in an oven at 105^{o}C until their wt stabilized. The MC% values were calculated on the dry wt basis.

5.3.5.5 Thermogravimetric analysis (TGA)

Thermogravimetric analysis (TGA Model Q500, TA Instrument, New Castle, DE) was used to characterize the thermal properties of all specimens. Specimens were dried in an air circulating oven at 45^{o}C for 12 hr prior to conducting the tests. All TGA tests were performed between 25 and 800^{o}C under a nitrogen atmosphere (gas flow rate of 60 ml/min) and at a scanning rate of 10^{o}C/min.

5.3.5.6 Differential scanning calorimetry (DSC)

Differential scanning calorimetry (DSC, Model Q2000, TA Instrument, New Castle, DE) was used to analyze the glass transition temperature (T_g), melting temperature (T_m), enthalpy of fusion (ΔH_f) and crystallinity of PVA, HNT-PVA nanocomposites (10% HNT loading) and their corresponding MA crosslinked specimens. All specimens were dried in an oven at 105^{o}C for 12 hr prior to conducting the test. All DSC analyses were performed under an inert atmosphere by flowing nitrogen at the rate of 50 ml/min, between -20 and 250^{o}C and at a scanning rate of 10^{o}C/min.

5.4 Results and discussions

5.4.1 HNTs individualization

Unlike other nanolayered clays that must be exfoliated, HNTs naturally occur as small cylinders which average 30 nm in diameter. The HNT specimen used in this research was unprocessed and hence the nanotubes within were clustered. This was confirmed from the SEM photomicrographs in a previously published report [6]. Therefore, many separation techniques

were employed in the present study to individualize HNT clusters. These techniques include: high speed mechanical stirring, ultrasonication, addition of non-ionic surfactant and changing the solution pH.

Shear force from high speed mechanical stirring was used to effectively break down the HNT clusters. Ultrasonication generates intense and high frequency sound. The sound itself consists of regions of high and low pressure that move through a material as waves. As these waves pass through the liquid in the bath, each tiny portion of liquid vibrates back and forth in response to these pressure fluctuations which results in breaking of the clusters of HNTs [6].
Non-ionic surfactant Tween® 80 was used as a dispersant to improve the separation of HNTs [29].

The change of pH value is one of the key factors to separate HNTs. HNTs carry a negative charge on the basal or 'face' surface of their crystals but the charge on crystal edges varies with the pH of the ambient environment. The amphoteric nature of the edge surface may be ascribed to the protonation and deprotonation of hydroxyl groups coordinated with exposed Al ions under acid and alkaline pH conditions, respectively [5]. It has been reported that at pH 7.5 and above, the HNTs tend to repel each other since the charge on both the edge and face surface is negative [30]. As a result, the system deflocculates, and loses cohesion. In the present study, uniform and stable HNT dispersion was obtained after using these separation techniques sequentially. This stable HNT dispersion was used for fabricating HNT-PVA nanocomposites.

5.4.2 Mechanism of uniform HNT dispersion in acidic crosslinking condition

The individualized HNTs in dispersion can aggregate (recluster) and deposit when pH value is changed to acidic values. However, after HNT dispersion was mixed with PVA solution, the reclustering did not occur for many days, even in acidic condition, during PVA crosslinking.

This is possibly because the high viscosity of the PVA solution prevents them from coming closer due to the change of charges on edge surfaces of the HNTs in acidic environment. Figure 5.1 shows a schematic of this mechanism. It shows individualized HNTs can recluster with each other in acidic situation during opposite charge attracting. However, as mentioned earlier, high viscosity of PVA solution can help individualized HNTs to retard or even prevent clustering by immobilizing them.

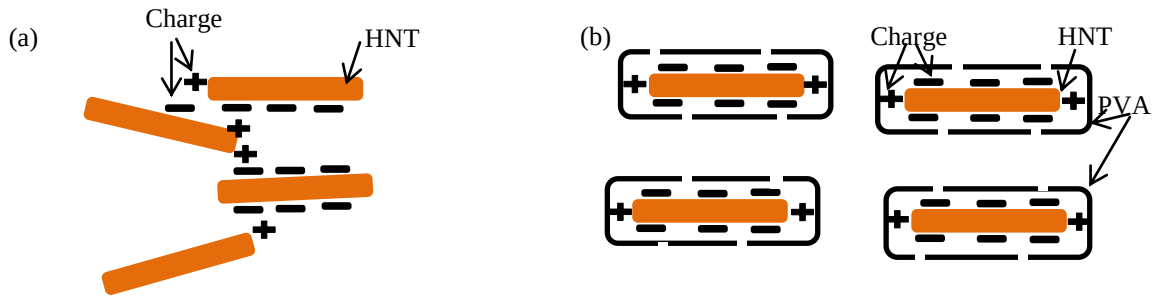

Figure 5.1 HNT clustering (a) and PVA surrounded HNTs without clustering (b) in acidic environment

5.4.3 TEM analysis of HNT dispersion in PVA and crosslinked PVA

Figure 5.2 shows typical TEM images of (a) HNT-PVA nanocomposite and (b) MA crosslinked HNT-PVA nanocomposite. Both nanocomposites had 10% HNT loading. Both TEM images clearly show that the HNTs were individualized and the uniformly dispersed within the PVA or crosslinked PVA. As mentioned earlier high viscosity of the PVA solution can help individualized HNTs to retard or even prevent clustering by immobilizing them. The degree or uniformity of dispersion of the HNTs within the polymer plays an important role on its mechanical properties [31]. Also, since the HNTs are uniformly dispersed, both mechanical and thermal properties of the nanocomposites would also be expected to be uniform [6].

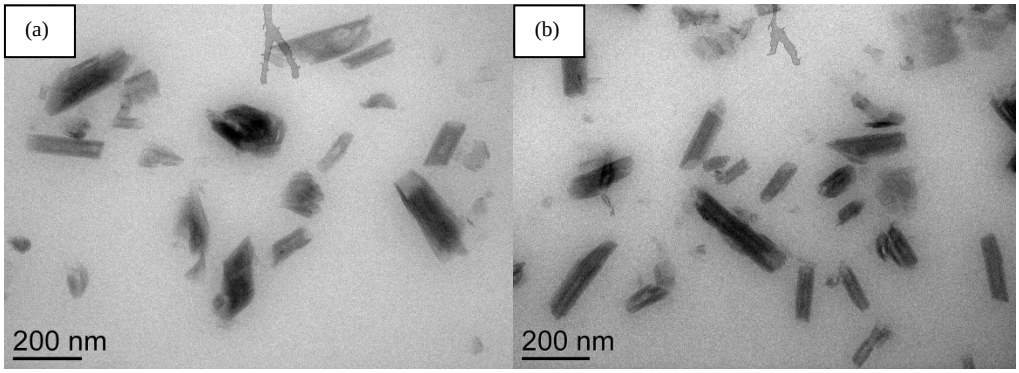

Figure 5.2 TEM images of HNT-PVA nanocomposite (a) and crosslinked HNT-PVA nanocomposite (b). Both contain 10% HNT loading

5.4.4 Sol-gel and swelling analyses

A study of crosslinking PVA with dicarboxylic acids, including MA, with sulfuric acid as a catalyst has been described earlier [27]. However, our preliminary study showed no difference in the extent of crosslinking between MA crosslinked PVA catalyzed by sulfuric acid and phosphoric acid. As a result, in all subsequent experiments phosphoric acid was used as a catalyst to crosslink PVA and HNT-PVA nanocomposites because of its lower toxicity compared to sulfuric acid [25].

Sol-gel and swelling analyses were performed for noncrosslinked (control) and crosslinked PVA, as well as for the resin in the crosslinked HNT-PVA nanocomposites to evaluate the level of crosslinking. Table 5.1 presents the sol-gel and swelling results for MA crosslinked PVA as well as control PVA. The results show that the PVA gel (crosslinked component) percentages of the crosslinked PVA and the resin in the crosslinked HNT-PVA nanocomposites were 93.1% and 94.8%, respectively, while the control PVA dissolved completely during the sol-gel test. The high gel percentage suggests that the PVA was crosslinked by MA in the presence of catalyst phosphoric acid. The results also show that the swelling powers of crosslinked PVA and the resin in the crosslinked HNT-PVA nanocomposites were 52.3% and 51.0%, respectively, much lower than control (noncrosslinked) PVA (107.3%), confirming the crosslinking.

Table 5.1 Sol-gel and swelling power results of PVA and MA crosslinked PVA

Tests	Control PVA	Crosslinked PVA	PVA in crosslinked HNT-PVA nanocomposites
Gel percentage (%)	0	93.1 (8.3)*	94.8 (7.2)
Swelling power (%)	107.3 (5.2)	52.3 (9.2)	51.0 (8.0)

**: values in the parentheses are % coefficient of variation*

5.4.5 ATR-FTIR analysis

When MA is made to react with PVA, the carboxylic groups (COOH) in MA react with the hydroxyl groups (OH) in the PVA forming ester linkages. Figure 5.3A shows typical carboxylic ester linkages in MA crosslinked PVA. Figure 5.3B shows the ATR-FTIR spectra for control HNT-PVA nanocomposite (a) and MA crosslinked HNT-PVA nanocomposite (b). Since HNTs cannot crosslink with MA, ATR-FTIR spectra only indicate the chemical structure change of PVA in HNT-PVA nanocomposites before and after crosslinking. A broad band at 3500-3200 cm^{-1} wavenumber seen in both spectra is a result of the O-H stretching vibration resulting from the strong intra-molecular and inter-molecular hydrogen bonding [32-34]. The absorption band observed between 3000 and 2820 cm^{-1} wavenumbers is due to the stretching of aliphatic C-H bonds [33]. The absorbance intensity ratio for O-H to C-H bands showed a decrease from 1.82 in spectrum (a) for control PVA compared to 1.23 for spectrum (b) for crosslinked PVA. This lower absorption clearly indicates a reduction in the O-H groups and confirms the crosslinking of PVA by MA [33]. Absorption at 1750-1650 cm^{-1} (stretching of C=O) for noncrosslinked specimen (spectrum (a)) was weak (intensity ratio of C=O to C-H = 0.36) and indicates the presence of carbonyl (C=O) in the nanocomposites from the nonhydrolyzed acetate group remaining in the PVA (98-99% hydrolyzed), confirming the earlier results obtained by Gohil et al. [32] and Mansur et al. [33]. In the ATR-FTIR spectrum (b), however, a sharp absorption

(intensity ratio of C=O to C-H = 0.61) observed at 1750-1650 cm^{-1} wavenumber indicates presence of C=O in the crosslinked PVA of the nanocomposites as expected. This shows that in addition to the nonhydrolyzed vinyl acetate groups, some residual unreacted carboxylic groups from MA and carboxylic ester groups (shown in Figure 5.3A) from crosslinked PVA also exist in the crosslinked HNT-PVA nanocomposites, both contributing to the stronger C=O absorption.

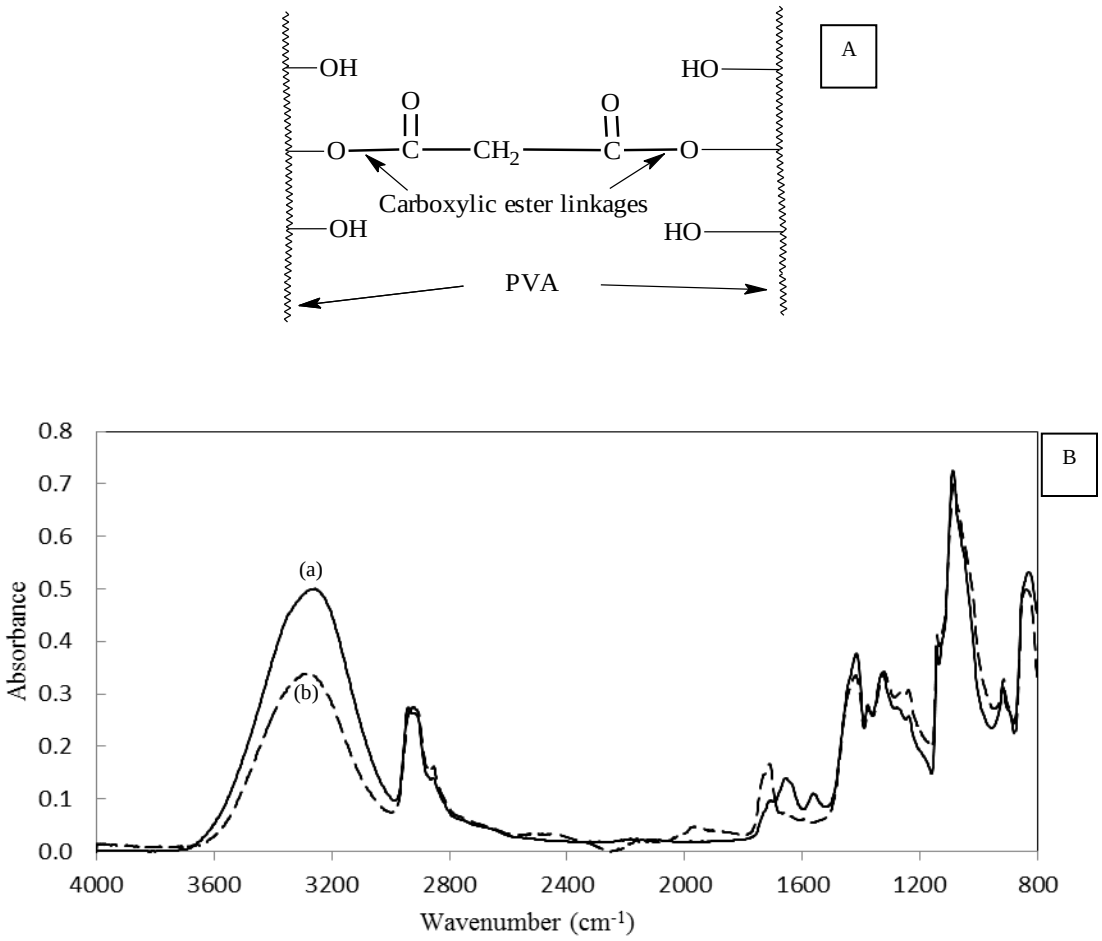

Figure 5.3 A: Schematic of the carboxylic ester linkage in MA crosslinked PVA structure; B: ATR-FTIR spectra of HNT-PVA nanocomposite (a) and MA crosslinked HNT-PVA nanocomposite (b). Both contain 10% HNT loading

Overall, the ATR-FTIR results indicate that the PVA in HNT-PVA nanocomposites were crosslinked based on the decreased intensity of bands for O-H stretching vibration combined with the increased intensity of bands for C=O stretching vibrations.

5.4.6 Tensile properties and moisture content

Table 5.2 presents tensile test results and moisture content values for pure (control) PVA and noncrosslinked HNT-PVA nanocomposites with HNT loading from 5 to 20% and their MA crosslinked specimens. The Young's modulus value for the control PVA was 245 MPa. The Young's modulus value for the HNT-PVA nanocomposites were higher than that obtained for PVA and increased with the HNT loading, as was expected. For nanocomposites with 5 and 10% HNT loading, the Young's moduli were 286 MPa and 388 MPa, respectively, and when the HNT loading increased to 20% the Young's modulus increased to 466 MPa, about 2 times that of control PVA. This phenomenon is commonly observed for most polymers loaded with inorganic nanoparticles due to the increased tortuosity of the polymer molecules, significantly harder nanoparticles and increased nanoparticle-polymer interface [1, 35, 36, 37, 38]. The facture stress for the control PVA was 34.3 MPa. The fracture stress values for HNT-PVA nanocomposites with 5 and 10% HNT loading were 29.1 MPa and 27.7 MPa, respectively, and decreased to 22.0 MPa when the HNT loading increased to 20%, respectively. This is attributed to the significantly reduced fracture strain values brought about by HNT agglomeration in some areas of the nanocomposites, particularly at 20% loading, again, a phenomenon seen in most polymers. However, lower fracture strain may also be a result of the weaker bonds between the nanoparticles (HNTs) and PVA as noted by others [39]. The fracture strain for control PVA was 336%. As seen from data in Table 5.2, facture strains for the HNT-PVA nanocomposites are much lower than that obtained for control PVA and decreased as the HNT loading increased. The reduced fracture strain as a function of nanoparticle loading has been observed by many [37]. The moisture content for control PVA was 9.2%, whereas for HNT-PVA nanocomposites with 5, 10 and 20% HNT loading the moisture content values were 8.0, 7.4 and 6.6%, respectively. This

is because moisture content of HNTs is around 1.6%, lower than PVA.

The Young's moduli of the MA crosslinked PVA and MA crosslinked HNT-PVA nanocomposites with 5, 10 and 20% HNT loading increased to 1023 MPa, 1105 MPa, 1185 MPa and 1244 MPa, respectively, from 245 MPa for control PVA and from 286 MPa, 388 MPa and 466 MPa for noncrosslinked HNT-PVA nanocomposites with the corresponding HNT loading. It is obvious that the increase in Young's modulus for the crosslinked PVA and HNT-PVA nanocomposites is solely due to the crosslinking of the PVA which makes the structure rigid [40]. The reduction in moisture content from 9.2% for the noncrosslinked PVA to 6.3% after crosslinking and from 8.0%, 7.4% and 6.6% for the HNT-PVA nanocomposites with 5, 10 and 20% HNT loading, respectively, to 6.2%, 6.0% and 6.0% for the crosslinked HNT-PVA nanocomposites with the corresponding HNT loading is also responsible, at least partially, for higher Young's modulus. With lower moisture content, i.e., less plasticization, the structure maintains its higher rigidity or stiffness [41]. Crosslinking also increased fracture stress values of PVA from 34.3 MPa to 46.4 MPa and HNT-PVA nanocomposites with 5, 10 and 20% HNT loading from 29.1 MPa, 27.7 MPa and 22.0 MPa to 42.1 MPa, 38.8 MPa and 36.1 MPa, respectively. From data presented in Table 5.2, it is also clear that after crosslinking, fracture strain values of PVA and HNT-PVA nanocomposites are significantly lower as expected [35, 36]. The fracture strains, particularly in the case of crosslinked nanocomposites decreased significantly with HNT loading. The decrease in fracture stress is closely related to the decreased fracture strains.

Table 5.2 Tensile properties and moisture content for PVA, HNT-PVA nanocomposites and their corresponding MA crosslinked specimens

Specimens	Young's modulus (MPa)	Fracture stress (MPa)	Fracture strain (%)	Moisture content (%)
PVA	245 (20.6)*	34.3 (13.6)	336 (10.1)	9.2 (5.3)
Crosslinked PVA	1023 (19.1)	46.4 (8.5)	186 (30.2)	6.3 (7.6)
HNT-PVA (5% HNTs)	286 (16.2)	29.1 (8.7)	297 (32.1)	8.0 (5.6)
HNT-PVA (10% HNTs)	388 (17.0)	27.7 (9.8)	268 (22.9)	7.4 (1.0)
HNT-PVA (20% HNTs)	466 (11.3)	22.0 (10.7)	159 (34.8)	6.6 (1.0)
Crosslinked HNT-PVA (5% HNTs)	1105 (10.4)	42.1(9.5)	110.0 (22.3)	6.2 (4.2)
Crosslinked HNT-PVA (10% HNTs)	1185 (24.7)	38.8 (9.6)	74.9 (17.6)	6.0 (8.8)
Crosslinked HNT-PVA (20% HNTs)	1244 (0.4)	36.1 (0.6)	8.8 (22.9)	6.0 (6.1)

**: values in the parentheses are % coefficient of variation values*

It should be noted that tensile properties of HNT-PVA nanocomposites and crosslinked HNT-PVA nanocomposites are comparable or higher than many traditional polymers, including polyethylene (Young's modulus: 800 MPa; fracture stress: 15 MPa), polypropylene (Young's modulus: 1900 MPa; fracture stress: 40 MPa), and nylon 6 (Young's modulus: 1800 MPa; fracture stress: 70 MPa) [42]. As a result, these PVA based biodegradable nanocomposites can easily replace many of these traditional plastic materials. Also, after crosslinking their moisture sensitivity is lower, making them more useful. Biodegradable plastics based on PVA can reduce the current landfilling load significantly.

Figure 5.4 shows typical stress vs strain plots of HNT-PVA nanocomposite (a) and MA crosslinked HNT-PVA nanocomposite (b). The HNT loading in both specimens is around 10% by wt. Figure 5.4 (a) shows HNT-PVA nanocomposite initially showed elastic behavior but then

showed a plastic plateau (yielding) until reaching its fracture point. This plateau is due to PVA's high ductility. While stress vs strain plot for the crosslinked HNT-PVA nanocomposite shown in Figure 5.4 (b) also shows yielding, it shows no obvious plateau for plastic deformation because of the crosslinking.

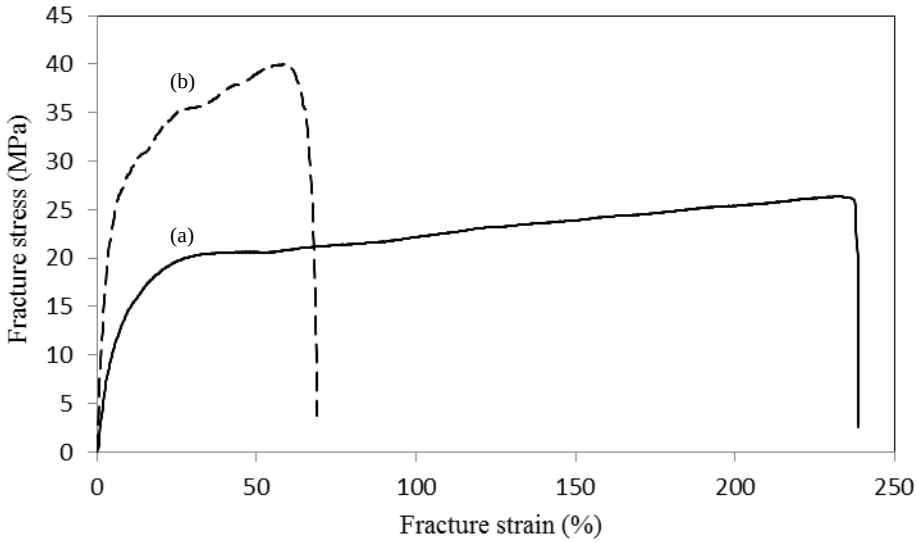

Figure 5.4 Typical stress vs strain plots for HNT-PVA nanocomposite (a) and MA cross-linked HNT-PVA nanocomposite (b). Both contain 10% HNT loading

5.4.7 Thermogravimetric analysis

Figure 5.5A presents typical TGA thermograms of PVA, HNT-PVA nanocomposites (10% and 20% HNT loading) and HNTs. Thermogram 5.5A (a) for control PVA shows two decomposition onset temperatures, (T_{d1}) and (T_{d2}), at 255^{o}C and 390^{o}C, respectively. Weight losses for the PVA were 30% at 266^{o}C, 50% at 276^{o}C and up to 94% at 800^{o}C. Two-step degradation of PVA has been reported earlier by Peng and Kong [41]. A likely explanation for this is that PVA first degrades into smaller molecular weight polymer at around 250^{o}C by chain scission and degrades further into carbon char at temperatures above 350^{o}C. Results of this study confirm the earlier findings [43]. Thermograms 5.5A (b) and (c) for HNT-PVA nanocomposites, with 10 and 20% HNT loading, respectively, also show two decomposition

onset temperatures. However, their T_{d1} and T_{d2}, 260°C and 393°C, respectively, are 3 to 5°C higher than those observed for PVA. This is again due to the addition of HNTs which makes it thermally more stable. Weight losses observed for the HNT-PVA nanocomposites (10% HNT loading) were 30% at 286°C, 50% at 305°C and 88% at 800°C. Weight losses observed for the HNT-PVA nanocomposites (20% HNT loading) were 30% at 295°C, 50% at 343°C (both temperatures are higher than those obtained for HNT-PVA nanocomposites with 10% HNT loading) and 74% at 800°C. These data confirm the higher thermal stability of the HNT-PVA nanocomposites. Thermogram 5.5A (d) for HNTs showed no sharp thermal degradation. Weight losses observed for pure HNTs were 10% at 471°C, 20% at 700°C, and 24% at 800°C, confirming higher thermal stability of HNTs [11]. Thus it is obvious that HNT loading is responsible for the higher thermal stability of the HNT-PVA nanocomposites.

Figure 5.5B presents typical TGA thermograms of PVA, HNT-PVA nanocomposite (10% HNT loading) and their corresponding MA crosslinked specimens. Thermograms 5.5B (a) and 5.5B (b) are for PVA and HNT-PVA nanocomposites, respectively, and have been described in the last paragraph. Thermogram 5.5B (c), for crosslinked PVA, also shows a two-step degradation pattern with T_{d1} and T_{d2} (no so obvious) observed at 305°C and 417°C, respectively. However, the steps are not as distinct compared to the control PVA. The weight losses observed were 30% at 329°C, 50% at 362°C and almost 100% at 800°C. These results indicate that the crosslinked PVA has significantly higher thermal stability compared to control PVA in the range of 240-430°C. Increased thermal stability after crosslinking has been observed earlier for many polymers [44-46]. Thermogram 5.5B (d) for crosslinked HNT-PVA nanocomposites also shows a single degradation pattern with T_d observed at 380°C. Weight losses observed were 30% at 329°C, 50% at 372°C and 86% at 800°C. As is expected these values are close to those obtained

for the crosslinked PVA, the major constituent in the nanocomposite. These results clearly indicate that crosslinking of PVA using MA can increase its thermal stability as well as that of HNT-PVA nanocomposites, in addition to enhancing their tensile properties.

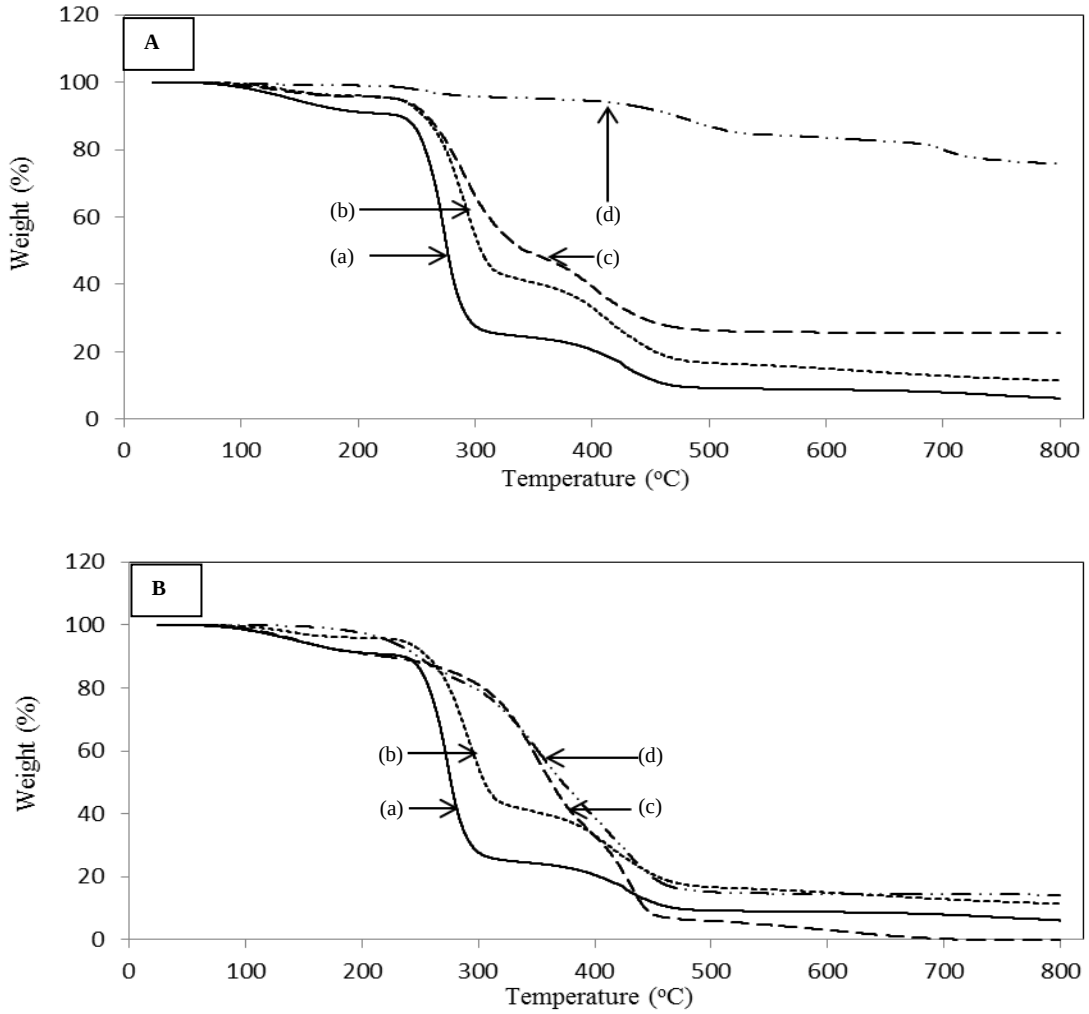

Figure 5.5 Typical TGA thermograms A: PVA (a), HNT-PVA nanocomposite (b: 10% HNT loading), HNT-PVA nanocomposite (c: 20% HNT loading) and HNTs (d); B: PVA (a), HNT-PVA nanocomposite (b: 10% HNT loading), MA crosslinked PVA (c) and MA crosslinked HNT-PVA nanocomposite (d: 10% HNT loading)

5.4.8 Differential scanning calorimetry

Typical DSC thermograms for PVA and MA crosslinked PVA are presented in Figure 5.6A. Thermogram 5.6A (a) for control PVA shows T_g and T_m of 92.0°C and 196.1°C, respectively. The ΔH_f of 81.1 J/g, compared to 138.6 J/g for 100% crystalline PVA resulted in a crystallinity

of 58.5% for control (pure) PVA [47-50]. Thermogram 5.6A (b) for the crosslinked PVA shows T_g and T_m of 102.1^{o}C and 189.7^{o}C, respectively. The ΔH_f and the crystallinity of the crosslinked PVA were 36.8 J/g and 26.6%, respectively. The lower ΔH_f and higher T_g further confirm that the PVA was effectively crosslinked by MA. The higher T_g and lower crystallinity after crosslinking are due to restricted segmental motion of the molecules, a phenomenon commonly observed in most polymers [1, 47, 51, 52].

Figure 5.6B presents typical DSC thermograms of (a) HNT-PVA nanocomposite and (b) MA crosslinked HNT-PVA nanocomposite. The T_g and T_m for the HNT-PVA nanocomposites were observed at 90.5^{o}C and 201.9^{o}C, respectively. The change in T_g for nanocomposite is insignificant. While the T_m value is about 5^{o}C higher than that of control PVA, the T_g is about 1.5^{o}C lower. This suggests that HNTs have the ability to lead to decrease T_g and increase T_m of polymers [19, 53]. Nakamura et al. also [16] observed similar decrease in T_g as a result of HNT addition. They argued that this was a result of free volume addition. The ΔH_f and the crystallinity of the PVA in HNT-PVA nanocomposites (10% loading) were 43.3 J/g and 31.2%, respectively, which were much lower than 85.9 J/g and 62.0%, respectively, obtained for control PVA. It is likely that the HNTs can inhibit the crystallization of PVA, as they are well dispersed [54]. However, higher T_m suggested that the average crystal size in nanocomposites was larger. Thermogram 5.6B (b) is for MA crosslinked HNT-PVA composites but mainly represents crosslinked PVA behavior. The T_g and T_m observed were 99.0^{o}C and 191.9^{o}C, respectively, and confirm earlier observation that MA crosslinking can increase T_g and decrease T_m of PVA. These changed characteristics are reflected in the crosslinked HNT-PVA nanocomposites. The ΔH_f and crystallinity of PVA in crosslinked HNT-PVA nanocomposites were 8.6 J/g and 6.2%, respectively. These are significantly lower than those for the PVA in HNT-PVA nanocomposites

and the MA crosslinked PVA, showing the combined effect of crosslinking and the ability of the HNTs to restrain the molecular motion needed for crystallization.

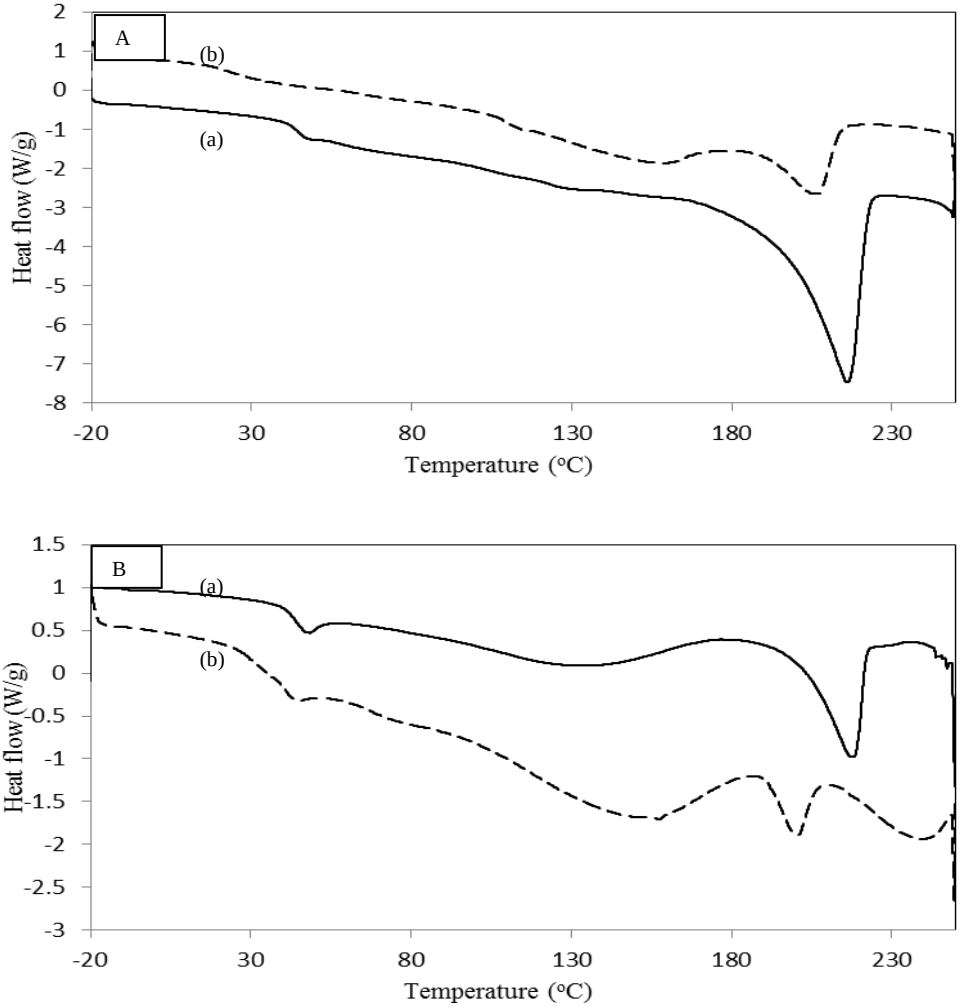

Figure 5.6 DSC thermograms A: PVA (a) and MA crosslinked PVA (b); B: HNT-PVA nanocomposite (a) and MA crosslinked HNT-PVA nanocomposite (b). Both contain 10% HNT loading

5.5 Conclusions

The biodegradable membrane-like HNT-PVA nanocomposites with differing HNT loadings were produced using blending and casting methods. Several separation techniques such as mechanical stirring, ultrasonication, non-ionic surfactant and desired solution pH, were used to individualize HNTs and obtain stable HNT dispersion. The TEM images indicated that HNTs

were uniformly dispersed in both PVA and MA crosslinked PVA. ATR-FTIR results confirmed that PVA can be crosslinked using MA as crosslinker and phosphoric acid as catalyst. MA crosslinked PVA was highly water-insoluble with decreased swelling ability. PVA and HNT-PVA nanocomposites showed higher mechanical properties and thermal stability after crosslinking. HNT loading also was responsible for higher thermal stability of the PVA based nanocomposites. Fracture strain was seen to decrease significantly with crosslinking. Fracture strain also decreased with HNT loading for both crosslinked and noncrosslinked PVA. The DSC results indicated that HNT loading decrease T_g as well as crystallinity while increasing the T_m of PVA. Crosslinking of PVA resulted in higher T_g, lower T_m and lower crystallinity as was expected.

5.6 Acknowledgements

This work was partly supported by the National Textile Center (NTC) and the Wallace Foundation. The authors also like to thank the Cornell Center for Materials Research (CCMR) for the use of their facilities.

References

[1] Young RJ, Lovell PA. Introduction to polymers, 3rd edition. Boca Raton, FL: CRC Press, 2011. p. 591-622.

[2] Cao G, Wang Y. Nanostructures and nanomaterials: synthesis, properties, and applications, 2nd edition. Singapore: World Scientific, 2011. p. 61-142.

[3] Dean KM, Petinakis E, Yu L. Biodegradable thermoplastic starch/poly(vinyl alcohol) nanocomposites with layered silicates. In: Mittal V, editor. Nanocomposites with biodegradable polymers: synthesis, properties and future perspectives. Oxford, UK: Oxford University Press, 2011. p. 58-70.

[4] Liu M, Guo B, Du M, Jia D. Drying induced aggregation of halloysite nanotubes in polyvinyl alcohol/halloysite nanotubes solution and its effect on properties of composite film. Appl Phys A 2007; 88: 391-395.

[5] Joussein E, Petit S, Churchman J, Theng B, Righi D, Delvaux B. Halloysite clay minerals-a review. Clay Miner 2005; 40: 383-426.

[6] Rathi P. Soy protein based nanophase reins for green composites. Ithaca, NY: A project report, Cornell University, 2007. p. 13-18.

[7] Liu M, Guo B, Du M, Cai X, Jia D. Properties of halloysite nanotube-epoxy resin hybrids and the interfacial reactions in the systems. Nanotechnology 2007; 18 (45): Art. No. : 455703.

[8] Ye Y, Chen H, Wu J, Ye L. High impact strength epoxy nanocomposites with natural nanotubes. Polymer 2007; 48: 6426-6433.

[9] Deng S, Zhang J, Ye L, Wu J. Toughening epoxies with halloysite nanotubes. Polymer 2008; 49: 5119-5127.

[10] Ning N, Yin Q, Luo F, Zhang Q, Du R, Fu Q. Crystallization behavior and mechanical properties of polypropylene/halloysite composites. Polymer 2007; 48: 7374-7384.

[11] Du M, Guo, B, Jia D. Thermal stability and flame retardant effect of halloysite nanotubes on poly(propylene). Eur Polym J 2006; 42: 1362-1369.

[12] Marney DCO, Russell LJ, Wu DY, Nguyen T, Cramm D, Rigopoulos N, Wright N, Greaves M. The suitability of halloysite nanotubes as a fire retardant for nylon 6. Polym Degrad Stabil 2008; 93: 1971-1978.

[13] Du M, Guo B, Lei Y, Liu M, Jia D. Carboxylated butadiene-styrene rubber/haolloysite nanotube nanocomposites: interfacial interaction and performance. Polymer 2008; 49: 4871-4876.

[14] Guo B, Lei Y, Chen F, Liu X, Du M, Jia D. Styrene-butadiene rubber/halloysite nanotubes nanocomposites modified by methacrylic acid. Appl Surf Sci 2008; 255: 2715-2722.

[15] Pasbakhsh P, Ismail H, Fauzi MNA, Bakar AA. EPDM/modified halloysite nanocomposites. Appl Clay Sci 2010; 48: 405-413.

[16] Nakamura R, Netravali AN, Hosur M. Effect of halloysite nanotubes on interfacial property between carbon fiber and epoxy resin. J Adhes Sci Technol 2012; 26: 1295-1312.

[17] Nakamura R, Netravali AN, Morgan AB, Nyden MR, Gilman JW. Effect of halloysite nanotubes on mechanical properties and flammability of soy protein based green composites. Fire Mater 2012; DOI: 10.1002/fam.2113.

[18] Stevens ES. Green plastics: an introduction to the new science of biodegradable plastics, Princeton, NJ: Princeton University Press, 2002. p.10-30.

[19] Liu M, Guo B, Du M, Jia D. Drying induced aggregation of halloysite nanotubes in polyvinyl alcohol/halloysite nanotubes solution and its effect on properties of composite film. Appl Phys A 2007; 88: 391-395.

[20] Zhou WY, Guo B, Liu M, Liao R, Rabie ABM, Jia D. Poly(vinyl alcohol)/halloysite nanotubes bionanocomposite films: properties and *in vitro* osteoblasts and fibroblasts response. J Biomed Mater Res A 2010; 93 (4): 1574-1587.

[21] Thermo Scientific. Thermo scientific pierce-crosslinking technical handbook, http://www.piercenet.com/files/1601673_Crosslink_HB_Intl.pdf, Accessed November 2011.

[22]. Yeom CK, Lee KH. Pervaporation speration of water-acetic acid mixtures through poly (vinyl alcohol) membranes crosslinked with glutaraldehyde. J Membrane Sci 1996; 109: 257-265.

[23] Zhang Y, Zhu PC, Edgren D. Crosslinking reaction of poly(vinyl alcohol) with glyoxal. J Polym Res 2010; 17 (5): 725-730.

[24] BASF. Glyoxal as a cellulose crosslinker. http://www.intermediates.basf.com/chemicals/glyoxal/crosslinker-for-cellulose. Accessed November 2011.

[25] MSDS. http://www.msdsonline.com, Accessed November 2011.

[26] Weiner N. Malonic acid. Org Synth 1943; Collective 2: 376.

[27] Jian S, Ming SX. Crosslinked PVA-PS thin-film composite membrane for reverse osmosis. Desalination 1987; 62: 395-403.

[28] Majumdar S, Adhikari B. Polyvinyl alcohol: A taste sensing material. Sensors Actuators B-Chem 2006; 114: 747-755.

[29] Karatepe N. Adsorption of a non-onic dispersant on lignite particle surface. Energ Convers Manage 2003; 44 (8): 1275-1284.

[30] Churchman, G. J., Theng, B. K. G., Interactions of halloysites with amides: Mineralogical factors affecting complex formation. Clay Miner 1984; 19: 161–175.

[31] Yano K, Usuki A, Okada A. Synthesis and properties of polyimide-clay hybrid films. J Polym Sci Pol Chem 1997; 35: 2289-94.

[32] Gohil JM, Bhattacharya A, Ray P. Studies on the cross-linking of poly (vinyl alcohol). J Polym Res 2006; 13: 161-169.

[33] Mansur HS, Sadahira CM, Souza AN, Mansur AAP. FTIR spectroscopy characterization of poly (vinyl alcohol) hydrogel with different hydrolysis degree and chemically crosslinked with glutaraldehyde. Mater Sci Eng C 2008; 28: 539-548.

[34] Kim JH, Moon EJ, Kim CK. Composite membranes prepared from poly (m-animostyrene-co-vinyl alcohol) copolymers for the reverse osmosis process. J Membrane Sci 2003; 216: 107-120.

[35] He Y, Kong W, Wang W, Liu T, Gong Q, Gao J. Modified natural halloysite/potato starch composite films. Carbohyd Polym 2012; 87 (4): 2706-2711.

[36] Vaia RA, Jandt KD, Kramer EJ, Giannelis EP. Microstructural evolution of melt intercalated polymer-organically modified layered silicates nanocomposites. Chem Mater 1996; 8 (11): 2628-2635.

[37] Kumar H, Hosur M, Netravali AN. Characterization of interface properties of clay nanoplatelets filled epoxy resin and carbon fiber by single fiber composite technique, J Adhes Sci Technol 2010; 24: 217-236.

[38] Lew C, Choudhury F, Hosur M, Netravali AN. The effect of silica (SiO_2) nanoparticle and ethylene/ammonia plasma on the carbon fiber/nanoepoxy interfacial shear strength. J Adhes Sci Technol 2007; 21(14): 1407-1424.

[39] Zhao D, Zhang Y, Gong H, Zhu B, Zhang X. BN nanoparticles/Si3N4 wave-transparent composites with high strength and low dielectric constant. J Nanomater 2011; Art. ID 246847.

[40] Zhang L, Chen P, Huang J, Yang G, Zheng L. Way of strengthening biodegradable soy-dreg plastics. J Appl Polym Sci 2003; 88: 422-427.

[41] Zhang J, Mungara P, Jane J. Mechanical and thermal properties of extruded soy protein sheets. Polymer 2001; 42 (6): 2569-2578.

[42] Tensile property testing of plastics - MatWeb.

http://www.matweb.com/reference/tensilestrength.aspx, 2010, Accessed November 2011.

[43] Peng Z, Kong LX. A thermal degradation mechanism of polyvinyl alcohol/silica nanocomposites. Polym Degrad Stabil 2007; 92: 1061-1071.

[44] Chabba S, Matthews GF, Netravali AN. 'Green' composites using cross-linked soy flour and flax yarns. Green Chem 2005; 7: 576-581.

[45] Rodrigues FT, Martins VCA, Plepis AMG. Porcine skin as a source of biodegradable matrices: alkaline treatment and glutaraldehyde crosslinking. Polimeros 2010; 20 (2): 92-97.

[46] Liu BS, Yao CH, Fang SS. Evaluation of a non-woven fabric coated with a chitosan Bi-layer composite for wound dressing. Macromol Bioscience 2008; 8 (5): 432-440.

[47] Warner SB. Fiber Science. Upper Saddle River, NJ: Prentice Hall; 1995. p. 205-206.

[48] Blaine RL. Determination of polymer crystallnity by DSC. TA Instruments, www.tainstruments.com/library_download.aspx?file=TA123.PDF, Accessed December 2011.

[49] Sichina WJ. DSC as problem solving tool: measurement of percent crysallnity of thermoplastics. PerkinElmer Instruments,

http://www.perkinelmer.com/Content/applicationnotes/app_thermalcrystallinitythermoplastics.pdf , Accessed December 2011.

[50] Guirguis OW, Moselhey MTH. Thermal and structural studies of poly (vinyl alcohol) and hydroxypropyl cellulose blends. Nat Sci 2012; 4 (1): 57-67.

[51] Kim JH, Kim JY, Lee YM, Kim KY. Properties and swelling characteristics of cross-linked poly (vinyl alcohol)/chitosan blend membrane. J Appl Polym Sci 1992; 45 (10): 1711-1717.

[52] Mtshali TN, Krupa I, Luyt AS. The effect of cross-linking on the thermal properties of LDPE/wax blends. Thermalchim Acta 2001; 380: 47-54.

[53] Liu M, Guo B, Du M, Chen F, Jia D. Halloysite nanotubes as a novel β-nucleating agent for isotactic polypropylene. Polymer 2009; 50: 3022-3030.

[54] Boudenne A, Ibos, L, Candau Y, Thomas S. Handbook of multiphase polymer systems. Chichester, West Sussex, UK: John Wiley & Sons Ltd; 2011. p. 455.

Chapter 6 A composting study of membrane-like polyvinyl alcohol based resins and composites

Kaiyan Qiu, Anil N. Netravali*
Fiber Science Program, Cornell University, Ithaca, NY 14853-4401

6.1 Abstract

This study presents the effect of biodegradation in a composting medium on membrane-like polyvinyl alcohol (PVA) based resins and composites. The materials studied include PVA, glyoxal crosslinked PVA (GX-PVA), malonic acid (MA) crosslinked PVA (MX-PVA), and microfibrillated cellulose (MFC)-PVA and halloysite nanotube (HNT)-PVA nanocomposites. The composting process was monitored for up to 120 days and the biodegradation of these materials was characterized by weight loss, attenuated total reflectance Fourier-transform infrared spectroscopy (ATR-FTIR), differential scanning calorimetry (DSC), sol-gel analysis and energy dispersive X-ray (EDX) analysis. The changes in the PVA based materials' surface topography and microstructure during composting were also characterized using scanning electron microscopy (SEM). The results from the analyses suggest biodegradation of PVA based materials in compost medium was mainly by enzymes secreted by fungi. The results also indicate that the enzymes degraded the amorphous regions of the specimens first. The surface roughness of the specimens significantly increased with the composting time which could facilitate microorganism to stay and propagate. All specimens broke in to many pieces as a result of deep biodegradation between 90 and 120 days of composting. The results also showed that crystallinity played an important role in PVA biodegradation. Crosslinking decreased the PVA biodegradation rate slightly. Highly crystalline MFC and naturally occurred HNTs also

were a factor as their presence decreased the biodegradation rate when present in PVA based composites.

Keywords: Polyvinyl alcohol; Crosslinking; Composites; Biodegradation; Composting

6.2 Introduction

Most commercially available polymers at present are non-biodegradable. Furthermore, most of them are made using petroleum as raw material, a non-renewable resource. With increased use of plastics and polymers in every part of our life, their waste disposal has become a serious problem. To resolve these issues there has been increased research on biobased and biodegradable polymers and their composites in the past decade. The research, in recent years, has been accelerated both by environmental awareness among people as well as by governmental regulations and support [1-9].

Biobased and biodegradable polymers are generally defined as those polymers that can decompose in natural aerobic (composting) and anaerobic (landfill) environments [8]. Most biobased polymers are those that are inherently biodegradable and have been derived from renewable raw materials [8, 10, 11]. They almost always have oxygen or nitrogen atoms in their polymer backbones which is the feature that is mainly responsible for their biodegradability [8]. Biobased polymers can be further subdivided into two categories, natural biopolymers and synthetic biopolymers [8]. The term, 'natural biopolymers' is often used to refer to biobased polymers that are found directly in nature such as carbohydrates (starch, cellulose, chitin, agar, carrageenan, etc.), lignin, proteins and bacteria-produced polyesters, etc. [8, 10, 11]. Synthetic biopolymers are polymers that are not found in nature but are made commercially from

monomers that are found abundantly in nature [8]. Polylactic acid (PLA) and polyamino acids (PAA) are examples of synthetic biopolymes that are rapidly becoming mainstream [8]. Biodegradable polymers normally refer to petroleum-based biodegradable synthetic polymers, such as polyvinyl alcohol (PVA), polyglycolic acid (PGA), polycaprolactone (PCL), polyethylene oxide (PEO), etc. [8-11].

Biodegradation is regarded as a process in which the degradation results from the action of microorganisms such as bacteria, fungi or algae [12, 13]. Biodegradation can be generally divided into two steps [13]. The first step is depolymerization or chain cleavage where the polymer chain undergoes backbone scission and fractures into smaller oligomeric fragments with the help of enzymes generated by microorganisms. The second step is mineralization which occurs inside the cell in which small oligomeric fragments are converted to biomass, minerals and salts, water and gaseous substances such as carbon dioxide under aerobic environments and methane under anaerobic environments [13]. Biobased and biodegradable polymers and their composites may be broken down by the enzymes secreted by microorganisms. Once broken down to monomeric level, it is used as the carbon source and metabolized by the microorganisms. The biodegradation process is chemical in nature but the source of the attacking chemicals (enzymes) comes from microorganisms [14-18]. The susceptibility of polymers and their composites to microbial attack generally depends on enzyme availability, availability of a site in the polymers for enzyme attack, enzyme specificity for that polymer and the presence of coenzyme [19]. Biodegradation results in the changes in surface properties since it begins at the surface where the microorganisms are present. Once progressed, it results in loss of strength, degradation by enzymes or breakage of backbone chains, subsequent reduction in the average molecular weight of polymers and assimilation by microorganisms [12, 13-21].

The biodegradation and its mechanism under the effect of microorganisms for different polymers and their composites, including poly (butylene succinate) (PBS) and its silicate reinforced nanocomposites, PLA and its silica and calcium carbonate reinforced nanocomposites, whey protein, soy protein isolate (SPI), PCL, poly (hydroxybutyrate-co-hydroxyvalerate) (PHBV), noncrosslinked PVA, etc., have already been extensively studied [1, 2, 3, 8, 12, 22-33]. Many factors have been shown to influence the biodegradation process, including surface area, hydrophilic/hydrophobic properties, chemical structure, molecular weight, crystallinity and melting temperature. Polyesters with side chains and higher melting temperature are less assimilated than those without side chains [22-33]. PCL with higher molecular weight degraded more slowly than that that with low molecular weight [22-33]. The rate of biodegradation of PLA was shown to decrease with an increase in crystallinity since the enzymes mainly attack the amorphous domains of polymers [1, 2, 3, 12, 23-26]. Addition of a dispersed phase also has an effect on the rate of biodegradation [30-33]. The relative rate of biodegradation for PBS-silica nanocomposites was faster than that of neat PBS which was attributed to the relatively low crystallinity of PBS in the PBS-silica nanocomposites [30, 31]. It was also observed that addition of layered silicate and calcium carbonate increased the rate of biodegradation of PLA [32, 33]. Besides, the degradation rate of PLA in compost was observed to decrease with the introduction of crosslinks [34].

PVA is a widely used thermoplastic and biocompatible polymer. However, unlike most petroleum based polymers, it is one of the rare polymers with a carbon-carbon single bond backbone that is fully biodegradable in the presence of suitably acclimated microorganisms [1, 2, 8]. In addition, because of the hydroxyl (-OH) groups on alternating carbon atoms, PVA is strongly hydrophilic and soluble in water, which also helps to promote its degradation through

hydrolysis [1, 2, 8, 9, 35]. Therefore, both enzymatic and hydrolytic degradations can occur in PVA as it absorbs moisture [3]. Nevertheless, degradation of hydrophobic polymers, e.g. poly(hydroxybutyrate-co-hydroxyvalerate) (PHBV) in compost medium is enzymatic rather than hydrolytic and occurs from the surface [2].

The first microorganisms capable of assimilating PVA as their sole carbon source were isolated from soil samples and identified as *Pseudomonas* species [2, 9, 28, 29, 36]. Further studies confirmed that other aerobic bacteria, such as Alcaligenes and Bacillus, were also active in the PVA degradation [9, 27, 36-38]. Fungal strains, such as *Aspergillus niger, Pycnoporus cinnabarinus, Fusarium and Phanerochaete chrysoporium*, have been reported to have the ability to change not only the polymer (like PVA) surface from smooth to rough, but even to break down the polymer [9, 39, 40]. It was observed that specific microbial strains were able to induce a rapid decrease of the viscosity of aqueous culture media containing PVA [9, 27, 36-40]. It was, therefore, assumed that at least the initial microbial attack should be consistent with a random cleavage of the polymer chains. At the same time, the occurrence of oxidative reactions of the tertiary carbon atoms of PVA chains, leading to the formation of hydrolysable β-hydroxylketone and 1, 3-diketone groups along the polymer backbone, was established. These reactions were catalyzed by specific oxidases and dehydrogenases that were isolated mainly as extracellular proteins from different bacterial species [1, 2, 9, 27]. However, biodegradation of PVA can not be finished by a single kind of microorganism in a real biodegradative environment, instead, it is the combinative process by many microorganisms [36-40].

PVA has been shown to degrade under different environmental conditions, including aerobic composting, soil burial, aqueous media and even anaerobic conditions [27, 41-44]. Among these ways of biodegradation, composting is an effective technique to characterize the biodegradation

of PVA and other biodegradable polymers and their composites [2]. Composting is defined as an exothermic bio-oxidative decomposition of organic materials by indigenous microorganisms in a controlled moist and warm aerobic environment leading to the production of 'compost', a mixture of carbon dioxide, water, minerals and a stabilized organic matter [28, 45]. As the compost pile becomes active, a succession of mesophilic and thermophilic microorganisms secrete depolymerase enzymes. These enzymes attack the substrate as nutrient in the presence of optimal moisture, temperature and nutrients [28, 45]. This being an exothermic process causes the temperature to rise above the ambient temperature of 23^{o}C. If the temperature increases to 40-45^{o}C, the mesophilic bacteria, actinomycetes and fungi give way to thermophilic organisms and if it reaches 70-75^{o}C, the microbial activity is drastically reduced resulting in cooling down of the material and eventual maturity [28, 45]. It has been reported that hydrolytic degradation can occur in some polymers with high moisture sensitivity under the slightly acidic pH conditions [2, 3, 28, 29].

In this study, typical composting technique has been utilized to characterize the biodegradation of PVA based materials, including PVA, glyoxal crosslinked PVA (GX-PVA), malonic acid crosslinked PVA (MX-PVA), MFC-PVA composite and HNT-PVA composite. Various characterization methods, including scanning electron microscopy (SEM), attenuated total reflectance Fourier-transform infrared spectroscopy (ATR-FTIR), differential scanning calorimetry (DSC) and sol-gel analysis were used. Weight loss was also monitored to characterize the extent of biodegradation.

6.3 Materials and methods

6.3.1 Materials

PVA powder (M_w 31,000-50,000, 98-99% hydrolyzed), glyoxal solution (25 wt% solution), MA powder and Tween® 80 (non-ionic surfactant) were purchased from Sigma-Aldrich, St. Louis, MO. Phosphoric acid (85 wt% solution in water) was purchased from Mallinckrodt Baker, Phillipsburg, NJ. MFC in water (KY-100G) was obtained from Daicel Chemical Industries, Japan. HNTs in unprocessed raw form were obtained from Nanoclays and Technology Inc, Utah (Division of Atlas Mining). Composting chicken manure was obtained from Poultry Research Farm, Cornell University, Ithaca, NY. Composting sawdust (Fine Pine Shavings) was purchased from Tractor Supply Company, Ithaca, NY.

6.3.2 Specimen preparation

6.3.2.1 Preparation of PVA, GX-PVA and MX-PVA

PVA powder was added to the deionized water at a weight ratio of 1:9 to form PVA solution which was kept in a water bath at 80^{o}C and stirred for 30 min. Glyoxal solution and MA powder were then added separately, to PVA solutions. The glyoxal:PVA weight ratio was 3:100 and MA:PVA weight ratio was 10:100 [6, 7]. The pH of both mixtures was adjusted to 1 using phosphoric acid. Both mixtures were stirred at 90^{o}C for 1 hr to precure. The precured mixtures were then cast on Teflon® coated glass plates and slowly dried in an air circulating oven at 40^{o}C to form precured crosslinked PVA sheets. The precured crosslinked PVA sheets were further hot pressed in a Carver hot press (model 3891) at 100^{o}C under a pressure of 0.2 MPa for 60 min to form cured crosslinked PVA sheets. Acetal linkage are expected to from between hydroxyl groups of PVA and carbonyl groups of glyoxal at high temperature during the hot pressing, while the ester linkages are expected to form between hydroxyl group of PVA and carboxylic groups

of MA at high temperature during the hot pressing [6, 7, 46, 47]. The MA crosslinked (cured) PVA was then immersed into deionized water at RT for 12 hr in order to remove phosphoric acid and remaining unreacted MA. Cured GX-PVA sheets were not treated by water. The specimens were then dried at 40^{o}C to form final glyoxal and MX-PVA sheets. The PVA was prepared by casting PVA solution without the addition of glyoxal or MA as control, for comparison. Average thicknesses of the sheets were approximately 0.2 mm.

6.3.2.2 Preparation of MFC-PVA and HNT-PVA composites

MFC in water and HNT powder were initially prepared into MFC suspension and individualized HNT dispersion, respectively, for fabrication of composites, based on our previous reports [6, 7]. Briefly, the MFC was added into deionized water at a weight ratio of 1:199. The mixture was stirred using high speed mechanical stirrer (Polymix®, PX-SR 90 D, Kinematica Inc., Bohemia, NY) at 90^{o}C and 1000 rpm for 1 hr and followed by ultrasonication (Branson Ultrasonics, Model 2510, Mumbai, India) at 65^{o}C for 1 hr in order to individualize the fibrils as much as possible and form MFC suspension (0.5% MFC by wt). HNT powder was initially added into deionized water at a weight ratio of 1:49. Tween® 80 (HNT:Tween® 80 (w/w)=10:1) was then added into the mixture, as non-ionic surfactant, to assist in individualizing the HNTs. The pH value of the mixture was adjusted to 10 using NaOH solution, to further avoid clustering of HNTs [48]. The mixture (at pH=10) was stirred using a mechanical stirrer at 90^{o}C and 1000 rpm for 1 hr and followed by ultrasonication at 65^{o}C for 1 hr to form original HNT dispersion. The original HNT dispersion was kept standing for 2 days until it was stabilized. The supernatant of the HNT dispersion was used as final individualized HNT dispersion while the solution at the bottom with HNT deposition was removed. The HNT content loading in the final individualized HNT dispersion was 0.5% by wt.

The PVA solution (10% by wt) was then added to the MFC suspension and the final individualized HNT dispersion, separately, at desired weight ratios. The MFC-PVA solution and HNT-PVA solution mixtures were stirred at 90^{o}C for 1 hr and ultrasonicated at 65^{o}C for 1 hr. Both mixtures were cast on Teflon® glass plate and slowly dried in an oven at 40^{o}C to form MFC-PVA (10% MFC content, by wt) and HNT-PVA composite sheets (10 HNT loading, by wt, in the composites). The MFC-PVA and HNT-PVA composites were hot pressed at 100^{o}C and 0.2 MPa for 60 min to form the final composites with smooth surfaces and thicknesses of about 0.2 mm.

6.3.3 Composting set-up

The composting medium was prepared by blending chicken manure (droppings) and sawdust in the ratio 1:1 (w/w) to obtain a C/N ratio of 50/50 [28]. Organic matter, sawdust, was added to increase the C/N ratio to achieve the optimum degradation of organic carbon and retention of nitrogen through microbial biomass formation. One 94.5 L plastic container was concentrically placed inside another 121 L plastic container. Wooden spacers were placed at the bottom of the outer cylinder to maintain uniform spacing of about 75 mm between the two containers. The inside container had circular holes on its wall for improved air circulation. The walls of the outer cylinder were covered with 50 mm thick insulating plastic foam to reduce the heat loss from the surface. This helped in maintaining the necessary temperature inside the composting unit [2, 3, 28].

All types of composites were dried in an oven at 105^{o}C for 12 hr and then placed in porous non-woven polypropylene (NPP) bags, which were then placed in the compost mix for microbial degradation. The NPP bags facilitated easy retrieval of the buried sheet specimens and its open structure allowed moisture, air and microorganism to move in and out freely during composting.

The composting conditions such as moisture, temperature, pH were monitored periodically. The moisture content of the compost mix was maintained at 50% by adding water initially and periodically. The temperature of the compost mix was maintained at 32^{o}C (in mesophilic phase) throughout the composting. This assured that the degradation was primarily attributed to the activity of mesophilic microorganisms, actinomycetes and fungi. The pH of the compost was measured to be acidic in the range of 5.5-6.0 during composting. During 120 days of composting, the specimens were retrieved at different time intervals, including 30, 45, 60, 75, 90 and 120 days of composting. These specimens at different stages of composting were dried in an oven at 105^{o}C for 12 hr again and then characterized for various properties [2, 3, 28].

6.3.4 Characterization

6.3.4.1 Surface characterization during composting

The PVA, GX-PVA, MX-PVA and MFC-PVA and HNT-PVA composite specimens during the composting were sputter coated with gold to prevent charging and improve the image contrast. Their surface topographies were observed with scanning electron microscope (SEM Leica 440, Leica Microsystems, Cambridge, UK) at an accelerating voltage of 15 kV.

6.3.4.2. Weight loss

All the specimens in the study were dried in an air-circulating oven at 105^{o}C for 12 hr and then weighed using a microbalance. The percent weight (wt) loss was calculated using the ratio of lost wt to original wt of the corresponding specimen.

6.3.4.3 Attenuated total reflectance-Fourier transform infrared (ATR-FTIR) spectroscopy

Chemical analysis of all the above mentioned specimens was carried out using an FTIR spectrophotometer (Nicolet Magna-IR 560, Thermo Scientific, Waltham, MA) in attenuated total reflection (ATR) mode using a split pea accessory. Spectra, averaged over 64 scans, were taken

in the range of 4000-800 cm^{-1} wavenumber at a resolution of 4 cm^{-1}. All the specimens were dried prior to conducting the ATR-FTIR spectroscopy.

6.3.4.4 Differential scanning calorimetry

Differential scanning calorimetry (DSC, Model Q2000, TA Instrument, New Castle, DE) was used to analyze the glass transition temperature (T_g), melting temperature (T_m), enthalpy of fusion (ΔH_f) and crystallinity of all the above mentioned specimens. All the specimens were dried in an oven at 105^oC for 12 hr prior to conducting the test. All DSC analyses were performed under a nitrogen atmosphere by keeping the flow rate of 50 ml/min, between -20 and 250^oC and at a scanning rate of 10^oC/min.

6.3.4.5 Sol-gel analysis of the resins

PVA, GX-PVA and MX-PVA specimens taken out and after specific composting periods and fully dried at 105^oC for 12 hr prior to conducting the sol-gel test. The specimens were weighed to obtain their initial dry wt and then immersed in distilled water in 150 mL glass bottles. The glass bottles with the specimens were then placed on a shaker table (MAXQ 4450, Thermo Scientific, Waltham, MA) maintained at 80^oC and 150 rpm for about 2 hr until the control (noncrosslinked) PVA was completely dissolved. The remaining solid contents for the crosslinked specimens were then washed three times with distilled water and filtered using a Whatman® filter paper (Number 4, 20-25 μm pore size) to obtain final residues. The water soluble part (sol) and particles smaller than 25 μm were removed during filtration. The final residues of the GX-PVA and MX-PVA specimens were dried at 105^oC for 12 hr to obtain their dry wt (gel). Ratios of the dry gel wt of the crosslinked PVA to their corresponding initial dry wt were used to determine the PVA gel (crosslinked) percentages.

6.3.4.6 Engery dispersive X-ray analysis

The elemental compostion of crystals observed on the surface of GX-PVA and MX-PVA specimens were analyzed by energy dispersive X-ray technique (EDX, Bruker AXS Microanalysis GmbH Berlin, Germany) with primary enegy of 9 KeV with 90-second scans.

6.4 Results and discussion

6.4.1 Surface characterization (SEM and EDX) during degradation

Typical SEM photomicrographs showing the surface characteristics of PVA (control), GX-PVA, MX-PVA and MFC-PVA (10 wt% MFC content) and HNT-PVA composites (10 wt% HNTs loading) as a function of composting days are presented in Figures 6.1, 6.2, 6.3, 6.4 and 6.5, respectively.

As seen in Figure 6.1 (A), the control PVA specimens showed a relatively clean and smooth surface before composting. After 30 days of composting no significant difference was observed on its surface topography (Figure 6.1 (B)). However, some traces were obvious on the surface of the resin after 45 days of composting (Figure 6.1 (C)). These traces, branched filamentous structures, are known as fungal hyphae [49, 50]. In most fungi, hyphae are the main mode of vegetative growth. In the present case these were thought to be generated when the composting was in the mesophilic phase confirming earlier studies [49, 50]. The number of fungal hyphae on the resin kept increasing after 60 days and 75 days of composting shown in (Figure 6.1 (D)) and (Figure 6.1 (E)), respectively, and even crisscrossed with each other. Some obvious grooves along with more fungal hyphae were observed on the surfaces of control PVA specimens after 90 days of composting indicating deeper biodegradation of the specimens (Figure 6.1 (F)). Fungal hyphae and deeper cracks spread everywhere on the surface of PVA specimen that resulted in specimens breaking down into many pieces after 120 days of composting (Figure 6.1 (G)).

In the case of GX-PVA, a different sequence of biodegradation was observed. As seen in Figure 6.2 (A), the GX-PVA specimens also showed a relatively smooth surface before composting. After 30 days of composting, surface of the resin began to get rougher but had a layer with crystal-like elements (Figure 6.2 (B)). This indicates that residual catalyst phosphoric acid had leached out and crystalized on the surface during composting [49]. The presence of residual phosphoric acid and possibly its salts on the surface were confirmed using energy-dispersive X-ray (EDX) analysis which showed a strong peak for phosphrous. After 45 days of composting, the surface roughness of the resin increased as the thickness of that crystal layer increased as well (Figure 6.2 (C)). The crystalline structure of the layer became more obvious on the surface of the resin after 60 days of composting (Figure 6.2 (D)). The crystal layer spread all over the surface of the specimen along with some grooves after 75 days of composting (Figure 6.2 (E)). After 90 days of composting, some grooves became more obvious and deeper indicating deep biodegradation of GX-PVA (Figure 6.2 (F)). While the specimen broke down in to many pieces after 120 days of composting, some deep cracks were seen on the remaining surface (Figure 6.2 (G)). Fungal hyphae were not seen in during composting. However, it is possible that they were covered by thick crystalline phosphoric acid or salt layer.

The MX-PVA specimens showed a relatively clean smooth surface before composting as seen in Figure 6.3 (A). After 30 and 45 days of composting, no obvious changes except some small crystals were observed on surface of the resin (Figure 6.3 (B) and 6.3 (C)). These crystals, as mentioned earlier, resulted from leached residual phosphoric acid and/or its salts. This was confirmed through EDX analysis which showed a strong peak for phosphrous. However, the amount was much less than GX-PVA [51]. After composting for 60 days or more, crystals were seen on specimen surfaces (Figure 6.3 (D)). This again indicates the possibility of residual

catalyst phosphoric acid leaching out during composting [51]. The amount of residual phosphoric acid was less on the surface of MX-PVA than on the surface of GX-PVA. One obvious reason for this is that less phosphoric acid was needed in fabrication of MX-PVA since MA also helped lowering the pH to 1 used for crosslinking. Another reason is that the MA crosslinked specimens were treated by water to partially remove some phosphoric acid after crosslinking. After 75 days of composting, many fungal hyphae appeared on the specimen surfaces (Figure 6.3 (E)) and after 90 days of composting a few grooves were seen along with more fungal hyphae (Figure 6.3 (F)). Some deep cracks were also seen on the surface and the specimen broke down to many pieces after 120 days of composting which indicates deep biodegradation of MA-PVA (Figure 6.3 (G)).

It can be clearly seen from Figure 6.4 (A) that the MFC fibrils are randomly organized but uniformly distributed on the specimen surface. It may be assumed that the MFC fibrils are uniformly distributed within the MFC-PVA composite. After 30 days of composting, no significant difference can be seen in the composite surface (Figure 6.4 (B)). However, some fungal hyphae were observed on the surface of the composite after 45 days of composting (Figure 6.4 (C)). The number of fungal hyphae increased significantly after 60 days of composting (Figure 6.4 (D)) and some non-obvious grooves were also observed on surfaces of the specimens after 75 days of composting (Figure 6.4 (E)). After 90 days of composting, the grooves became bigger and deeper resulting in the specimen breaking apart in to smaller fragments (Figure 6.4 (F)). Some deeper cracks were seen on the surface and the specimen finally broke down into many smaller pieces after 120 days of composting (Figure 6.4 (G)).

The HNT-PVA composites (Figure 6.5 (A)) also had relatively clean and smooth surfaces prior to composting. After 30 days of composting, no obvious change was observed on surface

of the specimens (Figure 6.5 (B)). Few spots and even cracks were observed on the specimen surface after 45 days of composting (Figure 6.5 (C)). However, as in most cases, some fungal hyphae were observed on the specimen surfaces after 60 days of composting (Figure 6.5 (D)). The number of fungal hyphae increased significantly and they were randomly distributed on surface of the composite after 75 days of composting (Figure 6.5 (E)). After 90 days of composting deeper grooves were observed which lead the specimen to break up (Figure 6.5 (F)). Some deeper cracks were seen on the surface and the specimen finally broke down into many pieces after 120 days of composting (Figure 6.5 (G)).

In summary, the SEM results indicated that the fungi played an important role during biodegradation of the PVA based materials. The fungi hyphae were seen to spread over the surface of the PVA based materials initiating the degradation process during composting [39-40]. In addition, surface roughness of specimens significantly increased with the composting time, especially after 75 days of composting. While the roughness causes the specimens to break into pieces, it can also expedite the biodegradation rate of the specimens by providing additional surface for the fungi to attack.

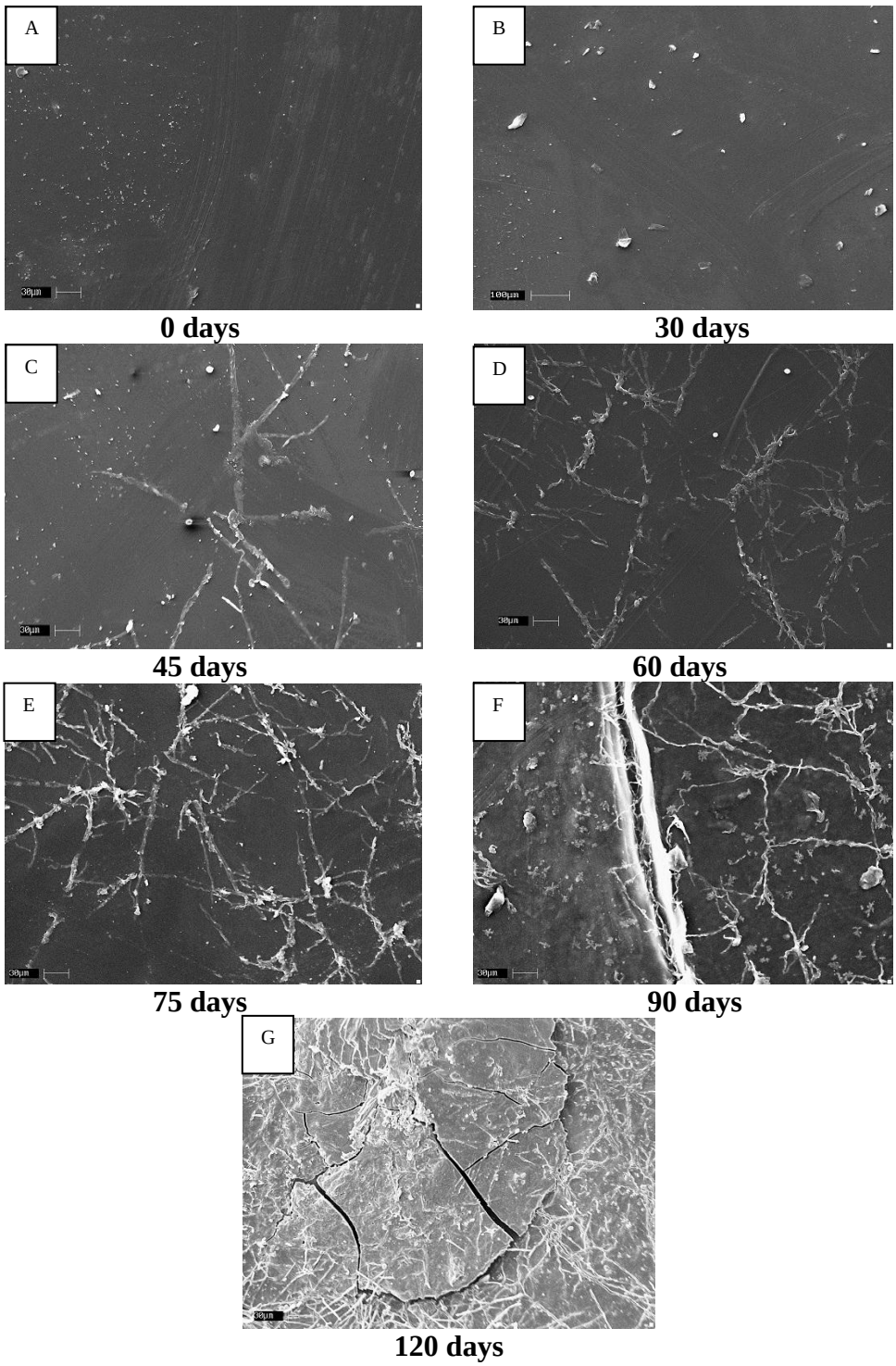

Figure 6.1 SEM photomicrographs showing effect of composting on the microscopic surface characteristics on PVA as a function of composting time

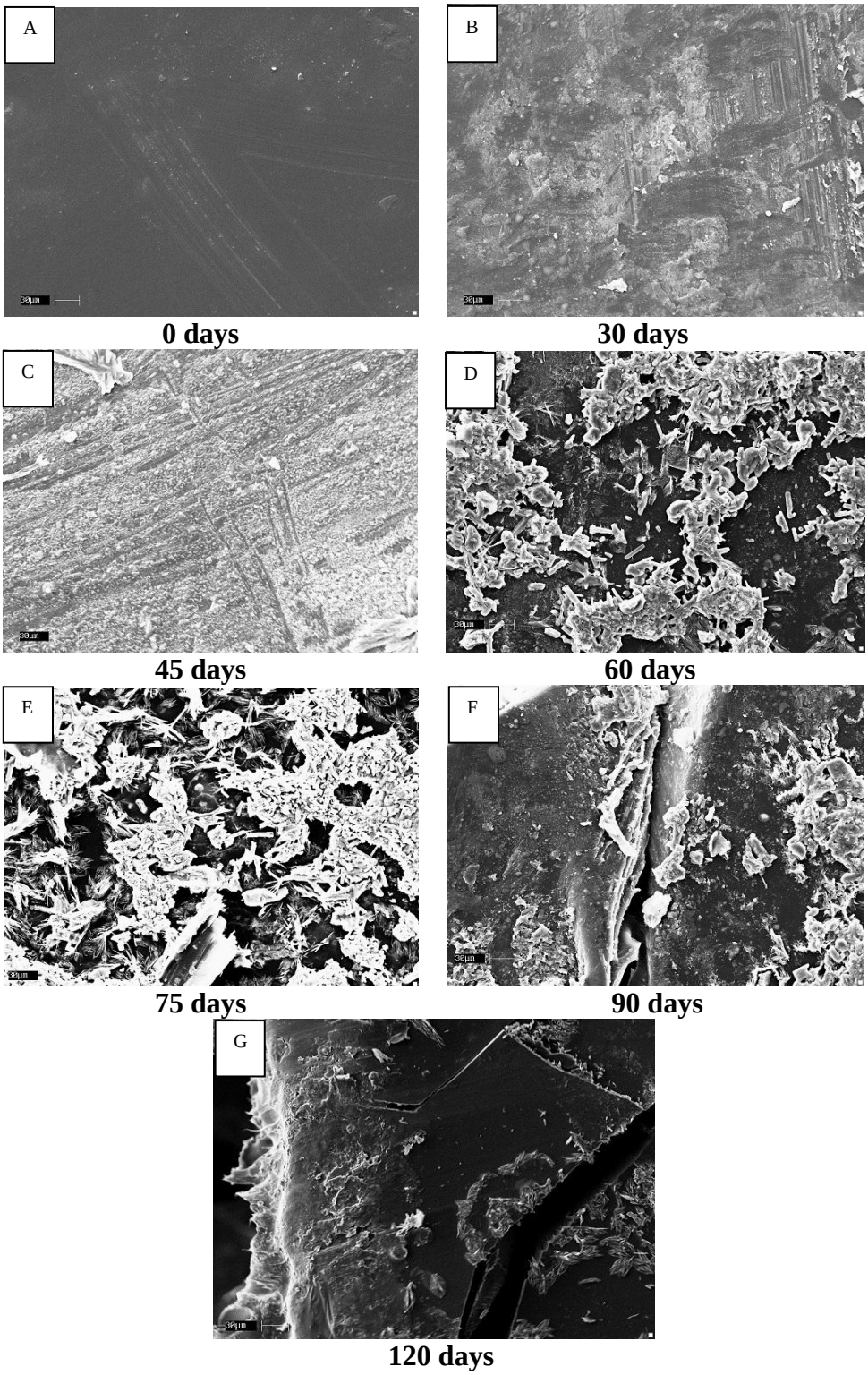

Figure 6.2 SEM photomicrographs showing effect of composting on the microscopic surface characteristics on GX-PVA as a function of composting time

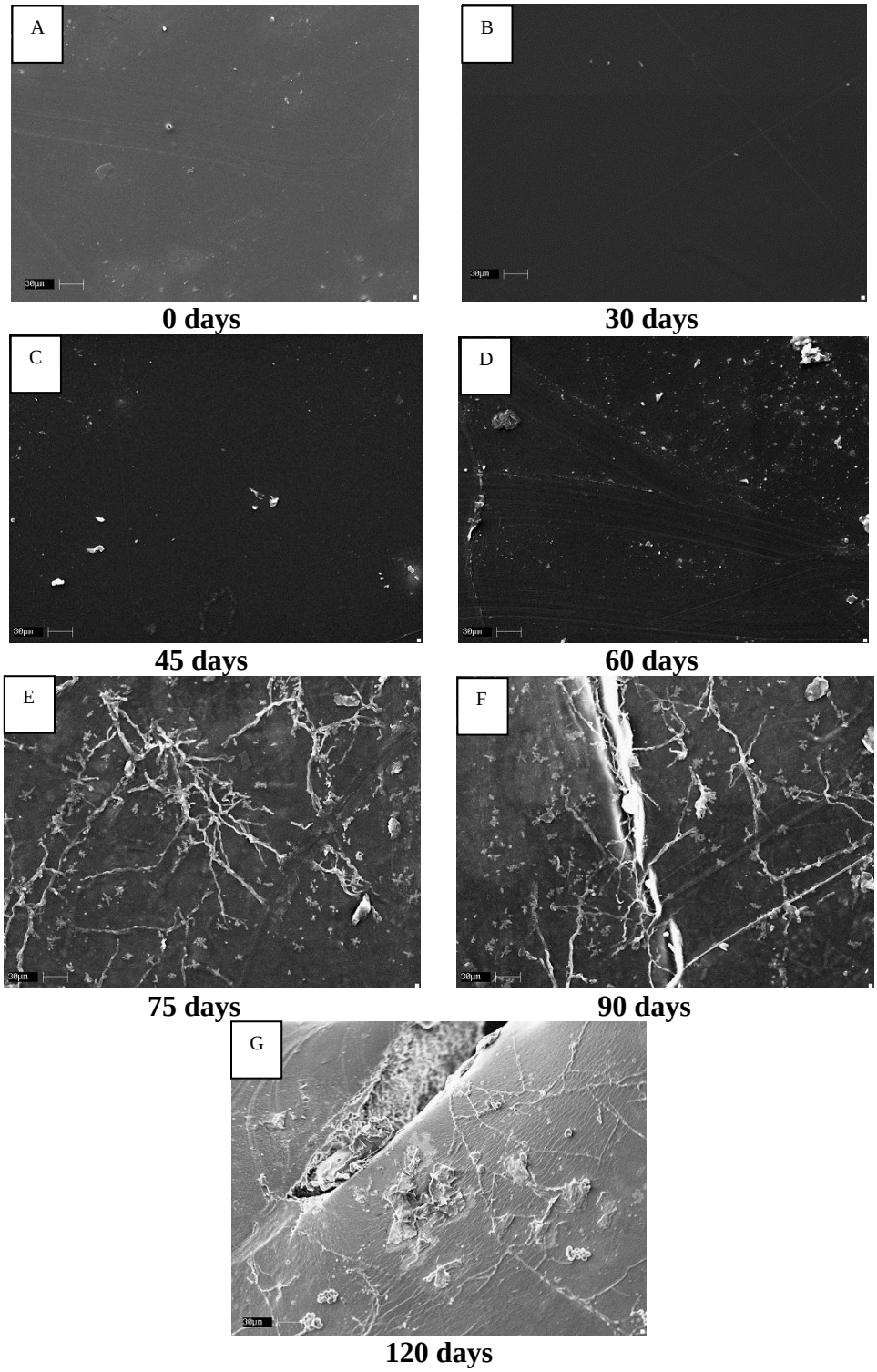

Figure 6.3 SEM photomicrographs showing effect of composting on the microscopic surface characteristics on MX-PVA as a function of composting time

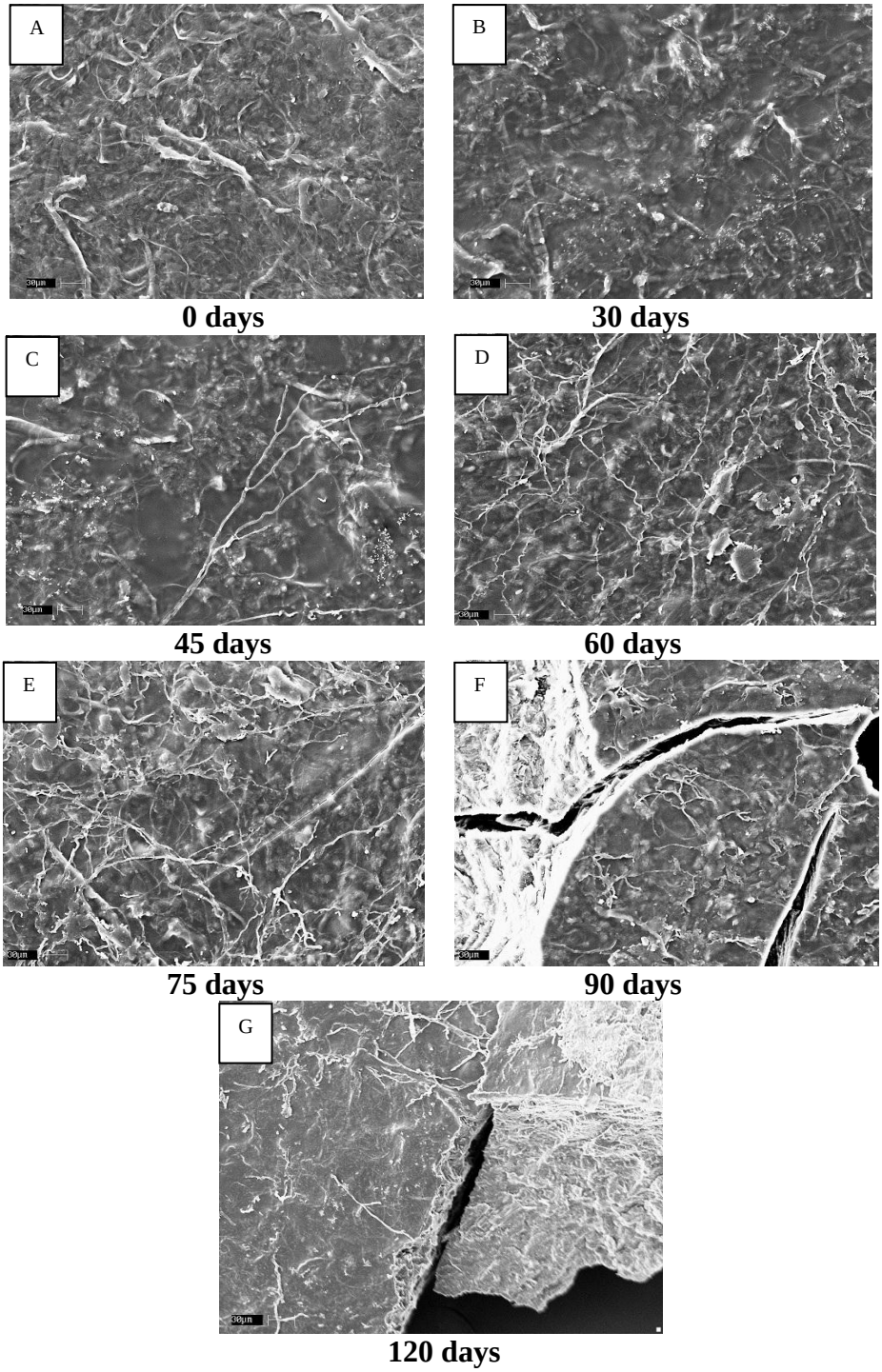

Figure 6.4 SEM photomicrographs showing effect of composting on the microscopic surface characteristics on MFC-PVA composites (10 wt% MFC content) as a function of composting time

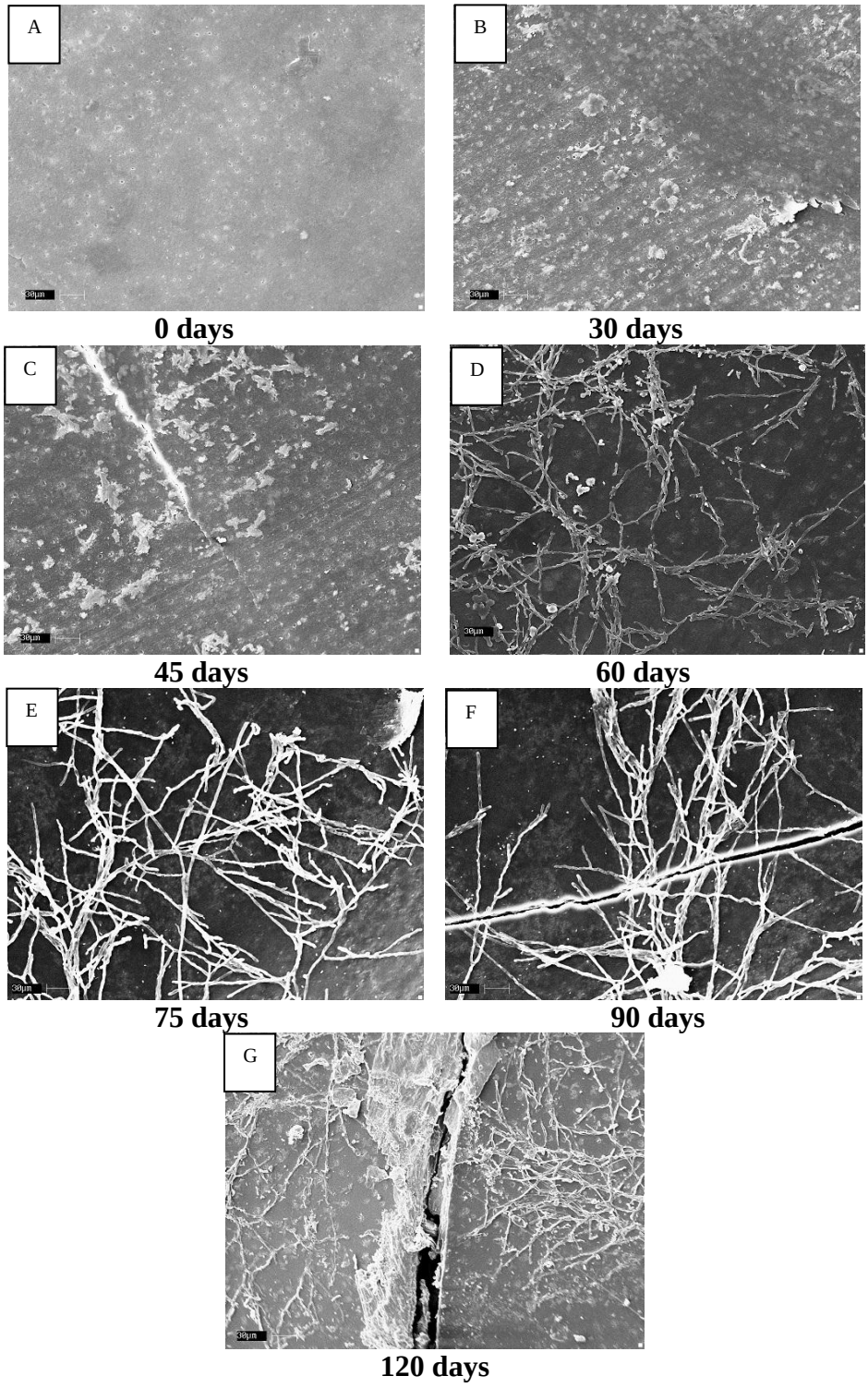

Figure 6.5 SEM photomicrographs showing effect of composting on the microscopic surface characteristics on HNT-PVA composites (10 wt% HNTs loading) as a function of composting time

6.4.2 Weight loss during composting

The effect of composting time on the weight loss of the PVA, GX-PVA, MX-PVA and MFC-PVA and HNT-PVA composite specimens is presented in Figure 6.6. The data in Figure 6.6 indicate, the weight loss for PVA specimen is 0.2, 2.1, 2.7, 3.2, 5.2 and 20.1% after 30, 45, 60, 75, 90 and 120 days of composting, respectively. The weight loss change was especially significant between 90 and 120 days of composting. Such rapid weight loss after 90 days of composting has beed recorded by other researchers [8]. As mentioned earlier, the specimens break into many pieces providing larger and larger areas for the fungi to be active. However, GX-PVA specimens showed a relatively higher weight loss at the beginning. The weight loss for GX-PVA specimens was 3.2% after 30 days of composting. This, however, was found to be due to the leaching of residual catalyst phosphoric acid present in the resin. Once the phosphoric acid was leached out the rate of weight loss of gloxal crosslinked PVA specimens decreased and was slightly lower than control PVA specimens, although the total weight loss was higher. After 120 days of composting, the weight loss of GX-PVA specimens only reached to 15.1%, lower than control PVA specimens. This is because gloxal crosslinking, though partial, decreased biodegradation rate as has been reported earlier [6, 34, 52]. The weight loss for MX-PVA specimens reached 0.8% after 30 days of composting. While this was higher than that obtained for PVA specimens, it was lower than GX-PVA specimens. This, again, is due to the leaching out of residual catalyst phosphoric acid present in the resin. As mentioned earlier, much lower amount of phosphoric acid was used in the case of MX-PVA specimens since MA was able to reduce the pH. Once the phosphoric acid had leached out, the biodegradation rate of MX-PVA specimens was found to decrease and was lower than both control PVA and GX-PVA specimens. The weight losses for MX-PVA specimens were 0.9, 1.0, 1.1, 2.1 and 10.1% respectively after

45, 60, 75, 90 and 120 days of composting. This is because MA being a better crosslinking agent compared to glyoxal, results in higher crosslink percentage and hence shows even lower biodegradation rate [6, 7, 34]. This conclusion was further confirmed by sol-gel results which have been described later in section 6.4.5. It indicates that gel percentage of MX-PVA specimens (90.3%) is much higher than GX-PVA specimens (7.0%). For MFC-PVA composites and HNT-PVA composites, the initial weight losses were close to those of PVA specimens, both were 0.1% after 30 days of composting. However, weight losses for MFC-PVA and HNT-PVA composites were lower than PVA after 45 days (1.1% and 0.9%), 60 days (1.4% and 1.3%), 75 days (1.8% and 1.8%), 90 days (3.1% and 3.0%) and 120 days (11.8% and 11.5%) of composting, respectively. These results contradict with some of the previous reports that addition of dispersed phase can increase the biodegradation rate of polymers [30-33]. However, in the present case, it is because MFC (10% by weight in the composite) is highly crystalline and does crack bridging that delays breaking apart of the PVA film. In the case of HNTs (10% by weight in the composite) they themselves do not degrade and influence the process in composting. From Figure 6.6, sharp increase in weight losses can be observed for all specimens from 75 to 120 days of composting. This confirms the SEM results which indicated that most of the specimens started to break down after 75 days of composting. The increased roughness of the surfaces of specimens may also be responsible for the sharp weight loss with composting time. This is because the roughness provides additional surface for the fungi to act. It can also facilitate the microorganisms to stay and propagate on the specimens and expedite the biodegradation.

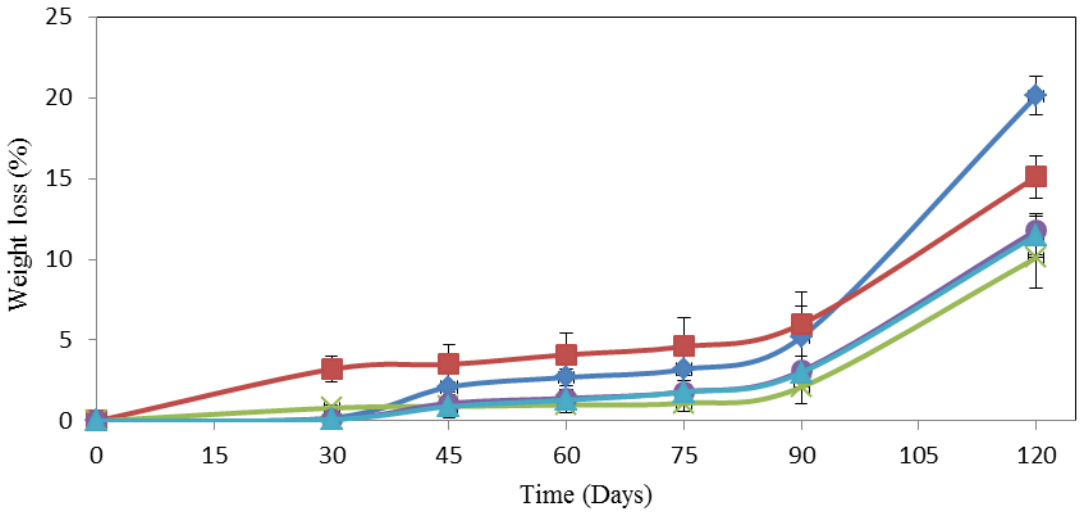

Figure 6.6 Effect of composting time on the weight loss (%) of PVA based materials
Symbols: ♦, PVA; ■, GX-PVA; ×, MX-PVA; ●, MFC-PVA composite; ▲, HNT-PVA composite

6.4.3 ATR-FTIR spectroscopy

The effect of composting time on the PVA specimen surface chemistry by ATR-FTIR is presented in Figure 6.7, where spectra (a), (b) and (c) represent PVA specimens after 0, 60 and 120 days of composting, respectively. A broad band at 3500-3200 cm^{-1} wavenumber seen in all three spectra is a result of the O-H stretching vibration resulting from the strong intra-molecular and inter-molecular hydrogen bonding in PVA [53-55]. The absorption band observed between 3000 and 2820 cm^{-1} wavenumbers is due to the stretching of the aliphatic C-H bonds [54]. The absorbance intensity ratio of O-H to C-H bands showed a decrease from 1.81 in spectrum (a) for control PVA specimen compared to 1.32 for spectrum (b) (60 days of composting) and 1.11 for spectrum (c) (120 days of composting). The lower ratio clearly indicates a reduction in the O-H groups and confirms degradation of PVA on surface of the specimen with composting time as explained by Chiellini et al. [9]. Absorption at 1750-1600 cm^{-1} (stretching of C=O) for PVA without composting (spectrum (a)) was weak (intensity ratio of C=O to C-H = 0.51) and indicates the presence of carbonyl (C=O) in the resin from the nonhydrolyzed acetate group

remaining in the PVA (98-99% hydrolyzed), confirming the earlier results obtained by Gohil et al. [53] and Mansur et al. [54]. In the ATR-FTIR spectrum (b), however, a slightly sharper absorption (intensity ratio of C=O to C-H = 0.55) observed at 1750-1600 cm^{-1} wavenumber indicates presence of more C=O in the PVA after 60 days composting. This confirms PVA biodegradation that results in the formation of β-hydroxylketone and 1, 3-diketone groups by a random endocleavage of the polymer chains with the help of enzymes, as observed by others [9, 36, 37]. In the ATR-FTIR spectrum (c), a much higher absorption (intensity ratio of C=O to C-H = 1.13) observed at 1750-1600 cm^{-1} wavenumber indicates presence of much more C=O in the PVA after 120 days of composting. This is as expected due to continued biodegradation that proceeds with composting time. These results also indicate formation of ketone groups during composting based on the decreased absorption intensity for O-H stretching vibration combined with the increased intensity of bands for C=O stretching vibrations.

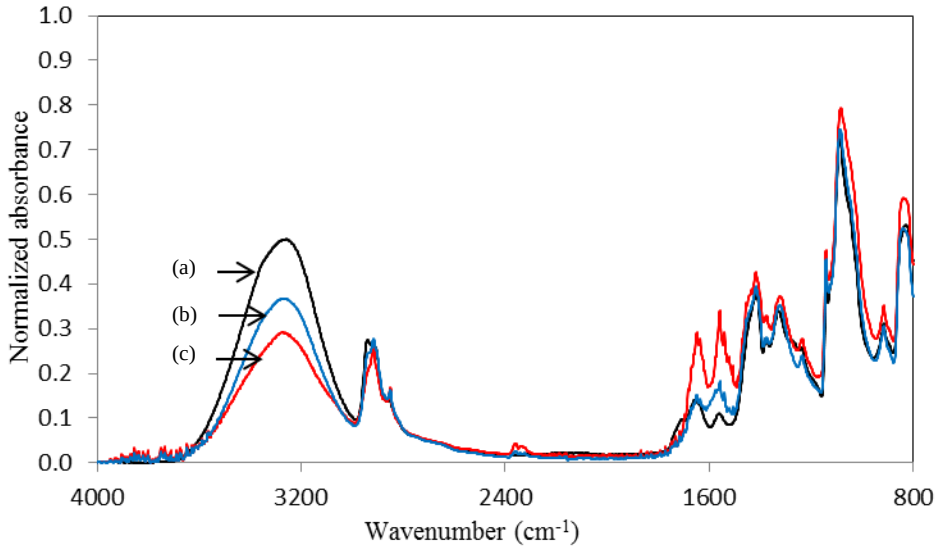

Figure 6.7 ATR-FTIR spectra of PVA after 0 days (a), 60 days (b) and 120 days (c) of composting time

The effect of composting time on the GX-PVA specimen surface chemistry by ATR-FTIR is presented in Figure 6.8, where spectra (a), (b) and (c) represent GX-PVA after 0, 60 and 120

days of composting, respectively. Two broad bands at 3500-3200 cm^{-1} and 3000-2820 cm^{-1} wavenumber are the results of the O-H stretching vibration resulting from the strong intra-molecular and inter-molecular hydrogen bonding and the stretching of aliphatic C-H bonds, respectively [53-55]. For spectrum (a), the two bands are separated well, and the absorbance intensity ratio of bands for O-H to C-H is 1.28, which is lower than that obtained for pure PVA, as can be expected, due to crosslinking through which the O-H groups are consumed. However, for spectra (b) and (c), no obvious separation was observed between these two bands. This is because of the residual phosphoric acid (catalyst) and crosslinker (glyoxal) leaching out during composting. In addition, the absorbance intensity ratio of O-H to C-H bands decreased to 1.11 and 0.87, respectively, for spectra (b) and (c). The lower absorption indicating a reduction in the O-H groups confirms degradation of PVA with composting time. Absorption at 1750-1600 cm^{-1} (stretching of C=O) for non-composted GX-PVA (spectrum (a)) was weak (intensity ratio of C=O to C-H = 0.63) and indicates the presence of carbonyl (C=O) in the specimens from residual unreacted aldehyde groups from glyoxal and the nonhydrolyzed acetate groups in PVA (98-99% hydrolyzed). In the ATR-FTIR spectra (b), however, a much sharper absorption (intensity ratio of C=O to C-H = 1.09) observed at 1750-1600 cm^{-1} wavenumber indicates presence of larger number of C=O groups in the GX-PVA after 60 days composting. The increase of intensity is due to the ketone groups obtained from the biodegradation of GX-PVA [1, 2, 9, 27]. In the ATR-FTIR spectrum (c), the intensity ratio of C=O to C-H observed at 1750-1600 cm^{-1} wavenumber is 1.08, almost similar with that in spectrum (b). As glyxoal has been reported as a readily biodegradable chemical and can be degraded during composting [52]. Therefore, more ketone groups generated from degrading GX-PVA helped to maintain the intensity of C=O in spectrum (c). Overall, the ATR-FTIR results confirm the biodegradation of

GX-PVA.

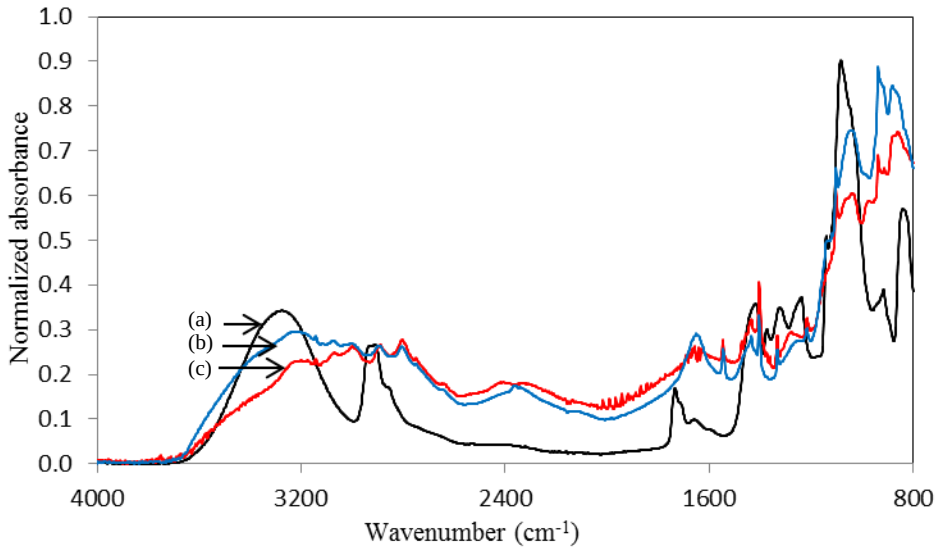

Figure 6.8 ATR-FTIR spectra of GX-PVA after 0 days (a), 60 days (b) and 120 days (c) of composting time

The effect of composting time on the MX-PVA specimen surface chemistry by ATR-FTIR is presented in Figure 6.9, where spectra (a), (b) and (c) are, respectively, representing corresponding MX-PVA after 0, 60 and 120 days of composting. As seen in spectra (a), (b) and (c), during composting, the absorbance intensity ratio for O-H to C-H bands showed a decrease from 1.42 in spectrum (a) for control MX-PVA compared to 1.37 for spectrum (b) (60 days of composting) and 1.22 for spectrum (c) (120 days of composting). The lower absorption indicates a reduction in the O-H groups and confirms degradation of MX-PVA on surface of the specimen with composting time. Absorption at 1750-1600 cm^{-1} (stretching of C=O) for MX-PVA without composting (spectrum (a)) was relatively weak (intensity ratio of C=O to C-H = 0.46) and indicates the presence of carbonyl (C=O) in the resin from residual MA and the nonhydrolyzed acetate group remaining in the PVA (98-99% hydrolyzed) [53, 54]. In the ATR-FTIR spectrum (b), however, a slightly sharper absorption (intensity ratio of C=O to C-H = 0.50) observed at 1750-1600 cm^{-1} wavenumber indicates presence of higher number of C=O groups in the MX-

PVA after 60 days composting. It confirms the biodegradation of MX-PVA and formation of β-hydroxylketone and 1, 3-diketone groups by a random cleavage of the polymer chains with the help of enzymes shown by others [9, 36, 37]. In the ATR-FTIR spectrum (c), a sharper absorption (intensity ratio of C=O to C-H = 0.62) observed at 1750-1600 cm^{-1} wavenumber indicates presence of much more C=O in the MX-PVA after 120 days of composting. This indicates that with composting time as degradation proceeded, more ketone groups were generated. Overall, the ATR-FTIR results confirm the biodegradation of MX-PVA, though the change is not as significant as pure PVA or GX-PVA, due to its high gel (crosslinked) percentage.

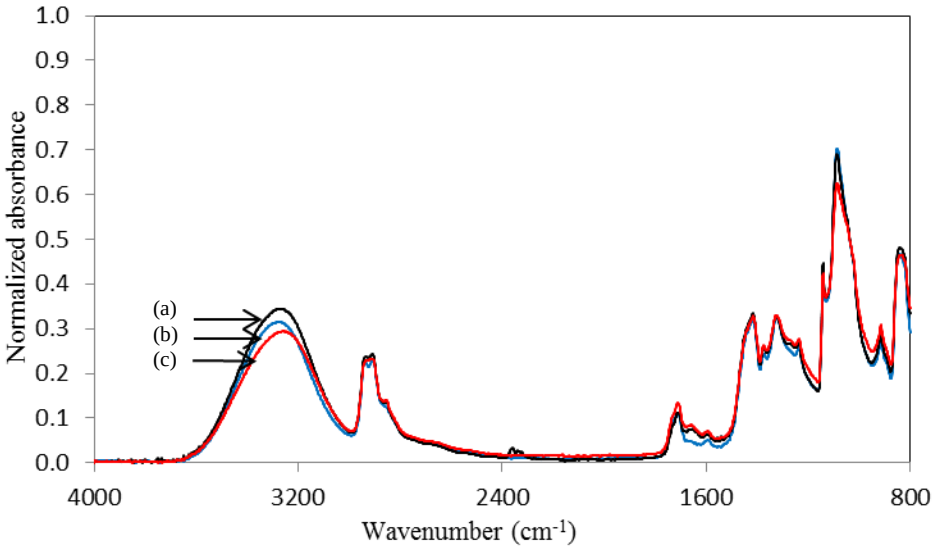

Figure 6.9 ATR-FTIR spectra of MX-PVA after 0 days (a), 60 days (b) and 120 days (c) of composting time

The effects of composting time on the MFC-PVA composite and HNT-PVA composite were identical to pure with PVA based on ATR-FTIR spectra where only PVA degraded leaving MFC and HNT intact, within the 120 days of composting.

6.4.4 DSC study

The melting temperatures (T_m), associated enthalpies (ΔH_f) of fusion and corresponding crystallinity observed in the DSC scans for PVA based resins and composites after different

composting times (up to 120 days) are presented in Table 6.1. It is interesting to note that both T_m and ΔH_f for all specimens, including PVA, GX-PVA, MX-PVA, MFC-PVA and HNT-PVA composite specimens increased quickly with the composting time the initial 45 days of composting. The percent crystallinity for all the specimens were calculated based on 138.6 J/g for 100% crystalline PVA and are shown in Table 6.1 [56-59]. After 45 days of composting, T_m and crystallinity for PVA increased from 196.1^{o}C and 44.8% to 210.1^{o}C and 53.6%, for GX-PVA increased from 175.6^{o}C and 39.9% to 200.8^{o}C and 49.5%, for MX-PVA increased from 188.2^{o}C and 33.8% to 193^{o}C and 50.0%, for MFC-PVA composite increased from 198.6^{o}C and 37.2% to 208.3^{o}C and 50.4%, for HNT-PVA composite increased from 199.7^{o}C and 40.0 to 210.1^{o}C and 47.6%. The increase of crystallinity is a result of two main factors. The first, as mentioned earlier, is that the enzymes from microbes (fungi) attack the amorphous domain first and digest it away. As the amorphous fraction decreases, the percentage of crystalline domains in the remaining resin increases with composting time [3]. In addition, hydrolytic degradation also occurs primarily in the amorphous region which again contributes to the increase in crystallinity [2, 3, 60, 61]. Similar increase in crystallinty has been shown to occur during the degradation of polyester fibers and soy protein isolate films [2, 3, 57, 58]. The second factor for the increase of crystallinity is that the PVA chain segments remaining in the amorphous regions acquire more chain mobility during composting, both because of moisture absorption as well as reduced molecular weight and thus enable them to be incorporated into the existing crystals [60-62]. This process, involving an increase in the density due to higher crystallinity, is called chemicrystallization [60-62]. The increase in the T_m and ΔH_f also indicates possible lamella thickening linked to the chemicrystallization process [60-62]. Changes in T_m and ΔH_f values for all the specimens, however, were less significant from the results between 45 and 75 days of

composting. Both T_m and ΔH_f increased quickly again between the 75 days to 90 days of composting. This indicates more amorphous PVA was biodegraded or incorporated into existing crystals during this period which has been confirmed the observations from SEM and weight loss and explained earlier. However, both T_m and ΔH_f for all the specimens remained constant or even slightly decresed between the 90 days to 120 days of composting, though all the specimens degraded significantly during this period. This is very likely that enzymes and moisture affecting the crystalline regions of the specimens and starting to degrade it [63].

Based on the results presented in Table 6.1 and results obtained in our previous research, following conclusions may be made [6, 7]. After glyoxal crosslinking, the T_m, ΔH_f and crystallinity values decreased from 196.1^{o}C, 62.1 J/g and 44.8% for control PVA to 175.6, 55.3 J/g and 39.9% whereas after MA crosslinking, these values decreased to 188.2, 46.9 J/g and 33.8%, respectively, prior to composting. The lower ΔH_f and crystallinity after crosslinking is quite common as the crosslinked polymer cannot crystallize and has been observed in most polymers [6, 7, 53, 64-66]. The T_m for the MFC-PVA composite was observed at 198.6^{o}C which is close to that obtained for PVA. No T_m for cellulose can be observed since it degrades prior to melting [67, 68]. As a result, the DSC thermogram mainly represented the PVA behavior. The ΔH_f and the crystallinity of the PVA in MFC-PVA composite were 51.6 J/g and 37.2%, respectively, which were much lower than 62.1 J/g and 44.8%, respectively, obtained for control PVA. It is likely that the nano- and micro-fibrils in the MFC can inhibit the crystallization of PVA, as they are well dispersed. The fibrils can suppress the free movement of polymeric chains restricting their ability to fold and thus lower the crystallinity [69]. The T_m for the HNT-PVA composite was observed at 199.7^{o}C, about 3.6 ^{o}C higher than that of control PVA. This suggests that HNTs have the ability to lead to slightly increase T_m of polymers [70]. The ΔH_f and the

crystallinity of the PVA in HNT-PVA composite (10% loading) were 55.4 J/g and 40.0%, respectively, which were much lower than 62.1 J/g and 44.8%, respectively, obtained for control PVA. It is likely that the HNTs can inhibit the crystallization of PVA, as they are well dispersed [71].

Table 6.1 Effect of composting time on the melting temperature and melting enthalpy of PVA based resins and composites

Composting time (Days)/Properties	PVA	GX-PVA	MX-PVA	MFC-PVA composite (10% MFC)	HNT-PVA composite (10% HNTs)
0 / T_m (^oC)	196.1	175.6	188.2	198.6	199.7
Enthalpy (J/g)	62.1	55.3	46.9	51.6	55.4
Crystalinity (%)	44.8	39.9	33.8	37.2	40.0
30 / T_m (^oC)	206.9	199.2	192.4	204.8	208.2
Enthalpy (J/g)	68.6	64.6	47.9	58.1	61.2
Crystalinity (%)	49.5	46.6	34.6	41.9	44.3
45 / T_m (^oC)	210.1	200.8	193.0	208.3	210.1
Enthalpy (J/g)	74.3	68.6	50.0	69.8	66.0
Crystallinity (%)	53.6	49.5	36.1	50.4	47.6
60 / T_m (^oC)	210.8	199.2	192.7	209.9	211.7
Enthalpy (J/g)	76.6	70.3	50.1	70.0	66.5
Crystallinity (%)	55.3	50.7	36.1	50.5	48.0
75 / T_m (^oC)	210.6	202.4	193.1	210.6	211.4
Enthalpy (J/g)	76.8	69.7	50.4	68.4	65.6
Crystallinity (%)	55.4	50.3	36.4	49.4	47.3
90 / T_m (^oC)	212.5	205.9	194.0	211.5	213.0
Enthalpy (J/g)	81.0	74.1	54.7	72.0	69.8
Crystallinity (%)	58.4	53.5	39.0	51.9	50.4
120 / T_m (^oC)	211.8	205.3	195.0	211.0	212.6
Enthalpy (J/g)	81.4	72.8	54.3	71.1	69.4
Crystallinity (%)	58.7	52.5	39.2	51.3	50.1

6.4.5 Sol-gel analysis of PVA based materials

The gel (crosslinked) percentages for PVA, GX-PVA and MX-PVA specimens after different composting times (up to 120 days) are presented in Table 6.2.

As seen in Table 6.2, the gel percentage before and during composting was 0%, for the control PVA specimens. However, in the case of GX-PVA, the gel percentage slightly increased from 7.0% to 7.5% after 30 days of composting. This initial increase in gel percentage is mostly due to preferential leaching out of the non-crosslinked part during the first 30 days of composting as can be expected. Thereafter, gel percentages of the specimen decreased and reached 4.6% and 4.4% after 90 days and 120 days of composting respectively. This indicates composting process can break crosslinks and reduce the gel percentage of the specimen, although, the process seems to be slow. In the case of MX-PVA the reduction in gel percentage is similar as GX-PVA. After 30 days of composting, the gel percentage increased to 90.5% from 90.3%. Thereafter, gel percentages of the specimen decreased only slightly to 87.9% after 120 days of composting. Slow cleavage/breakage of crosslinks and hence slower degradation may be used advantageously to increase the life of the resin or the composite.

Table 6.2 Effect of composting time on the gel (%) of PVA, GX-PVA and MX-PVA

Composting time (Days)	PVA	GX-PVA	MX-PVA
0	0	7.0	90.3
30	0	7.5	90.5
45	0	4.9	89.1
60	0	4.9	88.6
75	0	5.0	88.5
90	0	4.6	88.5
120	0	4.4	87.9

6.5 Conclusions

In this study the biodegradation of polyvinyl alcohol (PVA) based materials, crosslinked, non-crosslinked and nanocomposites, in a composting medium was characterized. Chicken dropping-based compost medium was used. The composting process was monitored for up to 120 days and various techniques, including weight loss, SEM, EDX, ATR-FTIR, DSC, sol-gel analysis and EDX were used to characterize the biodegradation. The results of these analyses suggest that biodegradation of PVA based materials in compost medium is mainly by fungal means and the enzymes from fungi degraded amorphous regions of the specimens first. The surface roughness of the specimens signicantly increased with the composting time which could facilitate microorganism to stay and propagate, acceperating the degradation. All specimens broke up into smaller pieces after 120 days of composting. The results also showed that crosslinking and addition of specific fillers such as high crystalline MFC and nanoclay HNTs can decrease the biodegrdation rate. These results suggest that both crosslinking and addition of

suitable fillers may be used to increase the service life of the PVA based biodegradable composites.

6.6 Acknowledgements

This work was partly supported by the National Textile Center (NTC), the Wallace Foundation and the Department of Fiber Science & Apparel Design. The authors also thank the Cornell Center for Materials Research (CCMR) and Cornell Poultry Research Farm for the use of their facilities and materials.

References

[1] Cho Daehwan, Netravali AN, Joo YL. Mechanical properties and biodegradability of electronspun soy protein isolate/PVA hybrid nanofibers. Polym Degrad Stab 2012; 97: 747-754.

[2] Luo S, Netravali AN. A study of physical and mechanical properties of poly(hydroxybutyrate-co-hydroxyvalerate) during composting. Polym Degrad Stab 2003; 80: 59-66.

[3] Lodha P, Netravali AN. Effect of soy protein isolate resin modifications on their biodegradation in a compost medium. Polym Degrad Stab 2005; 87: 465-477.

[4] Qiu K, Netravali AN. Biodegradable composites of polyvinyl alcohol reinforced with microfibrillated cellulose. J Mater Sci 2012; 47 (16): 6066-6075.

[5] Qiu K, Netravali AN. 'Green' composites based on bacterial cellulose produced using novel low cost carbon source and soy protein resin. Recent advances in adhesion science & technology: Mittal festschrift. Netherlands: Brill; 2011 Accepted.

[6] Qiu, K, Netravali, AN. Fabrication and characterization of biodegradable composites based on microfibrillated cellulose and polyvinyl alcohol. Compos Sci Technol 2012; 72 (13): 1588-1594.

[7] Qiu, K, Netravali, AN. Halloysite nanotube reinforced biodegradable nanocomposites using noncrosslinked and malonic acid crosslinked polyvinyl alcohol. Compos Part A-Appl S 2012; Submitted.

[8] Stevens ES. Green plastics: an introduction to the new science of biodegradable plastics, Princeton, NJ: Princeton University Press, 2002. p.10-30.

[9] Chiellini E, Corti A, D'Antone S, Solaro R. Biodegradation of poly (vinyl alcohol) based materials. Prog Polym Sci 2003; 28: 963-1014.

[10] Netravali AN, Chabba S. ‘Composites get greener’. Mater Today, 2003, 6 (4): 22-29.

[11] Georgia Tech Research Institute . ‘Breaking down plastics: new standard specification may facilitate use of additives that trigger biodegradation of oil-based plastics in landfills’. http://gtresearchnews.gatech.edu/biodegradation-of-plastics/, Accessed November 201.

[12] Mittal V. Nanocomposites with biodegradable polymers: synthesis, properties and future perspectives. Oxford, UK: Oxford University Press, 2011. p. 1-27.

[13] Bohlmann GM. General characteristics, processability, industrial applications and market evolution of biodegradable polymers. In: Bastioli C. Handbook of biodegradable polymers. Shawbury, UK: Rapra Tech Ltd 2005. p. 183-218.

[14] Lemm W, Krukenberg T, Regier G, Gerlach K, Bucherl ES. Biodegrdation of some biomaterials after subcutaneous implantation. Proc Eur Sco Artif Org 1981; 8:71-75.

[15] Potts JE, Clendinning RA, Ackart WB, Neigisch WD. The biodegradability of synthetic polymers. In; Guillet J. Polymers and ecological problems. New York: Plenum Press 1973. p. 61-80.

[16] Swift G. Biodegrdable polymers in the environment: are they really biodegradable? . Pro ACS Div Polym Mater Sci Eng 1992; 66: 403-404.

[17] Ratner BC, Gladhill KW, Horbett TA. Analysis of *in vitro* enzymatic and oxidative degradation of polyurethane. J Biome Mater Res 1988; 22: 509-527.

[18] Hergenrother RW, Wabers HD, Cooper SL. The effect of chain extenders and stabilizers on the in vivo stability of polyurethanes. J Appl Biomater 1992; 3: 17-22.

[19] Reich L, Stivala SS. Elements of polymer degradation. New York: McGraw-Hill 1971.

[20] Kronenthal RL. Biodegradable polymers in medicine and surgery. In: Kronenthal RL, Oser Z, Martin E. Polymers in medicine and surgery. New York: Plenum Press 1975. p. 119-133.

[21] Gilding DK. Biodegradable polymers. In: Williams DF. Biocompatibility of clinic implant materials. Boca Raton, FL: CRC Press 1981. p. 209-232.

[22] Itavaara M, Karjomaa S, Selin JF. Biodegradation of polyolactide in aerobic and anaerobic thermophilic conditions. Chemosphere 2002; 46: 879-885.

[23] Tokiwa Y, Suzuki T. Hydrolysis of polyesters by rhizopus delemar lipase. Agric Biol Chem 1978; 42: 1071-1072.

[24] Tokiwa Y, Suzuki T. Hydrolysis of copolyesters containing aromatic and aliphatic ester blocks by lipase. J Appl Polym Sci 1981; 26: 441-448.

[25] Tokiwa Y, Suzuki, T, Ando T. Synthesis of copolyamide-esters and some aspects involved in their hydrolysis by lipase. J Appl Polym Sci 1979; 24: 1701-1711.

[26] Tokiwa Y, Calabia BP, Ugwu CU, Aiba S. Biodegradability of plastics. Int J Mol Sci 2009; 10: 3722-3742.

[27] Corti A, Solaro R, Chiellini E. Biodegradation of poly (vinyl alcohol) in selected mixed microbial culture and relevant culture filtrate. Polym Degrad Stab 2002; 75 (3): 447-458.

[28] Lodha P. Fundamental approaches to improving performance of soy protein isolate based 'green' plastics and composites. Ithaca, NY: PhD Dissertation, Cornell University 2004; p. 101-129.

[29] Semenov SA, Gumargalieva KZ, Zaikov GE. Biodegrdation and durability of materials under the effect of microorganisms. Boston, MA: VSP BV, 2003.

[30] Han SI, Lim JS, Kim DK, Kim MN, Im SS. In situ polymerized poly (butylene succinate)/silica nancomposites: physical properties and biodegradation. Polym Degrad Stab 2008; 93: 889-895.

[31] Yang HS, Yoon JS, Kim MN. Dependence of biodegradability of plastics in compost on the shape of specimens. Polym Degrad Sta 2005; 87: 131-135.

[32] Ray SS, Okamoto M. Biodegradable polylactide and its nancomposites; opening a new dimension for plastics and composites. Macromol Rap Comm 2003; 24: 815-840.

[33] Fukuda N, Tsuji H, Ohnishi Y. Physical properties and enzymatic hydrolysis of poly (-latide)-$CaCO_3$ composites. Polym Degrad Stab 2002; 78, 119-127.

[34] Quynh TM, Mitomo H, Nagasawa N, Wada Y, Yoshii F, Tamada M. Properties of crosslinked polylactides (PLLA & PDLA) by radation and its biodegradability. Euro Polym J 2007; 43: 1779-1785.

[35] Solaro R, Corti A, Chiellini E. Biodegradation of poly (vinyl alcohol) with different molecular weight and degree of hydrolysis. Polym Adv Technol 2000; 11 (8-12): 873-878.

[36] Watanabe Y, Morita M, Hamada N, Tsujisaka Y. Formation of hydrogen peroxide by a polyvinyl alcohol degrading enzyme. Agric Biol Chem 1975; 39: 2447-2448.

[37] Suzuki T, Ichihara Y, Yamada M, Tonomura K. Some characteristics of *Pesudomonas* O-3 which utilize polyvinyl alcohol. Agric Biol Chem 1973; 37: 747-756.

[38] Sakai K, Hamada N, Watanabe Y. Studies on the poly(vinyl alcohol)-degrading enzyme. Part VI. Degradation mechanism of poly(vinyl alcohol) by successive reactions of secondary alcohol oxidase and β-diketone hydrolase from *Pseudomonas* sp. Agric Biol Chem 1986; 50: 989-996.

[39] Jecu L, Grosu E, Raut I, Ghiurea M, Constantin M, Stoica A, Stroescu M, Vasilescu G. Fungal degradation of polymeric materials: morphological aspects. http://www.inginerie-electrica.ro/acqu/2011/P_1_Fungal_degradation_of_polymeric_materials_Morfological_aspects.pdf. Accessed 2012.

[40] Larking DM, Crawford RJ, Christie GBY, Lonergan GT. Enhanced degradation of polyvinyl alcohol by *Pysnoporus cinnabarinus* after pretreatment with Fenton's reagent. Appl Environ Microbiol 1999; 65 (4): 1798-1800.

[41] Chiellini E, Corti A, Solaro R. Biodegradation of poly (vinyl alcohol) based blown films under different environmental conditions. Polym Degrad Stab 1999; 64: 305-312.

[42] Jayasekara R, Harding I, Bowater I, Christie GBY, Lonergan GT. Biodegradation by composting of surface modified starch and PVA blended films. J Polym Environ 2003; 11 (2): 49-56.

[43] Solaro R, Corti A, Chiellini E. A new respirometric test simulating soil burial conditions for the evaluation of polymer biodegradation. J Environ Polym Degrad 1998; 6: 203-208.

[44] Matsumura S, Tanaka T. Novel malonate-type copolymers containing vinyl alcohol blocks as biodegradable segments and their builder performance in detergent formulation. J Environ Polym Degrad 1994; 2: 89-97.

[45] Diaz LF, Savage GM, Eggerth LI, Golueke CG. Composting and recycling-municipal solid waste. Boca Raton, FL: Lewis Publishers, 1993.

[46] Jian S, Ming SX. Crosslinked PVA-PS thin-film composite membrane for reverse osmosis. Desalination 1987; 62: 395-403.

[47] Majumdar S, Adhikari B. Polyvinyl alcohol: A taste sensing material. Sensors Actuators B-Chem 2006; 114: 747-755.

[48] Rathi P. Soy protein based nanophase reins for green composites. Ithaca, NY: A project report, Cornell University, 2007. p. 13-18.

[49] Rudnik E. Compostable polymer materials. Oxford, UK: Elsevier, 2008. p. 89-112.

[50] Sang BI, Hori K, Tanji Y, Unno H. Fungal contribution to in situ biodegradation of poly (3-

hydroxybutyrate-co-3-hydroxyvalerate) film in soil. Appl Microbiol Biotechnol 2002; 58: 241-247.

[51] Taixing Shenlong Chemical Co., Ltd. Crystal ortho phosphorous acid. http://www.sl-chemical.com/pages/pro4_en.htm. Accessed June 2012.

[52] BASF. Glyoxal-the sustainable solution for your business. http://worldaccount.basf.com/wa/NAFTA/Catalog/ChemicalsNAFTA/doc4/BASF/PRD/30037091/.pdf?title=Brochure&asset_type=pi/pdf&language=EN&urn=urn:documentum:eCommerce_sol_EU:09007bb2800475c8.pdf, Accessed November 2011.

[53] Gohil JM, Bhattacharya A, Ray P. Studies on the cross-linking of poly (vinyl alcohol). J Polym Res 2006; 13: 161-169.

[54] Mansur HS, Sadahira CM, Souza AN, Mansur AAP. FTIR spectroscopy characterization of poly (vinyl alcohol) hydrogel with different hydrolysis degree and chemically crosslinked with glutaraldehyde. Mater Sci Eng C 2008; 28: 539-548.

[55] Kim JH, Moon EJ, Kim CK. Composite membranes prepared from poly (m-animostyrene-co-vinyl alcohol) copolymers for the reverse osmosis process. J Membrane Sci 2003; 216: 107-120.

[56] Warner SB. Fiber Science. Prentice Hall, Upper Saddle River, NJ, 1995, pp. 205-206.

[57] Blaine RL. Determination of polymer crystallnity by DSC. TA Instruments, www.tainstruments.com/library_download.aspx?file=TA123.PDF, Accessed December 2011.

[58] Sichina WJ. DSC as problem solving tool: measurement of percent crystallnity of thermoplastics. PerkinElmer Instruments, http://www.perkinelmer.com/Content/applicationnotes/app_thermalcrystallinitythermoplastics.pdf , Accessed December 2011.

[59] Guirguis OW, Moselhey MTH. Thermal and structural studies of poly (vinyl alcohol) and hydroxypropyl cellulose blends. Nat Sci, 2012, 4 (1): 57-67.

[60] Netravali AN, Krstic R, Crouse JL, Richmond LE. Chemical stability of polyester fibers and geotextiles without and under stress. ASTM; 1993. STP 1190 p. 207-217.

[61] Mathur A, Netravali AN, O'Rourke D. Chemical aging effects on the physic-mechanical properties on the polyester and polypropylene geotextiles. Geotext Geomembranes 1994; 13:591-626.

[62] Jailloux JM, Verdu J. Kinetic models for the life prediction in PET hygrothermal aging: a critical survey. In: Den Hoedt (Ed.), Proceedings of 4th international conference on geotextiles, geomembranes and related products. Rotterdam, Netherlands: Balkema; 1990. p. 727.

[63] Bikiaris DN, Papageorgious GZ, Achili DS. Synthesis and comparative biodegradability studies of three (alkylene succinate)s. Polym Degrad Stab, 2006, 91 (1): 31-43.

[64] Young RJ, Lovell PA. Introduction to polymers, 3rd edition. CRC Press, Boca Raton, FL, 2011, pp. 591-622.

[65] Kim JH, Kim JY, Lee YM, Kim KY. Properties and swelling characteristics of cross-linked poly (vinyl alcohol)/chitosan blend membrane. J Appl Polym Sci, 1992, 45 (10): 1711-1717.

[66] Mtshali TN, Krupa I, Luyt AS. The effect of cross-linking on the thermal properties of LDPE/wax blends. Thermalchim Acta, 2001, 380: 47-54.

[67] Gardner DJ, Oporto GS, Mills R, Samir MASA. Adhesion and surface issues in cellulose and nanocellulose. J Adhes Sci Technol, 2008, 22: 545-567.

[68] Yan C, Zhang J, Lv Y, Yu J, Wu J, Zhang J, He J. Thermoplastic cellulose-graft-poly (L-lactide) copolymers homogeneously synthesized in an lonic liquid with 4-deimethylaminopyridine catalyst. Biomacromolecules, 2009, 10 (8): 2013-2018.

[69] Boudenne A, Ibos, L, Candau Y, Thomas S. Handbook of multiphase polymer systems. John Wiley & Sons Ltd, Chichester, West Sussex, UK, 2011, p. 455.

[70] Liu M, Guo B, Du M, Chen F, Jia D. Halloysite nanotubes as a novel β-nucleating agent for isotactic polypropylene. Polymer 2009; 50: 3022-3030.

[71] Boudenne A, Ibos, L, Candau Y, Thomas S. Handbook of multiphase polymer systems. Chichester, West Sussex, UK: John Wiley & Sons Ltd; 2011. p. 455.

Chapter 7 Suggestions for future research

Biobased and biodegradable polymer nanocomposites are considered part of 'Clean' and 'Green' technologies. They are developed mostly from sustainable resources, rather than petroleum, and do not end up in landfills at the end of their life unlike the conventional ones, as they can be easily composted. While they have good mechanical and physical properties, the current research is towards to improving their properties further and broadening their applications.

Several biobased and biodegradable polymer nanocomposites have been fabricated and characterized in this research [1-5]. Their mechanical, thermal, physical properties have been enhanced while at the same time the water resistance has been improved [1-5]. It is envisioned that these nanocomposites can replace the traditional non-biodegradable plastic materials in many applications, including sports racket frames, ski poles, circuit board, automobile inside panels, etc. [1-5]. The biodegradation process and its mechanism for some of these polymer nanocomposites have been investigated in this research as well. The 'Green Composite' field is still in its infancy and is expected to grow exponentially in the future as the demand for the green products grows and petroleum reserves get depleted. Based on the present research following recommendations may be made.

First, besides soy protein based resin and polyvinyl alcohol (PVA), more biobased and biodegradable polymers can be used. Biobased polymers include cellulose, chitin, agar agar, carrageenan, lignin, proteins, bacterial produced polyesters, polylactic acid (PLA) and polyamino acids (PAA). Many of these are inexpensive and available in all parts of the world. Biodegradable polymers include polyvinyl alcohol (PVA), polyglycolic acid (PGA),

polycaprolactone (PCL), polyethylene oxide (PEO), etc. [6-8]. These biobased and biodegradable polymers provide greener choices with varied properties for fabrication of polymer nanocomposites.

Second, as reinforcement and fillers, in addition to bacterial cellulose (BC), microfibrillated cellulose (MFC) and halloysite nanotubes (HNTs) used in this research other nanomaterials and natural fibers may also be used. These nanomaterials can be nanoparticles and heteroepitaxial core-shell nanomaterials (zero-dimensional nanostructure), nanowhiskers, nanofibers or fibrils, nanowires, nanorods, nanotubes and nancables (one-dimensional nanostructure), and thin films or sheets such as exfoliated nanoclay (two-dimension nanostructure) [9]. These nanomaterials can offer more functionalities for the polymer nancomposites to fit special requirements for materials. For example, polymer nancomposites with nanowires can be prepared with semi-conductive properties.

Third, in addition to solvent intercalation, other fabrication approaches may be used. These approaches include *in situ* polymerization synthesis and melt intercalation, which have special advantages for fabricating polymer nancomposites [10-12]. For example, *in situ* intercalative polymerization in the presence of filler provides distinct advantages as compared with other nancomposite synthesis techniques and offers possibility to polymerize a large range of thermoplastic and thermosetting polymers, handling of gaseous or liquid monomers, handling of high-pressure polymerization, and easy control of heat of polymerization owing to dispersion medium present in the system [13].

Fourth, besides glutaraldehyde (GA), glyoxal and malonic acid (MA) used in this research more benign crosslinkers can be used to make these nanocomposites truly green. Sugar derivatives with aldehyde or carboxylic groups obtained from oxidation of sugars such as

sucrose and glucose are good candidates for 'green' crosslinking. Many such benign crosslinkers have already been synthesized in our lab.

Fifth, detailed interface properties between polymer and nanomaterials should be investigated to understand factors controlling the additive/reinforcement-resin interface. For example, Föster resonance energy transfer (FRET) technique and laser scanning confocal microscopy (LSCM) are suggested to also jointly apply to reveal the interface between nanomaterial and polymer in polymeric nanocomposites [14]. The understanding about interface would allow manipulating desired mechanical properties of the nanocomposites.

Sixth, deeper understanding of biodegradation mechanisms for different biobased and biodegradable nanocomposites need to be investigated. This understanding will provide future methods to control the useful life of the products.

References

[1] Qiu K, Netravali AN. Biodegradable composites of polyvinyl alcohol reinforced with microfibrillated cellulose. J Mater Sci 2012; 47 (16): 6066-6075.

[2] Qiu, K, Netravali, AN. Fabrication and characterization of biodegradable composites based on microfibrillated cellulose and polyvinyl alcohol. Compos Sci Technol 2012; 72 (13): 1588-1594.

[3] Qiu K, Netravali AN. 'Green' composites based on bacterial cellulose produced using novel low cost carbon source and soy protein resin. Recent advances in adhesion science & technology: Mittal festschrift. Boston: Brill; 2012 Accepted.

[4] Qiu K, Netravali AN. Halloysite nanotube reinforced biodegradable nanocomposites using noncrosslinked and malonic acid crosslinked polyvinyl alcohol. Compos Part A-Appl S 2012; Submitted.

[5] Netravali AN, Qiu K. Bacterial Cellulose Based 'Green' Composites. International patent 2010; International Publication No.: WO 2010/135234 A2.

[6] Stevens ES. Green plastics: an introduction to the new science of biodegradable plastics, Princeton University Press, Princeton, NJ, 2002, pp.10-30.

[7] Netravali AN, Chabba S. 'Composites get greener'. Materials Today, 2003, 6 (4): 22-29.

[8] Georgia Tech Research Institute . 'Breaking down plastics: new standard specification may facilitate use of additives that trigger biodegradation of oil-based plastics in landfills'. http://gtresearchnews.gatech.edu/biodegradation-of-plastics/, Accessed November 2011.

[9] Cao G, Wang Y. Nanostructures and nanomaterials: synthesis, properties, and applications, 2nd edition. Singapore: World Scientific, 2011. p. 61-142.

[10] Alexandre M, Dubois P. Polymer layered silicate nanocomposites: preparation, properties and use of a new class of materials. Mater Sci Eng R: Rep 2000; 28: 1-63.

[11] Bordes P, Pollet E, Averous L. Nano-biocomposites: biodegradable polyester/nanoclay systems. Pro Polym Sci 2009; 34: 125-155.

[12] Pavlidoua S, Papaspyrides CD. A review on polymer-layered silicate nanocomposites. Prog Polym Sci 2008; 33: 1119-1198.

[13] Mittal V. In-site synthesis of polymer nancomposites. Weinheim, Germany: Wiley, John & Sons, Incorporated, 2011. p.1-44.

[14] Zammarano M, Maupin PH, Sung LP, Gilman JW, McCarthy ED, Kim YS, Fox DM. Revealing the interface in polymer nancomposites. ACS Nano 2011; 4 (4): 3391-3399.